UNIVERSITY OF OKLAHOMA

GRADUATE COLLEGE

DIRECT SIMULATION OF THE THERMAL TRANSPIRATION OF RAREFIED GASES IN SHORT CHANNELS

A DISSERTATION

SUBMITTED TO THE GRADUATE FACULTY

in partial fulfillment of the requirements for the

Degree of

DOCTOR OF PHILOSOPHY

By

JEFFREY W. LANTZ
Norman, Oklahoma
2009

DIRECT SIMULATION OF THE THERMAL TRANSPIRATION OF RAREFIED GASES IN SHORT CHANNELS

A DISSERTATION APPROVED FOR THE
SCHOOL OF AEROSPACE AND MECHANICAL ENGINEERING

BY

Dr. Harold Stalford, Chair

Dr. Lloyd A. Bumm

Dr. Kuang H. Chang

Dr. Rong Z. Gan

Dr. Feng C. Lai

DEDICATION

I want to dedicate this work to the following: my wife, Sarah, for the endless hours of listening, taking care of our two lovely daughters, and tireless patience while I was working. You are my better half. To Mom, Dad, Jon, Christy, Steve and Barbara: you always challenged me to pursue the goal and believed more than I, that I would achieve it. To my family at City Church of Albuquerque: for your continual prayer. And finally to my Father in heaven who saw fit to put me on this path and gave me the strength to keep going. To all of you I dedicate this work.

ACKNOWLEDGEMENTS

I first want to thank my advisor Dr. Harold Stalford for his continual support and encouragement. You are a prime example of what an advisor should be and you have a genuine care for the people working with you. I also want to thank Dr. Graeme Bird for his input, code development, and advice, and general good nature. To my colleagues: Paul Galambos, Conrad James, and Colleen Wakefield, thank you for offering advice, direction and encouragement. You wouldn't believe how small words could have such a big impact.

TABLE OF CONTENTS

LIST OF TABLES

LIST OF FIGURES

ABSTRACT

Thermal transpiration (also referred to as thermal creep, thermal diffusion and thermomolecular flux) is the process by which a gas under the influence of a temperature gradient will flow through a channel from a cold region to a hotter one. This dissertation presents molecular simulations of thermally induced flow in the transition and free molecular regime using the probabilistic modeling technique referred to as Direct Simulation Monte Carlo (DSMC). We show how the thermomolecular flux can create a pressure increase which can be used as a pumping mechanism as well as present results of the net flux as a function of temperature, gas density, channel length, and accommodation coefficient.

This disseration begins with a presentation of the historical background which led up to kinetic gas theory and inspired Martin Knudsen and his pump idea. We describe the Knudsen pump idea in depth and outline the experimental progress and various Knudsen pump designs in the last 100 yeas. We then take a comprehensive look at the various types of micropumps and their pumping mechanisms. The last section of the review focuses specifically on gas phase pumps and the performance of existing Knudsen pumps.

Afterwards, we provide the basic kinetic theory of thermal transpiration and describe the work in that area in the previous century. We then present the modern methods for solving the thermal transpiration method including an analysis of the strengths and weaknesses of each method. We discuss at length

the DSMC method, the errors involved in the method and the simulation parameters for my set of simulations.

Our DSMC simulations give the most complete DSMC results for both open and closed systems with the focus being on the thermomolecular flow through short channels throughout the transition and free molecular regimes. To our knowledge, our results are the first DSMC results to include both multiple pressure differences and temperature gradients and use those plots to derive maximum values for the flux, flowrate and pressure drop. We provide the first flowfield velocity profiles for both transition regime and free molecular regime flows as well as flux values for a variety of pressures differences at all Knudsen numbers. We also provide the pressure differences and pressure ratios when there is zero molecular flux along with flux data for pore arrays.

The results shown here are the first DSMC simulations looking at thermal transpiration for different aspect ratios and different tangential momentum accommodation coefficients for Knudsen numbers in the transition ($0.1<Kn<10$) and free molecular ($Kn>10$) regimes. We have run over 300 simulations where a single run takes anywhere from 12 hours to 7 days of computational time. For each flux or pressure difference data point, we ran several simulations at varying pressures using a single number density (Knudsen number) and temperature gradient.

Finally we provide four design scenarios which utilize the simulations results in various ways. We show how this phenomenon applies both to rarefied gases flowing through meso-sized channels as well as dense gases through micro/nano-channels. These designs show how the simulation results predict that a $1cm^2$ array of pores could achieve a maximum pressure difference of 7kPa and a maximum flowrate of over 1×10^8 sccm. The designs also emphasize the validity and usefulness of the DSMC simulations as well as provide the reader with a clearer understanding of the physics behind thermal transpiration and the potential performance of a Knudsen pump.

CHAPTER 1 INTRODUCTION

In recent years, microfluidic applications have continued to grow at an astounding rate. Much of the effort has been focused on biological and chemical sensors, ink-jet heads, fluidic manifolds, chemical power generators, flow sensors, filters, and many other applications [124]. One of the key components in microfluidic applications is the micropump (Chapter 2). In many of the above applications, while the fluidics channels and other active components are located on the chip, an external macroscopic pump is needed because existing micropumps aren't able to deliver fluid at the desired pressures and flowrates.

For those micropumps that provide the needed performance to the above applications, the majority are practical only as liquid phase pumps due to the high leak rates and low pressures and low flow. This is a result of the low viscosity of gas and the unique phenomena that occurs in the micro- and nano-scale regimes. This is a key obstacle since applications such as vacuum equipment, gas-phase microfluidics, mass spectrometry, metrology of gas flow, spacecraft design, gas sensing, and on-chip cooling all require robust gas-phase pumps.

In 1909 Martin Knudsen [131] determined that gas would flow continuously through the wall of a porcelain bulb under the influence of a temperature gradient from the cold side to the hot side. From this experiment he devised a gas phase pump with no-moving parts using a series of nano-scale channels

interconnected to larger capillaries. By applying a temperature gradient across the channels and capillaries, he envisioned that a continuous flow of gas would pass through the channels. What separates the Knudsen pump from other pump options is its lack of moving parts and the potential to use it passively where a known heat source is already available. There are others who have developed methods of studying Knudsen's phenomena using approximate numerical methods (section 4.5) and some experiments (section 1.3.3) have been performed. However, a rigorous study has yet to be made comparing thermal creep experiments in known channels with numerical simulations.

This report describes the results from an advanced modeling and simulation of gas flow and pressure/temperature differentials through the short channels using the molecular based simulation software developed by Dr. Graeme Bird: DSMC (Direct Simulation Monte Carlo) simulation. We will begin with a review of the work that led to Knudsen's pump concept followed by a comprehensive outline of current micropumps. Included in this section is a comprehensive look at the Knudsen pump and why it works. We then show the theory behind collisionless flow (Chapter 3) and its role in thermomolecular pumping. Chapter 4 adds the collision model to the equation with a derivation of the Boltzmann distribution along with an analysis of how it is used to calculate flux. The difficulty involved in solving this equation is presented which gives rise to the reason for using DSMC (Chapter 5) to solve the Knudsen flow problems. Our results in Chapter 6 show how the flux and pressure differential change with Knudsen

number followed by some examples (Chapter 7) where we apply our simulation results to design.

1.1 Historical Background

Today's work in Knudsen flow and rarefied gas flow can be traced back to the early philosophers [159] who speculated that substances in the world were made from smaller particles in constant motion. Lucretius, in his poem 'On the Nature of Things' described matter as being a "packed phalanx…tightly packed and closely joined cohere by virtue of their minim particles…" 1800 years later, Bernoulli published a paper which included a picture showing his ideas of a gas as a series of small particles, however, it wasn't until approximately 150 years ago that much of this theory was verified and the origins of modern gas theory began to take shape.

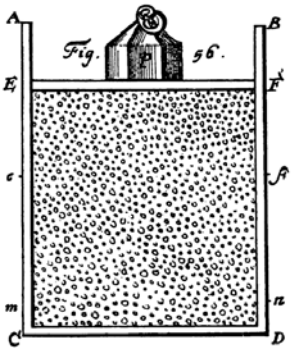

Figure 1-1: Bernoulli's Piston [23]

The year 1857 included a number of findings that truly jump-started the modern theory of gases. Using Boyle's law [32] and Graham's [94] experimental results

on the transpiration of gases, Dr. James Joule was able to derive an expression for the pressure in terms of the velocity of the molecules. Two contemporaries of Joule [119], Kronig and Clausius [49], reported experimental results that showed

Figure 1-2: James Prescott Joule (1818-1889)

that the motion of small gas particles wasn't centered on definite positions of equilibrium, but were continuous until they collided with other molecules or the container wall.

This presented a problem since, if this theory were true, it would seem the molecules would diffuse in a container much faster than was observed due to the molecules' high rate of speed. Clausius (Figure 1-3) answered this question with a description of the interaction between the molecules. He theorized gas molecules were large enough to collide with one another but were small enough so that, at any point in time, they would be separated by an average distance he termed the 'mean free path' of the gas.

Figure 1-3: Rudolph Clausius (1822-1888)

His equation for the mean free path of the gas was:

$$l = \frac{3}{4}\frac{1}{n\pi\sigma^2} \tag{1-1}$$

$$n = \frac{N}{V} \tag{1-2}$$

where n is the number density of the gas molecules, σ is the diameter of the particles, N is the total number of molecules and V is the volume. His equation was in error, however, by approximately 10% since he assumed the mean free path was based upon the motion of several particles around a single stationary particle.

Clausius also introduced the idea of entropy (the randomness of a gas) and was the first to make the statement "entropy always increases" [160]. Boltzmann (Figure 1-4) used Clausius' idea and made the first connection between entropy and probability which led to the derivation of the Maxwell-Boltzmann distribution which is one of the fundamental principles in gas flows.

Figure 1-4: Ludwig Boltzmann (1844-1906)

In 1863, Thomas Graham (Figure 1-5) [93, 169, 126] began an investigation into the study of gaseous flow through a porous plate. Chiefly, he showed that gaseous flow through these smaller pores was not necessarily a mechanism of the flow of the "gas in mass" but rather a summation of the individual motion and mobility of molecules in what he termed capillary transpiration. He was one of the first to study gaseous flow in small regimes where continuum theory breaks down.

Figure 1-5: Thomas Graham (1805-1869)

Osborne Reynolds (Figure 1-6) [213] continued this work by addressing areas that Graham and other observers of his work had not pursued. Graham focused on the pressure driven flow through a porous plate of both single and binary

gases and endeavored to maintain uniform temperature and low humidity. Reynolds, however, noticed that "a difference of temperature on the two sides of the (porous) plate might cause gas, without any difference of pressure or any difference in chemical constitution, to pass through the plate." He termed this temperature driven flow: "thermal transpiration" (also later to be known as

Figure 1-6: Osbourne Reynolds (1842-1912)

'thermal creep' or 'thermomolecular pumping'). He found experimentally that the relation between the temperature and pressure in a closed system was:

$$\frac{P_1}{P_2} = \sqrt{\frac{T_1}{T_2}} \tag{1-3}$$

Although Reynold's work was mainly a continuation of Graham's experiments, it was also influenced by a fascination he had with Sir Williams Crookes' (Figure 1-7) radiometer [207, 141]. This device measures light radiation using the rotary motion of black/white colored vanes suspended within a vacuum. In 'near' vacuum conditions, temperature variations at the edges of the vanes create pressure gradients which in turn put the device in motion.

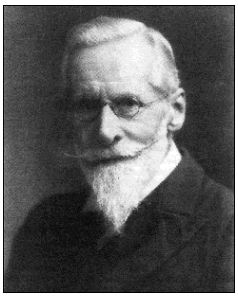

Figure 1-7: Sir William Crookes (1832-1919)

It took another scientist in 1879 to provide the mathematical conclusion to many of the theories addressed in the previous three decades. James Clerk Maxwell (Figure 1-8), who is best known for Maxwell's equations and his 1867 work "On the Dynamical Theory of Gases" [173],

Figure 1-8: James Clerk Maxwell (1831-1879)

further developed Kronig's and Clausius' theory of the motion of gases by introducing the concept of a statistical distribution of velocities. He determined that the velocity distribution of a molecule could be found using the equation:

$$f_o(\vec{v}) = n\left(\frac{m}{2\pi kT}\right)^{\frac{3}{2}} \exp\left(\frac{m\vec{v}^2}{2kT}\right) \tag{1-4}$$

where m is the mass, k is Boltzmann's constant, T is the temperature in Kelvin, and v is the velocity. This equation is explained in greater detail in section 0. From the velocity distribution Maxwell found the mean free path (the distance a molecule moves before it impacts another molecule) to be:

$$\lambda = \frac{1}{\sqrt{2}} \frac{1}{n\pi\sigma^2} \tag{1-5}$$

where

$$n = \frac{N}{V} \tag{1-6}$$

and n is the number density, N is the number of molecules and V is the volume. He went on to demonstrate that a variety of macroscopic variables of state can be derived from a statistical distribution of the velocities of the molecules. After reading Reynold's paper on thermal transpiration, Maxwell began to apply his ideas of interior gaseous behavior to the surface phenomena. Here he extended Reynold's work by developing some of the first mathematical models of thermal transpiration at the solid-gas interface.

1.2 Knudsen

It wasn't for another 30 years that thermal transpiration was to be used as a pumping mechanism. Martin Knudsen's initial endeavors went to prove experimentally that Maxwell's kinetic theory of the relation between temperature and pressure was accurate. He developed theories describing basic

kinetic theory, molecular effusion (the flow of gas into a vacuum), molecular reflection of surfaces, evaporation and condensation, gas flow in tubes at low pressures, and gas resistance to the motion of a body. He was having difficulty, however,

Figure 1-9: Martin Knudsen (1871-1949)

understanding why the direction of molecules reflecting from the surface of a solid were independent of the direction of approach . He agreed with Smoluchowski that energy was being transferred to the molecules so he developed the accommodation coefficient as a way to characterize the temperature difference of the impinging and reflecting molecules. Through his experimentation he began to see how the gas flow through small channels could be controlled and in 1910 published a pump design based on this phenomena. Today the pump carries his name.

1.3 The Knudsen Pump

The Knudsen pump (Figure 1-10) features an alternating set of small and large channels with a heater placed at every other channel junction. The small channel's diameter must be on the order of (or smaller than) the mean free path

of the gas molecules and the larger channels sized much greater than the mean free path so as to assure pressure driven flow. Because thermal flow is dominant in the small channels and Poisueille flow in the large channels, a continuous flow in one direction can be achieved. The pump has the advantage of having no moving parts and could also be passive if used with an existing heat source.

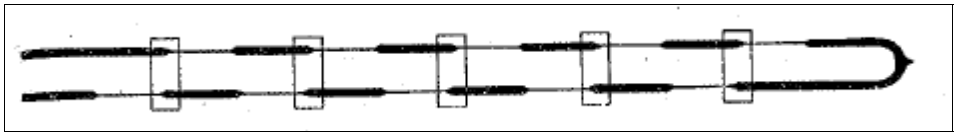

Figure 1-10: The Knudsen Pump [127]

1.3.1 Flow Regimes

Before we can understand how the Knudsen pump operates we must first take a look at the various flows regimes. Consider the flowfields in Figure 1-11. During hydrodynamic conditions the flow is dense enough that molecule-to-molecule interactions are happening continuously. In this flow, two things are occurring simultaneously. First, the pressure difference along the channel is being continually transmitted between molecules which "pushes" the flow through channel. Second, the influence of the wall is limited to a narrow area along the wall whose width is about the size of the mean free path of the gas. After the molecules impact the walls they are instantaneously impacting other molecules and transmitting/receiving energy. Thus, while the walls have influence on the flow, that influence can be overcome by the bulk state conditions.

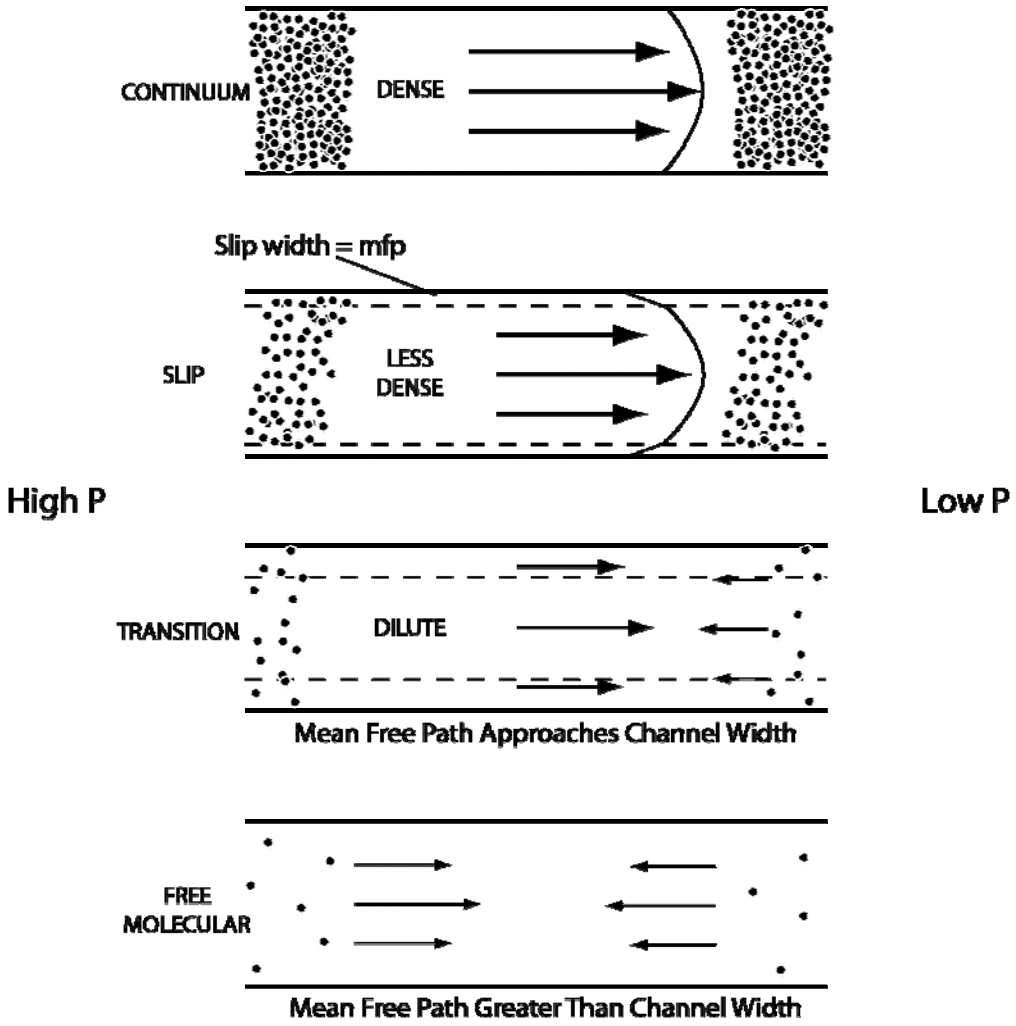

Figure 1-11: The Influence of Rarefaction

Now consider the situation where the ratio of the mean free path of the gas increases compared to the width of the channel. This can occur either by decreasing the width of the channel (i.e. microchannels) or by decreasing the pressure (and therefore the mean free path, as was shown in equation (1-6)).

This ratio is termed the Knudsen number (Kn) and is used to describe the "rarefaction" of the gas flow.

As the Knudsen number increases, the width of the boundary layer also increases in relation to the channel width. The intermolecular collisions begin to decrease in relation to the walls impacts. This in turn impacts the flowfield because there are not enough intermolecular impacts to transmit the pressure through the channel especially along the walls. The result is a "slip" condition where the velocity profile elongates and the slip length increases. This region is called the slip-flow and is defined where:

$$0.01 \leq Kn \leq 0.1 \tag{1-7}$$

If we continue to increase the rarefaction, the flow will eventually reach a point where the mean free path is greater than the channel width. In this case the wall impacts occur more frequently than intermolecular impacts which demands greater attention be paid to the surface properties of the channel; namely the energy and momentum accommodation coefficients. By increasing the rarefaction even more, it is entirely possible that a molecule could enter on one side of the channel and pass through the channel without hitting the wall or another molecule. There is not a clear line where this occurs but common practice sets this "free molecular" line where the Knudsen number is greater than 10. The area in between the free molecular and slip flow regimes is termed the transition regime.

1.3.2 The Knudsen Pump – Why It Works

Now consider flow through an ideal aperture (Figure 1-12) where the two sides of the wall are kept at different temperatures and pressures. We assume the size

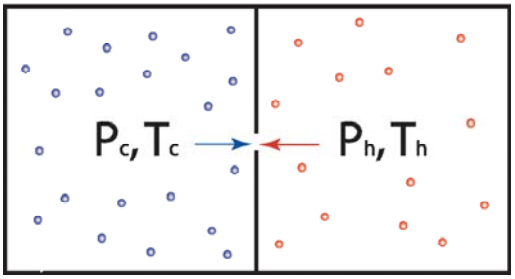

Figure 1-12: Flow Through an Aperture

of the hole is smaller than the mean free path of the gas and there are no collisions in the aperture. Based on the ideal gas law we know the following relations are true:

$$n \propto \frac{P}{T} \tag{1-8}$$

$$\bar{c} \propto \sqrt{T} \tag{1-9}$$

which means the number flux is proportional to P and inversely proportional to the square root of T:

$$\dot{N} \propto n\bar{c} \propto \frac{P}{\sqrt{T}} \tag{1-10}$$

The net flux through the orifice is related by:

$$\dot{N}_{\text{net}} \propto \left(\frac{P_H}{\sqrt{T_H}} - \frac{P_C}{\sqrt{T_C}} \right) \tag{1-11}$$

If the number flux is zero then we get the Reynolds' relation between the hot and cold sides from equation (1-3) which he termed "thermal transpiration". If we initially set $P_H=P_C$ then the net flow will begin to move from the colder side to the hotter side as long as the pressure is not allowed to build up beyond the ratio:

$$\frac{\sqrt{T_{hot}}}{\sqrt{T_{cold}}} \tag{1-12}$$

If P_H is kept continually at the same pressure as P_C (an open system with no walls) then there will be a continuous net flux based on the temperature difference (from lower temperature to higher temperature).

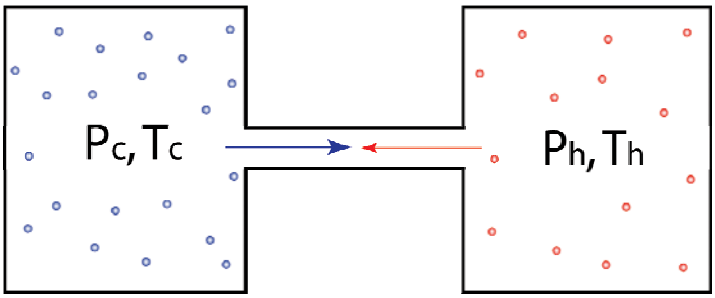

Figure 1-13: Channel Flow

Now let's extend this model to include a channel that separates the two reservoirs. In the free molecular case where there are very few intermolecular collisions, wall interactions now occur where energy and momentum are transferred. In a closed system the pressure ratio at steady state reaches the same value as before and the net flow is zero through the channel. Figure 1-14 shows the gas flow angles relative to the centerline (x) axis in a system with a

thermal gradient. In this flow the direction throughout the flow is random at steady state because molecules are streaming from both sides of the channel with very few collisions. The diffuse reflection of the walls has a random direction even though energy is transferred to the molecules.

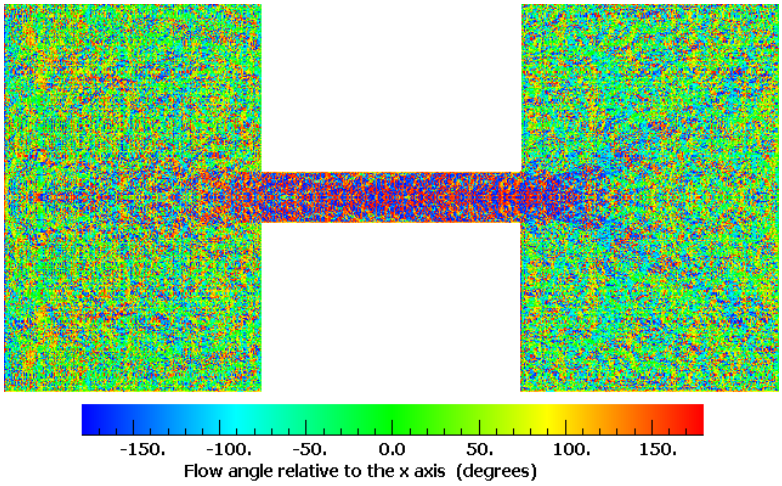

Figure 1-14: Free Molecular Flow Direction (Closed System)

If we look at the same system near the slip regime we see a slightly different response. The pressure ratio is much less than the square root of the temperature ratio since the pressure induces a Poiseuille flow in a direction opposite to the thermal creep. The velocity profile in Figure 1-15 shows a positive flow velocity along the walls and a negative velocity down the center of the channel showing how "thermal creep" occurs at the surface and pressure driven flow along the centerline of the channel. Figure 1-16 shows the flow angle for this case which confirms the direction of the flow. In an open system, both Sone [243] and Alexeenko [8] showed the thermal creep velocity profile was parabolic in the direction of the thermal gradient.

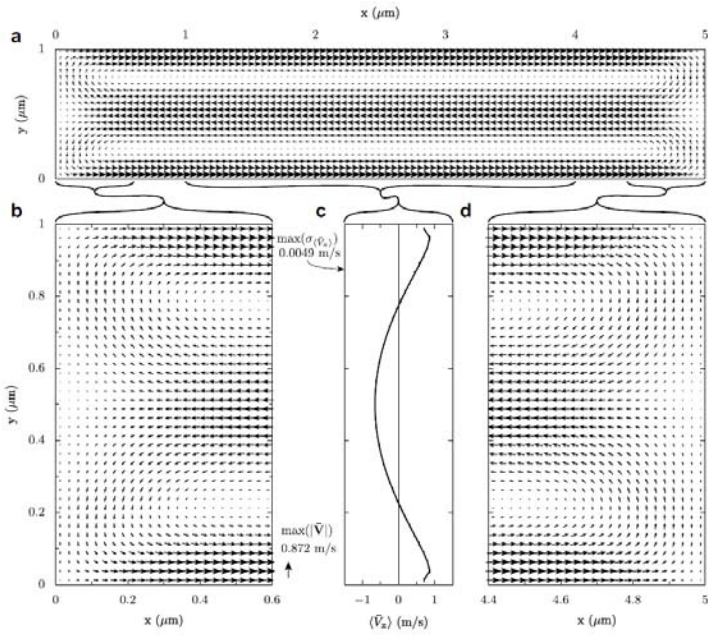

Figure 1-15: Near Slip-Flow Velocity (Closed System) [170]

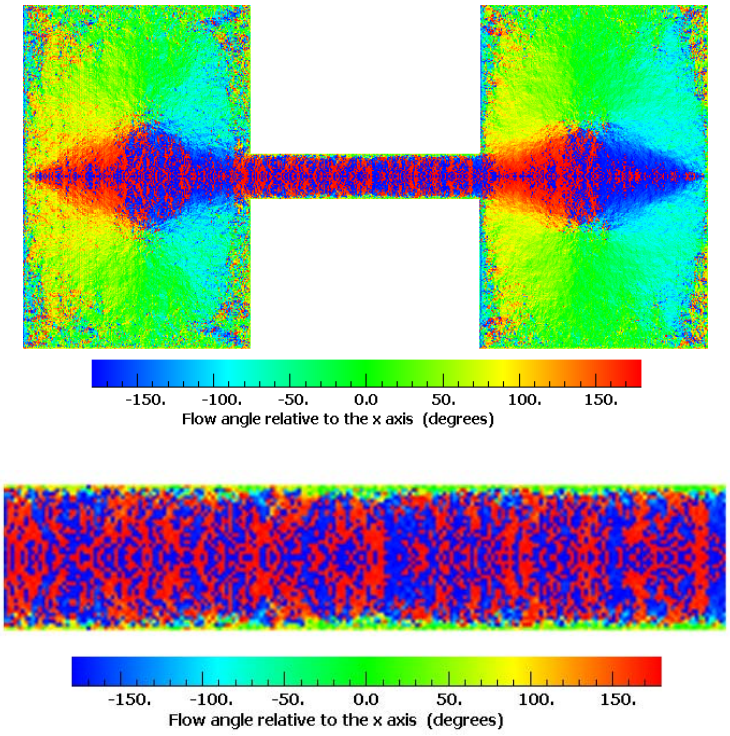

Figure 1-16: Near Slip-Flow Velocity (Closed System)

Now the width of the Knudsen layer (thermally driven flow) is on the order of the mean free path of the gas. Thus, the higher the Knudsen number, the greater the thermal effect in the channel. This can be accomplished either by shrinking the size of the channel or by reducing the gas density. Near the free molecular regime the width of the channel is on the order of the mean free path of the gas so thermal creep is at its maximum value. This effect is reduced to zero as the Knudsen number goes to infinity as well as when Kn approaches zero.

Knudsen's pump utilizes this thermomolecular pressure ratio by alternating narrow (high Knudsen number) channels and wide (low Knudsen number) channels. Thermally induced flow dominated the narrow channels and Poiseuille flow is dominant in the wide channels which creates a continual flow. If the channels are short (aspect ratio < 10) there is a contribution of flux due to the thermal creep at the walls as well as a contribution from molecules entering the channel. In long channels (aspect ratio > 10) the entrance effects are negligible. The effect is the same in either as the only requirement for Knudsen's pump to work is to have the alternating set of channels and thermal gradients. Sone [243] showed that the flux would stop if there were only the narrow channels without the larger ones.

1.3.3 Post-Knudsen (Continuing His Work)

A half century after Knudsen developed his pump concept the first significant effort was made with regard to the development and analysis of this type of pump. First, Liang [144, 145] ran experiments to study the thermal transpiration effects for various gases at different temperatures. Annis [9, 10] ran similar experiments with an emphasis on the temperature dependence. Turner [264] later developed a mathematical analysis of a macro-knudsen pump designed by Baum and Schumacher [223]. His conclusion was the limit of the pressures achieved would be 10-1 to 10-3 torr with a maximum flowrate of 66 liters/sec. Hobson [108-110] developed an accommodation pump based on a similar principal only instead of using a difference in channel size to control the direction of flow of the molecules, he changed the surface roughness between adjacent channels. His pump alternates two volumes at room temperature, the first being atomically rough and the second, atomically smooth. As the temperature of the alternate channel junctions are changed, flow is produced in the channels. A kinetic model of this method was presented by Branton [33] nearly a decade later.

Tracy [263] developed the first thermomolecular pump which used a heated 'director' placed directly above a small slit situated between two reservoirs . As the temperature of the director increased, the flow increased since the molecules striking the director were more likely to be directed normally toward the slit than not. Furuyama [82] and Yasumoto [288] took measurements of thermal

transpiration effects at various temperatures to study how the pressure and temperatures were related.

Young [289] was the first to mention the creation of a thermal/knudsen pump in the micro-regime and holds a patent for the same. Vargo, et. al. [269, 270], however, were the first to fabricate an actual microdevice. Their pump was comprised of an aerogel sandwiched between two silicon wafers with a pyrex cap on each side. The silicon had an array of 20um diameter holes and the aerogel a pore size of approximately 20nm. Muntz, et. al. [187] extended Vargo's analysis by developing models for the energy efficiency of the system.

In the last ten years, three different pump designs have been reported. Young [290, 291] replaced the aerogel in Vargo's design with a microsphere bed and performed an experimental comparison of the two . His conclusion was the microsphere bed's performance was equivalent to that of the aerogel, however, it would operate more efficiently at pressures under 100 mTorr. The benefit of the microsphere bed exists in its ability to be fabricated with varying pore sizes and thermal conductivities. Sone, et. al. [245, 246] developed a meso-scale vacuum pump (Figure 1-17) using two plane walls embedded in a circular pipe (15mm diameter/ 30 mm. length). The plates were etched with channels perpendicular to the direction of flow and a heater was placed in the middle of the pipe. He performed DSMC simulations on the pump for a 3:1 temperature

ratio and a high temperature of 150K. His experiments produced a maximum pressure drop of 12 Pa and a maximum volumetric flowrate of 28 cm^3/s.

McNamara, et. al. [174, 175] developed the smallest pump to date using a six mask silicon process. His device uses large channels fabricated 10um deep x 30um wide and small channels 100nm deep x 10um wide. It is a single stage device horizontally fabricated and is able to achieve .46 atm of pressure with less than 1W of input power. Han [99] continued the experimental work of Young and Vargo to study flows through the aerogel membrane. He outlined the "reverse" thermal creep that occurs in that system. In 2008, Copic [52] published a paper outlining the theoretical efficiency of a Knudsen pump.

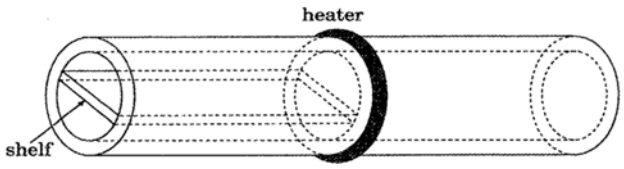

Figure 1-17: Sone's Pump Configuration [246]

CHAPTER 2 MICROPUMPS

It is now important to show how the Knudsen pump fits in context with other micropumps. In the mid-1980s, a surge in the development of lab-on-a-chip, micro-analysis, dosing, and thermal management systems created an entirely new field of Micro-Electro-Mechanical System (MEMS). Microfluidics sprang into being and thus spawned the need for pumps, valves, fluid channels, sensors, and a variety of other types of microfluidic components. Possibly the single most diverse area of component design was the micropump, which used a variety of actuation devices, integration schemes, and theoretical methods of providing fluid delivery at a wide range of pressures and flowrates.

When looking at the variety of gas phase micropumps, the Knudsen pump stood out because it utilized a phenomena unique to the micro-regime. This could also be said of other pumps (i.e. electrostatic), however the Knudsen pump had two characteristics no other gas pump could boast:

1. It has no moving parts.
2. It has the potential to be totally passive by using existing heat sources to drive the flow.

The review below outlines the taxonomy of mechanical and non-mechanical pumps followed by a description of the various actuation mechanisms. The section ends with comparison of gas phase pumps with special consideration to the Knudsen pump. It will be shown (Section 2.5) that the flux and pressure

difference data we present in Chapter 6 is needed to show the potential performance of the Knudsen pump.

2.1 Introduction (Taxonomy of pumps)

Micropumps can be divided into two main areas: mechanical and non-mechanical. Mechanical pumps convert electrical energy into mechanical energy through a variety of actuation mechanisms and generally use some sort of a moving boundary to create discrete fluid motion with each cycle. The most common of these is the membrane pump which has been fabricated in a variety of configurations some of which employ more than one membrane. Non-mechanical pumps, on the other hand, convert a variety of other (magnetic, entropy, electric field, optical, etc.) energy types into kinetic energy within the fluid. This is the more diverse of the two methods and employs a wide range of scientific phenomenon to actuate the pump.

2.2 Mechanical Pumps

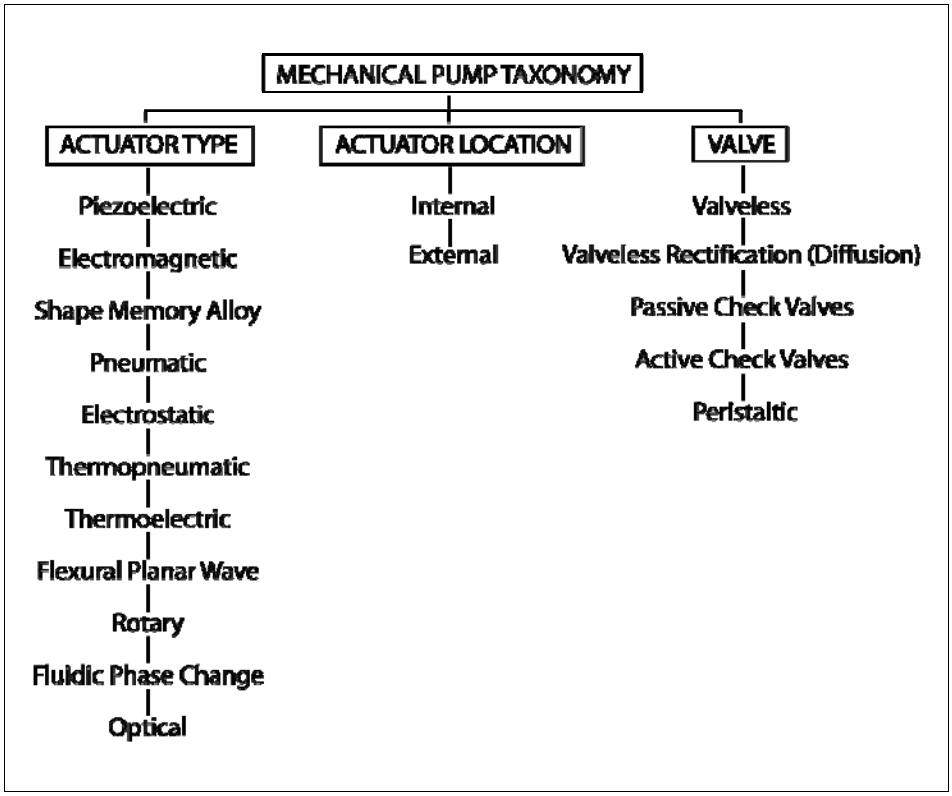

Figure 2-1: Classification of Mechanical Pumps

Mechanical pumps can be sub-categorized according to the type of valve system and whether the actuation device is integrated into the pump or is an external actuator. The first type of integrated valve system is a peristaltic valve. Figure 2-2 shows the

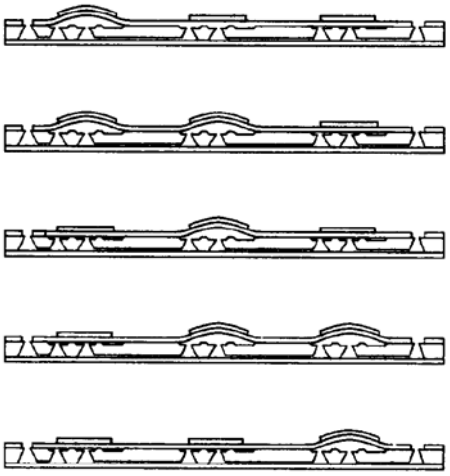

Figure 2-2: Peristaltic Pump [239, 240]

three individual actuators and the order of actuation to create controlled flow through the pump. Olsson [197-201] was the first to create (a gas version) of the second type of pump known as a valveless rectification or diffusion pump. Figure 2-3 shows how flow is directed

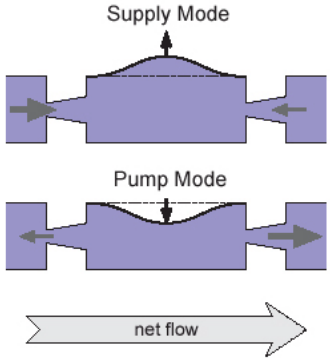

Figure 2-3: Valveless Rectification (Diffusion) Pump

through the pump using geometric design. Stemme [253] outlines a simple method of determining the flow through this type of valve. The pressure loss at one end of the diffuser is:

$$\Delta p = \frac{\rho v^2}{2}\xi \tag{2-1}$$

where ρ is the density, v is the average velocity, and ξ is the pressure loss coefficient. If we define η_F as the ratio between the pressure increase coefficients of the output and input diffusers, then the resulting flowrate is defined as:

$$\dot{Q} = V_x \left[\frac{\sqrt{\eta_F} - 1}{\sqrt{\eta_F} + 1} \right] \tag{2-2}$$

where V_x is the volume change each cycle. The third type of pump uses a check-valve analogous to the one designed by Makino [163-165] in Figure 2-4.

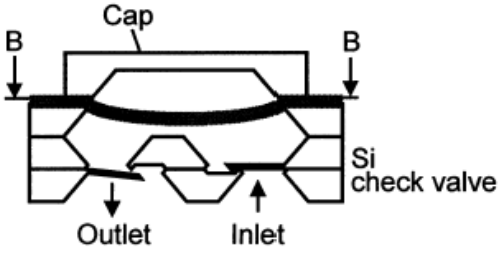

Figure 2-4: Integrated Checkvalve Pump

The check-valve material is generally a thin layer of silicon designed to deflect with small pressures. While check-valve designs tend to reduce the amount of backflow compared to diffusers, diffuser designs are more efficient. Neither, however, can match the ability to control delivery of small amounts of fluid like the peristaltic valve.

2.3 Mechanical Actuators

2.3.1 Piezoelectric (PZT)

Piezoelectric actuators are by far the most common external actuation method in mechanical micropump designs. It is most likely due to the ability to create high forces and high frequencies with just a small displacement. Typical piezo designs typically use one of three types of motors (Figure 2-5) that convert electrical energy into a variety of strains. The first

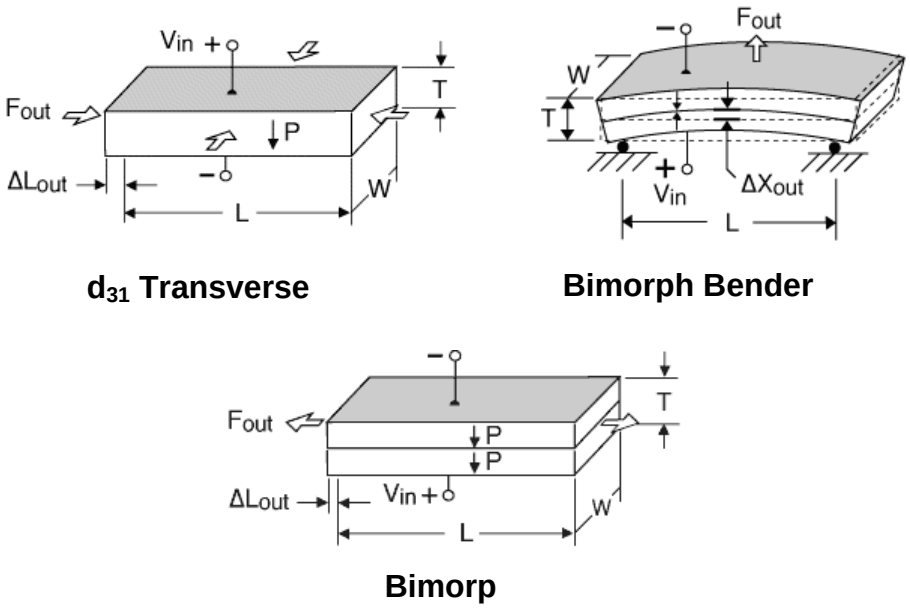

Figure 2-5: Piezoelectric Motor Configurations [209]

method of actuation is one of the most common and utilizes a transverse strain given by:

$$\Delta x = V d_{31} \tag{2-3}$$

where Δx is the linear displacement, V is the applied voltage, and d_{31} is the piezoelectric coefficient. These devices are typically bonded to the pump diaphragm which converts the transverse motion into the bending motion of the

diaphragm. Transverse PZT devices are widely used because of their larger strain (microns to tens of microns) compared to the d_{33} (longitudinal) type of PZT. Accoto [1] bonded this type of piezo actuator to a metallic sheet and used ball valves for his design, where as Hayamizu [105] bonded his to a silicon diaphragm and used variable signals to control the direction of flow. Shinohara [236] actually used two different piezo disks, one for the diaphragm and one for the valve. Stemme [253] developed one of the first d_{31} diffusion pumps and Williams [279] provided an analysis which optimized the pump based on the piezo size, valve size, and diaphragm thickness. Other devices using this type of actuation were developed by Bohm [30], Gass [88], Li [142], Linneman [147], Olsson [197-201], Van Der Wijngaart [268], and Van Lintel [267].

The bimorph (or bender) actuators are fabricated with two layers of pzt material, four electrode layers (two on each side of the actuator and two in the middle), and a center shim between the devices. Bonding the two devices adds stiffness, strength, and in general decreases the motion but can be operated with half the voltage if arranged in parallel. For the bending configuration, one device expands while the other contracts. It is possible with this type of design to produce up to tens of microns of displacement. The equation to determine the deflection of the bimorph is:

$$\Delta x = \frac{L^2 V d_{31}}{T^2} \tag{2-4}$$

where L is the length and T is the thickness of the bimorph. One design using this type of piezo actuator is presented by Smits [239, 240] which uses a

peristaltic configuration. Gerlach [89, 90] used a bimorph to actuate a diffusion pump.

Three other piezo actuated pumps are worth mentioning. The first was developed by Miyazaki [181] and uses composition changes under several piezo elements to create a flexural progressive wave. Matsumoto and Koch each used a different valve scheme in their pumps. Matsumoto [171] uses a viscous based valve system where he heats either the input or output valve to create local viscosity changes in the fluid where as Koch [133-135] uses simple 'flap' check-valves to control flow direction.

2.3.2 Electromagnetic (EM)

Another type of external mechanical pump which has some great benefits is the electromagnetic actuated device. EM actuators have a high stroke as well as a large force but are still driven by a low voltage. While they require simple drive electronics, their drawbacks lie, however, in the high power consumption, their size and the difficulty in mass producing integrated devices. The force model of EM actuator is shown in Figure 2-6 where the resulting sum of forces equation is:

$$m\frac{d^2x}{dt^2} + D\frac{dx}{dt} + k_s x = mg + F_e \tag{2-5}$$

and

$$F_e = \frac{1}{2} i^2 \frac{dL(x)}{dx} \tag{2-6}$$

where:

m = Mass of the actuator piston
x = Displacement

D = Coefficient of damping of the piston on the cylinder wall

k = Spring constant

g = Gravitational constant

F_e = Electromagnetic force

i = Current

L = Inductance of the electromagnetic coil

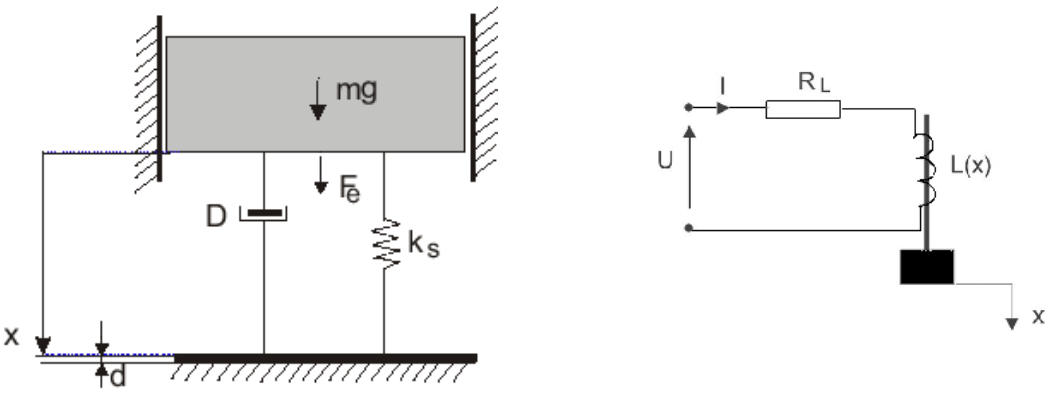

Figure 2-6: Model of Electromagnetic Actuator [296]

Bohm [30] was the first to develop an electromagnetic actuated micropump. His design used a surface micromachined diaphragm powered by either a piezo or a EM actuator. He showed the performance of the two devices were similar although the PZT device was much easier to fabricate and integrate with the system, not to mention the power requirements. Khoo [125] developed a device using a silicone membrane that was able to achieve fairly high flowrates due to

the volume displacement of the actuator. Meng [177] developed an EM pump as well but instead of having an external plunger, he embedded ferromagnetic pieces into a PDMS diaphragm. An external magnet was used to displace the membrane which provided similar performance while reducing the fabrication and packaging complexity.

2.3.3 Shape Memory Alloy (SMA)

The shape memory alloy (SMA) is a TiNi alloy sputtered onto a glass substrate. The use of these thin films takes advantage of a phase transformation between the two solid phases: austenite and martensite. The austenite phase is a high-temperature, high strength state whereas the martensite phase is a low-temperature, high ductile phase. Due to the migration of variant boundaries in the grain structure, as the film goes from one state to the next, it can undergo a deformation or apply a stress.

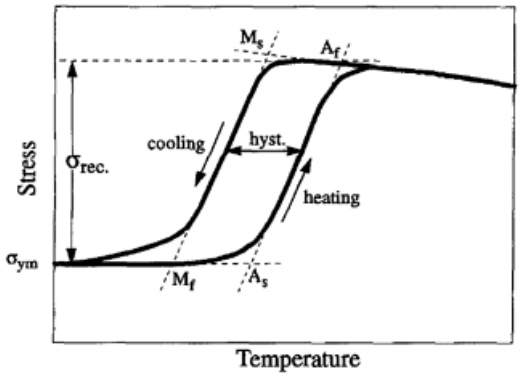

Figure 2-7: Hysteresis of Shape Memory Alloys

Figure 2-7 shows the hysteresis that occurs when the film undergoes a joule heating and conductive/convective cooling cycle. From this it becomes clear that SMA films are highly sensitive to heat and must have adequate heat transfer

to work efficiently. This requirement constrains the performance to low frequencies. Their popularity comes from the high force and displacement as well as the ability to fabricate a variety of shapes.

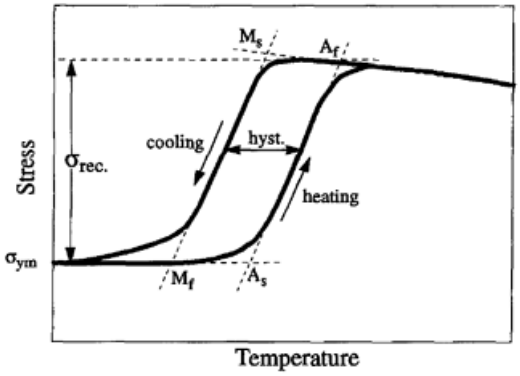

Figure 2-7: Hysteresis of Shape Memory Alloys

Benard [20] developed a pump using two different SMA films alternately heated and cooled attached on either side of a spacer. That portion of the design acts as a single diaphragm with the added benefit of increasing the actuation force. Kahn [123] used a similar configuration only the top SMA film was replaced by a silicon spring designed to increase the frequency of his device. Makino developed the most simple device in the form of a check-valved diaphragm pump using a single SMA film. Two designs that utilized the ability to configure the TiNi shape were Ikuta [117] and Xu [62]. Ikuta fabricated an SMA pump that used a cantilevered TiNi film similar to a piezo bending bi-morph and Xu created a serpentine film deposited on the top of a diaphragm. All reported devices achieved high pressures, however, the flowrate were low due to the low frequency.

2.3.4 Pneumatic

One of the interesting ideas in pump design is to use one actuation method to power another. One way to do this is through pneumatic pumps. Pneumatic pumps use an external pressure source (pressurized tank, air flow from a wing, etc.) to force air through channels on a chip into a cavity. As the pressure in that cavity increases, the membrane (one wall of the cavity) expands and creates a volume change in the adjacent channel.

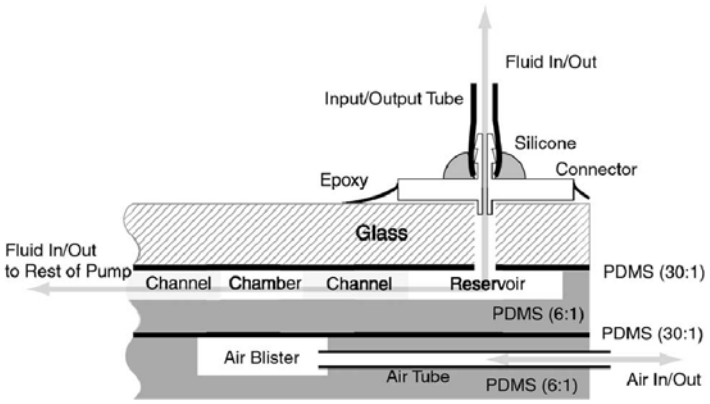

Figure 2-8: Pneumatic Pump [21]

Two designs have been realized in this area of external "actuation" devices other than the one mentioned above [177]. First, Schomberg [221, 37] created a single stage device that combines silicon membranes with LIGA structures galvanized on titanium membranes. Berg (Figure 2-8) used a PDMS structure and arranged several pneumatic actuators in series to create a perisaltic pump. While these devices have a wide range of uses due to the ability to achieve high pressures and displacements, the packaging difficulties and size make them not as desirable as other integrated devices.

2.3.5 Electrostatic

Electrostatic actuators show a lot of promise in the micropump field. They have the ability to achieve high frequencies with very low power (in comparison to other methods) which allows them to move large amounts of fluid, however, they can also control small amounts of fluid as well. They have a common characteristic of SMAs in the ability to control the deflection through the input signal and can generate high forces if the two plates are close enough. The trade-off is due to the force output being proportional to the displacement not to mention the instability that occurs at small gap spacing.

The electrostatic actuation force for a parallel plate capacitor array is calculated using [224, 225]:

$$F(x) = \frac{\varepsilon_o A}{2}\left(\frac{V}{d - d(x)}\right)^2 \tag{2-7}$$

where:

V = Voltage

A = Surface Area of plates

d = Gap space

ε_o = Dielectric permittivity

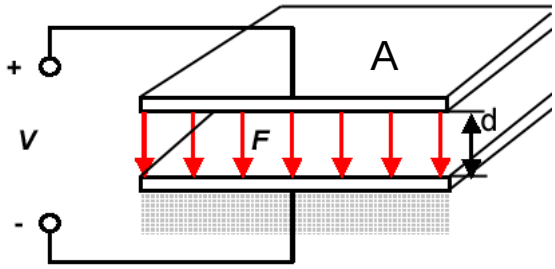

Figure 2-9: Parallel Plate Electrostatic Force

This equation shows how the force is directly proportional to the voltage and surface area and inversely proportional to the gap space. This makes the device a good candidate for surface micromachining as compared to other fabrication methods. It is important to note that in order to achieve the force required, the voltage might have to be quite high. In this instance it is important to stay below the dielectric breakdown voltage so as not to short out the device. One device that allows a larger displacement but can have some stability issues is an electrostatic comb device. It's motion is a result of the capacitive fringe fields rather than the direct "parallel-plate" forces. Theoretically, this type of comb device could have as long a displacement as the designer desired.

Zengerle [294] was the first to create an electrostatic actuated micropump. This first pump used a parallel plate actuator as the pumping membrane. A spacer layer in between the top electrode and the membrane provided electrical isolation to the membrane. He later improved upon the idea and created a bi-directional version [293] which used passive checkvalves designed with a specific resonant frequency. At higher frequencies the fluid moved in the

forward direction, at lower frequencies, the flow was reversed due to the phase shift between the response time of the valve and the pressure cycle. Bourouina [31] developed a device (Figure 2-10) similar to Zengerle only it used a single valve and functioning silicon channels and membrane sandwiched between two glass caps.

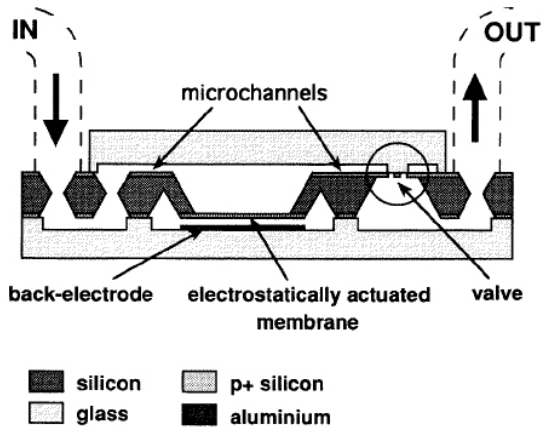

Figure 2-10: Electrostatic Pump (Bourouina, 1997)

Two different type of electrostatic actuators could both be called peristaltic pumps only they use two completely different configurations. The first presented by Judy [120] is a typical peristaltic valve like those shown in previous sections. Cabuz [38, 39] (Figure 2-11), however, uses two electrostatic membranes within a single cavity. Each membrane has holes offset from those in the other membrane. The membranes are actuated sequentially in a "zipping" like effect, which causes the holes to be covered by the adjacent membrane during inflow but uncovered during outflow.

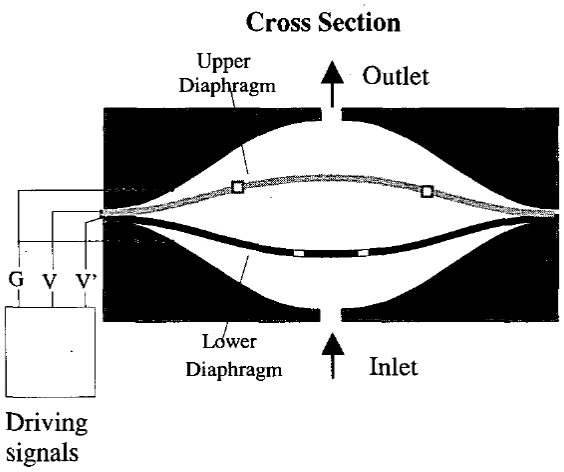

Figure 2-11: Dual Membrane Pump

2.3.6 Thermopneumatic

Thermopneumatic actuation is created by heating a fluid in a sealed chamber in order to create a volume change. The volume change equation for this type of system is given by:

$$\Delta V = V_0 \gamma_f \left(T_2 - T_1\right) \tag{2-8}$$

where V_0 is the initial volume, γ_f is the thermal expansion coefficient, and T is the temperature. Similar to this, the pressure change is:

$$P = P_o exp\left(\frac{-L_o}{RT}\right) \tag{2-9}$$

where P_0 is the initial pressure, L_0 is the molar latent heat of evaporation, and R is the universal gas constant. One of the advantages of thermopneumatic actuators is high displacement, low voltage, however, the cycle time is the limiting factor. As was shown by Elwenspoek [66], it is not only limited by the cooling temperature, it is also a function of the hydrodynamics and the thermal

conductance of the device material. Since the power consumption increases with size, the smaller the device, the better. This makes it especially suitable in the delivery of small, accurate amounts of fluid.

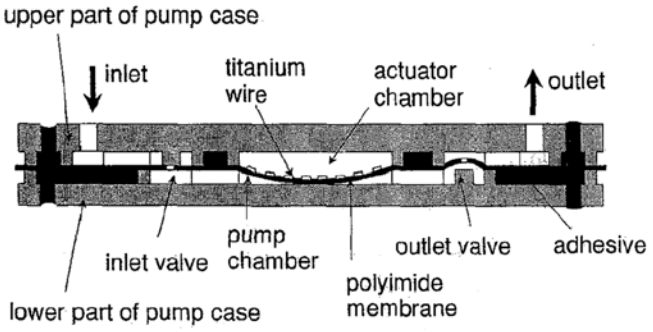

Figure 2-12: Thermopneumatic Actuator

Van De Pol [266] designed one of the first thermopneumatic pumps using silicon. Jeong [196] made a similar device using aluminum flap valves whereas Bustgens [37] (Figure 2-12) used a thermoplastic for his device. Mizoguchi [182] developed a light driven pump that uses light to heat small expandable cavities. This design could be used in applications avoiding the use of electrical devices. The other two thermopneumatic actuators designed by Folta [73] and Glosjean [95] utilize the peristaltic arrangement to produce highly accurate flows for possible use in medical devices.

2.3.7 Flexural Plate Wave (FPW)

Flexural Plate Wave pumps are also known as Flexural Planar Wave (Figure 2-13) and Ultrasonic pumps. FPWs have a membrane of silicon nitride over a large cavity etched out of silicon. Thin layers of piezo material are deposited on the silicon nitride in an interdigitated finger configuration. The piezo

transducers create acoustic planar waves along the membrane that can be used to move fluid. They also have the ability to be actuated magnetically, thus avoiding the requirement for a piezo material. These devices are excellent for creating flows in the nanoliter regime. The devices can be either uni-directional or bi-directional (Figure 2-14) depending on the arrangement of their fingers.

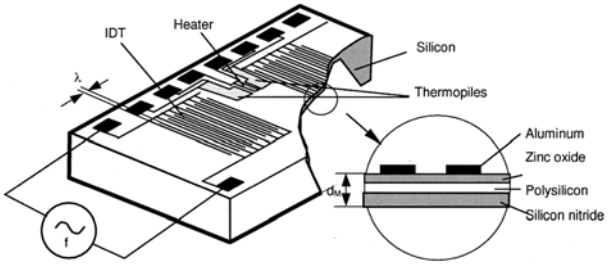

Figure 2-13: Flexural Planar Wave Device (Nguyen, 2000)

Moroney [184, 185] developed an FPW capable of moving fluids as well as granular solids. Kurusawa [136] developed an atomizer using the same principle. His desire was to use the device for hand-held nebulizers. Other devices were developed by Meng [176] and Nguyen [191, 192].

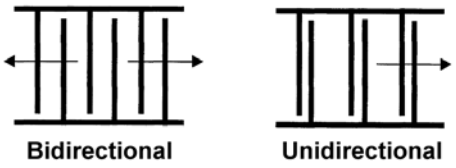

Figure 2-14: Flexural Plate Wave Finger Configuration

2.3.8 Rotary

The final type of mechanical pump that needs mentioning is the rotary design. This design in general takes macro scale or mini scale designs and shrinks them

down to the micro scale domain. A main problem associated with this is the gap spacing in the hub of the design that is required for fabrication. Critical spacing forces problems with backlash and the inherent wear of "friction" devices reduces reliability. The primary designs that has been fabricated was presented by Ahn [3] and is a rotary magnetic actuator with fully integrated coils and stator. His device was intended for conductive fluids and was successful in pumping insulin for potential drug-delivery applications.

2.4 Non-Mechanical Pumps

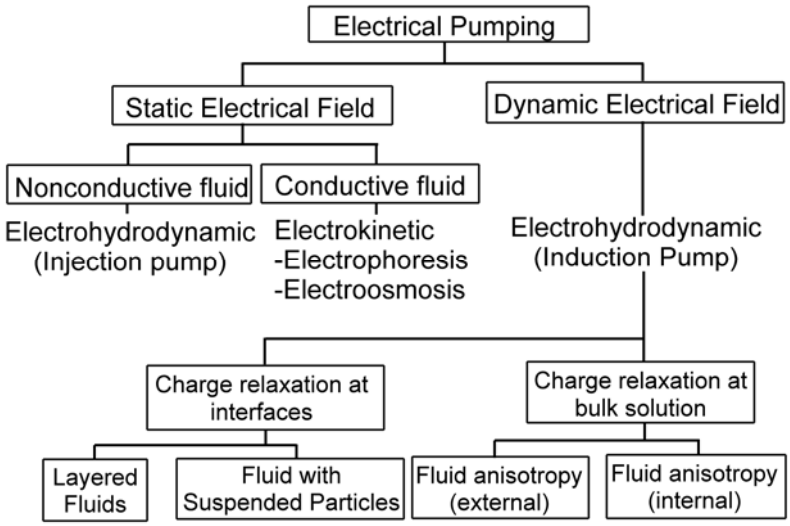

Figure 2-15: Electrical Pumping Methods [191]

Non-mechanical pumps use various methods to create fluid motion such as electrical and magnetic fields, surface tension, heat transfer, and phase changes. Since they do not usually require valves or any other moving parts they have a distinct advantage over mechanical pumps. The two most common types of non-mechanical pumps are the Electrokinetic (EK) and Electrohydrodynamic

(EHD) pumps. Although EHD pumps are typically called ion-drag pumps, the name could be applied to either. The primary difference between the two is EK pumps introduce ions into the fluid through a surface charge on the channel walls. This limits the effect of the electric field to a more localized area whereas the electric field of EHD pumps is applied to the entire pumping volume. Figure 2-15 shows a comparison between these two types of electrical pumps.

2.4.1 Electrohydrodynamic (EHD)

Electrohydrodynamic pumps (also known as ion-drag pumps) require either a free space charge in the fluid, a gradient in the electrical conductivity/permittivity gradient within a dynamic field (or traveling wave). This can be created by four different methods [79, 81]. First, for slightly conducting fluids, electro-convection can be induced at a fluid-gas or fluid-fluid interface. At this interface, there exists a charged double-layer, upon which a traveling wave can induce flow. Second, using the dielectrophoretic force on suspended particles within the fluid, it is possible to induce a flow in the fluid due to the viscous effects of the particle motion. With sufficient particle density, this "traveling wave dielectrophoresis" has the ability to move the entire fluid.

The third method of inducing motion is to create a thermal gradient (externally induced anisotropy) across a slightly conductive or electrolytic solution. This thermal gradient has the effect of changing the electrical conductivity and permittivity of the fluid which can be moved under a dynamic field by this

"electro-thermal" force. Finally, through localized heating around the electrodes, a similar gradient to the above can be generated. The effect of this method is highly dependant on the convection in the fluid which is a function of the configuration of the electrodes and the shape of the fluid channel. It can be seen that this technique becomes more useful as EHD devices become smaller.

All of these methods produce highly desired characteristics that makes the EHD pump popular for bio-transport, thermal cooling, and mixing applications. They require little power but produce large flow at low pressures. Even though they require a high voltage which can cause impurity collection at the electrodes and convection problems (depending on the size of the system…for small channels, the Peclet number is very small, since heat diffusion dominates heat convection), much of this can be eliminated using AC fields. Their main advantage lies in their simplicity and low cost.

Now, the governing equation [215] of force for an EHD pump is:

$$\boldsymbol{F} = q\boldsymbol{E} + \boldsymbol{P}\cdot\nabla\boldsymbol{E} - \frac{1}{2}\boldsymbol{E}^2\nabla\boldsymbol{\varepsilon} + \nabla\left[\frac{1}{2}\rho\frac{\delta\varepsilon}{\delta\rho}\boldsymbol{E}^2\right] \qquad (2\text{-}10)$$

where q_f is the free space charge density, E is the electric field, P is the polarization vector, ε is the permittivity, and ρ is the mass density of the fluid. The four components on the right hand side of the equation are:

1. Coulomb force on the free space charge
2. Kelvin polarization (dielectrophoretic) force
3. Dielectric (Korteweg-Helmholtz) force
4. Electrostrictive force

While the second term is generally small and doesn't have constant fluid motion in DC fields, dielectrophoresis is used frequently as a method to separate particle suspensions within the fluid. When an electrically neutral particle is placed in a spatially inhomogeneous electric field, charge polarization is induced at the interface between the particle and the surrounding medium. As seen in Figure 2-16, the field density is much larger on one side than the other which will draw the particle in that direction. If the field is reversed then the polarity of the charges will be reversed but the dielectrophoretic force will still be in the same direction. Particles with different material properties (permittivity and conductivity) can be separated using dielectrophoresis due to differences in the polarization induced in the particles by the inhomogeneous field [61].

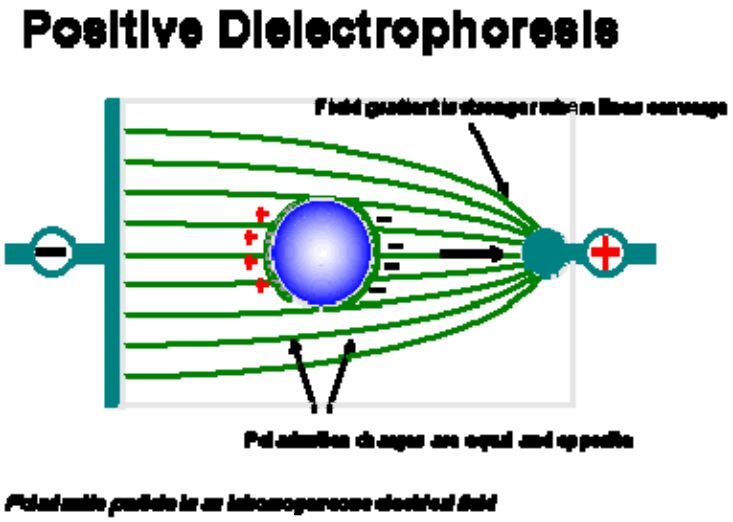

Figure 2-16: Dielectrophoretic Force Schematic [61]

Bart [17] was the first to design an EHD induction pump where he used a thermal gradient to pump highly insulating silicone oil (Figure 2-17).

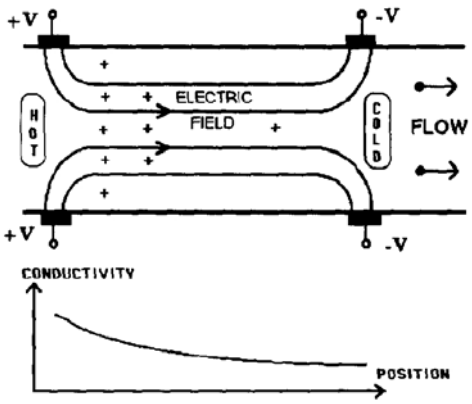

Figure 2-17: Heat Induced pump [17]

Both Darabi [54] and Seong [226] used similar methods the exception being localized heating in Seong's work. Fuhr [77, 78] also developed an induction pump which expanded the pumping materials to conductive liquids as well (Figure 2-18). Richter [214] and Ahn [3] both developed an EHD injection pump that used a dc field to induce coulomb forces on the particles.

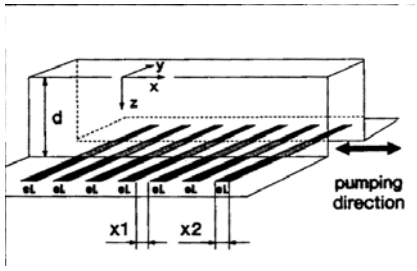

Figure 2-18: Traveling Wave Pump [76]

2.4.2 Electrokinetic (EK) and Electroosmotic (EO)

Electrokinetic pumps [45] are very useful for biological and chemical applications. They have the ability to transport aqueous solutions and not only have relatively high flows but can achieve high pressures as well. A couple of

unique attributes for EK pumps are the planar flow profile as well as the pulse-less pumping.

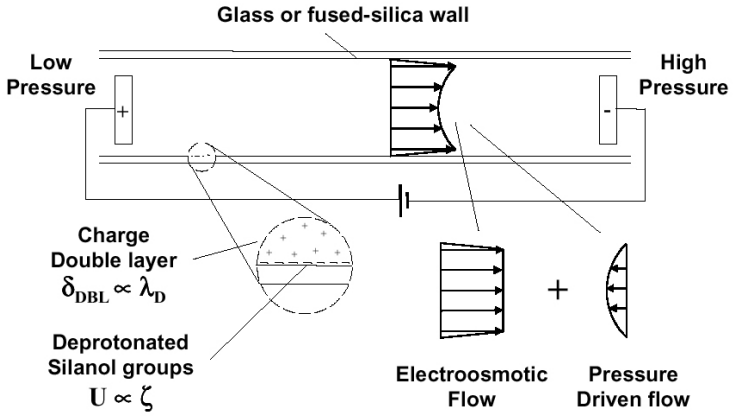

Figure 2-19: Electroosmotic flow [42]

EK pumps work through the use of electrolytic solutions which are comprised of both a buffer solution (which has nearly equal amounts of oppositely charged ions) and individual charged particles. The first of two types of actions that can occur under an induced electric field is called electro-osmosis. Oppositely charged fluid ions are drawn to the charged wall and create a electric double layer. This double layer is composed of immobile ions oppositely charged to that of the wall and another set of dispersed mobile ions of with the same charge. In an electric field the overall bulk concentration of dispersed ions is propelled through the tube and with it the rest of the fluid due to viscous forces. The flow builds until the velocity gradient reaches almost zero creating a flat or plug velocity profile.

The second type of pumping method is known as electrophoresis which moves the suspended charged particles separately from the surrounding fluid. Just as the wall developed a charged double layer, so do the individual particle (which are much larger than the double layer). The electric force caused by this charged layer create an electric force but that force is counteracted by a viscous drag force. In order to separate the particles, then, requires a determination of the desired electrophoretic and electroosmotic forces based on the buffer solution (pH), particle properties and wall coatings.

The type of EK pump mentioned above has been developed by Manz [168] and Harrison [103] who used an open channel. Zeng [237] used a pressure driven slurry packing method to fill the fluid column with silica particles. These particles increased the double layer surface area which created a much larger effect on the fluid. Mutlu [189] used a porous plug between the two electrodes which increased the surface area and minimized the corrosion and bubble creation at the electrodes. Another way to eliminate the reaction at the electrodes is to pulse the signal or keep voltages low. Two other issues common to EK pumps are the susceptibility to counter flows driven by hydrostatic pressure and the streaming/seditation potential that is created from the cross flow in the channel.

2.4.3 Magnetohydrodynamic (MHD)

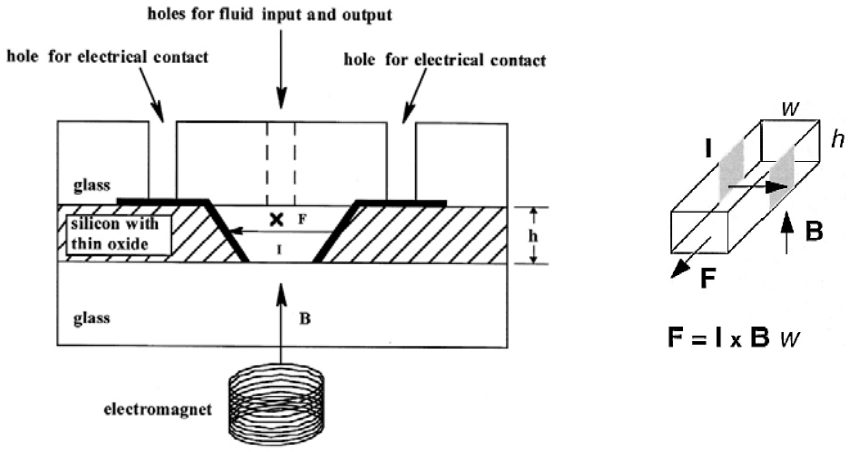

Figure 2-20: Magnetohydrodynamic pump (Lemoff)

Magnetohydrodynamic pumps exerts a force on either electrolytic solutions or ferro-fluids using a magnetic field. Lemoff [140] introduced a MHD pump that used Lorentz forces to direct an electrolytic flow within a silicon channel. As is seen in Figure 2-20, the force is equal to the cross product of electric current across the pump channel (I) times the magnetic flux density (B) and the width of the channel.

Two pumps designed for use with magnetic fluids (for instance, mercury) were Ozaki and Hatch. Ozaki [203] developed a linear pump the drives fluid through magnetized body forces as well as the particle vorticity created by the rotating magnetic field. Hatch [104] on the other hand used a ferro-fluidic plug within a circular channel. In this instance the ferro-fluid was only used as a means to "push" another fluid through the channel.

While the MHD pumps can create large forces as a function of the magnetic power, it requires specific fluids to work. If an aqueous solution is used then the current needs to be alternating to eliminate electrolysis, flow reducing bubbles, and electrode degradation. Ferro-fluids also require special handling and the overall magnetic actuator is generally bulky and difficult to integrate.

2.4.4 Phase-Transfer/Bubble-Based pumps

While somewhat different, phase-transfer and bubble-based pumps use very similar methods of pumping. Phase-Transfer pumps cyclically create vapor and liquid phases throughout sections of a capillary (Figure 2-21). Applying heat to the fluid produces, not only liquid to vapor

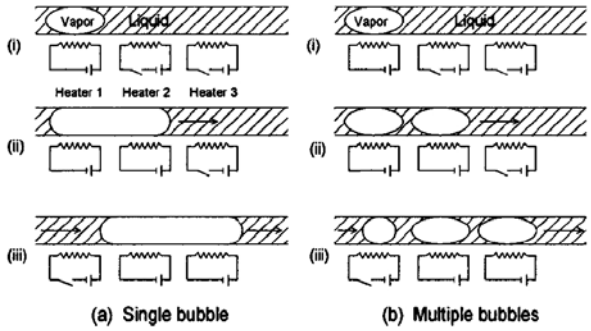

Figure 2-21: Phase Transfer Pump

transformation, but an increase in kinematic viscosity (and decrease in viscous resistance) as well. The pressure drop between one phase and the next can be found using:

$$\Delta P_n = -\frac{8\dot{m}L\nu}{\pi r_i^4} \tag{2-11}$$

Where m is the mass flowrate, L is the length of each area, ν is the kinematic viscosity, and r_i is the inner diameter of the channel. The continuity equation for the flow is:

$$\dot{m}_2 - \dot{m}_1 = AU\left(\rho_2 - \rho_1\right) \cong AU\rho_L \tag{2-12}$$

A is the cross sectional area, ρ_L is the density of the liquid phase, and U is the fluid velocity. Three different versions of this type of pump were designed by Jun [121], Ozaki [203], and Takagi [257].

Bubble pumps [58, 292] use one of two methods to create fluid flow. The first method is through the use of the Marangoni effect. The Marangoni (or thermocapillary) effect is caused when the surface tension of a fluid is changed due to a change in the temperature. If a bubble is located in a channel where one end of the capillary is hotter than the other then there will be a temperature gradient across the bubble. On the hot side of the bubble the surface tension will be lower which causes a pressure gradient that moves the bubble to the hotter end of the capillary. Two thermocapillary designs were designed by Takahashi [258] and Liepmann [146].

The other type of pump was developed by Geng [284] who created a device that uses a variance in channel curvature to move an electrically conductive liquid (although he suggests another method of pumping other fluids as well). As is shown in Figure 2-22,

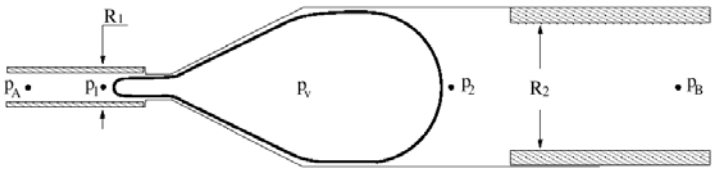

Figure 2-22: Geng's Bubble Pump

the pumping effect is caused by a variance in the curvature between different parts of bubble interface. After joule heating creates a vapor bubble at the channel joint, the surface tension generates a pressure differential between the inner part of the bubble and the surrounding liquid. Since this pressure will drive the bubble to conform to the shape of the channel, it will naturally flow from the smaller channel to larger channel. If operated continuously, flow will be created according to the relation:

$$\bar{p}_1 - \bar{p}_2 = -2\sigma\left(\frac{1}{R_1} - \frac{1}{R_2}\right)\frac{\tau + \Delta t}{T} \tag{2-13}$$

where σ is the surface tension coefficient, p is the pressure, R is the radius, τ is the duration of applied voltage, Δt is the difference between the bubble lifetime and τ, and T is the repetition time.

2.4.5 Continuous Electrowetting

Another type of pump mechanism that is similar to a thermocapillary pump is the Continuous Electrowetting (CEW) pump. The difference is instead of the surface tension being changed by a temperature gradient, it is changed using an electric field. The reason this works is because of its use of mercury as a fluid. The surface tension creates a

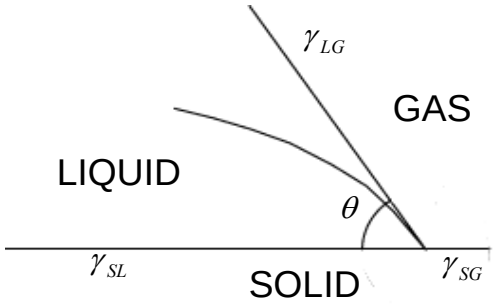

Figure 2-23: Surface Tension Diagram

pressure change between liquid, solid, and gas characterized by the equation:

$$\Delta P = \frac{2(\gamma_{SG} - \gamma_{SL})}{a} = \frac{2\gamma_L cos\theta}{a} \tag{2-14}$$

and

$$\gamma_{SL} + \gamma_{LG} cos\theta = \gamma_{SG} \tag{2-15}$$

where γ is the interface surface tension, a is the capillary radius, and θ is the liquid-solid contact angle. Colgate [51] showed that if an electric field is applied across the channel the surface tension would become:

$$\gamma_{SL} = \gamma_{SL}^{\max} - \frac{\varepsilon_r \varepsilon_o}{2\delta}\left(V - V^{zc}\right)^2 \tag{2-16}$$

Lee [122] developed a CEW pump that performed with low voltage and current, high speed, and could be designed in variety of configurations. Yun [137, 138] used the CEW process to actuate diaphragms in a hybrid non-mechanical actuated mechanical displacement pump.

2.5 Gas Phase Pumping and the Knudsen pump

Figure 2-24 shows the gas phase pump performance of existing pump designs. The maximum pressure drop achieved by the pump is shown on the x-axis and

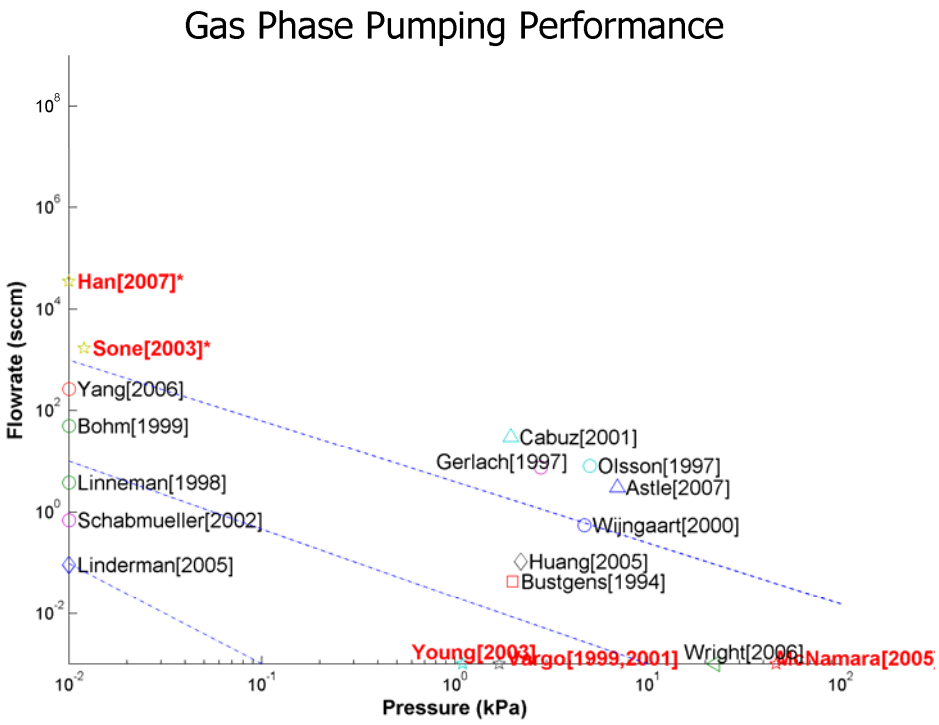

Figure 2-24: Gas Phase Pump Performance

the maximum flowrate reported is shown on the y-axis. Lines representing constant $Q_{max}*P_{max}$ are shown as dashed lines. Markers lying on the x or y axes represent pumps where only flowrate or pressure was listed in their literature. Some of these pumps have already been discussed above like the dual membrane pump of Cabuz or the electrostatic pump of Gerlach. Of those not mentioned, the pumps by Yang and Schabmueller are piezoelectric pumps. Schabmueller's design is typical of most piezoelectric diffusion pumps, however Yang uses a bi-morph to create the highest reported flowrates among the gas

pumps. Huang's design is a peristaltic pneumatic pump utilizes a PDMS layer between the actuation cavities and the working cavity. Wright obtains the largest pressure drop among non-Knudsen pumps using a titanium ion getter. The flowrate is unclear and is based upon the reaction of the titanium with the nitrogen and oxygen. Astle uses a bi-directional electrostatic pump that moves a membrane vertically between two electrodes. His performance as a function of both flowrate and pressure is the best among electrostatic devices.

The pumps featured using red text identify the Knudsen pumps which are of key importance to this dissertation . Since Vargo and Young did not report flowrate performance along with pressure it is important for this dissertation to give performance data in the context of gas phase pumps. Sone's pump was referenced in 1.3.3 where he provided both maximum pressure and flowrate data. In Chapter 7 we show how the performance of a Knudsen pump based on our simulation results fits in this plot which should allow the designer sufficient information to utilize the Knudsen pump mechanism.

CHAPTER 3 COLLISIONLESS FLOWS AND MAXWELL'S DISTRIBUTION

3.1 Introduction

As we determined in section 1.3.2, the first problem we need to solve relates to the collisionless flow of molecules through tubes. This chapter begins with a look at how the number density affects molecular impacts on a particular area (namely the entrance to a channel). This method is then extended to a two way flow through an ideal orifice in what is termed effusion. Next, Knudsen's equation for long tube flow is derived followed by modifications of von Smoluchowski, Clausing, and others.

3.2 Fundamental Assumptions

It is of key importance to begin with some fundamental assumptions regarding kinetic gas theory and its relation to collisionless flows. First, it is assumed any gas is comprised of a set of molecules and, if the gas is pure, these molecules are all alike. Second, it is assumed that the molecules move about in all directions. Since they are not considered infinitely small, they are capable of colliding with one another. Finally, it is assumed that the only pressure occurring in the gas is the one created by the motion of the molecules when in an ideal state.

The density of a gas is defined as:

$$\rho = N \cdot m \tag{3-1}$$

where N is the number of molecules in each cm^3 (number density) and m is the mass of each molecule which in pure gas is the same for every molecule.

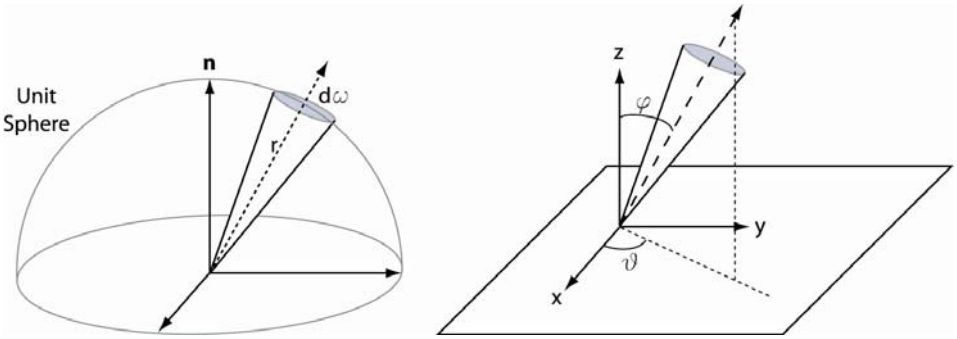

Figure 3-1: a) Diagram of Solid Angle b) Solid Angle in Spherical Coordinates

If a gas is in thermal and mechanical equilibrium, then the velocities of the molecules are varied, however, the direction of all the molecules having a particular velocity must be distributed equally in all directions. Now N_c is defined as the number of molecules having a particular velocity in the range c through c + dc. Within a solid angle, dω, the number of molecules within a certain velocity range is given by:

$$\frac{d\omega}{4\pi} N_c \tag{3-2}$$

where

$$d\omega = \iint_S \sin\phi \cdot d\vartheta \cdot d\phi \tag{3-3}$$

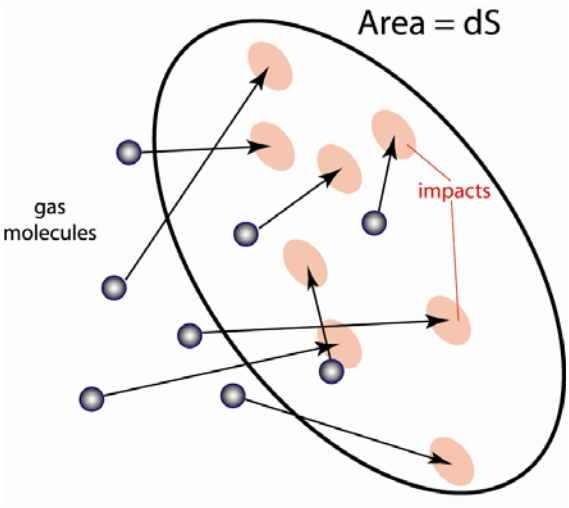

Figure 3-2: Pressure Induced by Molecular Impacts

Within a particular time, *dt*, the number of molecules in that solid angle hitting an area, *dS*, is equal to:

$$n_{c,x} = \frac{1}{2} N_c c(\cos\phi)(\sin\phi)\mathrm{d}\phi \cdot \mathrm{d}S \cdot \mathrm{d}t \tag{3-4}$$

If c is the arithmetical mean of the velocity, then after integrating φ between 0 and $\pi/2$, the number of impacts occurring each second on each cm^2 of the surface of a gas is equal to:

$$n = \frac{1}{4} N \cdot \bar{c} \tag{3-5}$$

The pressure is derived by multiplying the number of molecules by their momentum to yield:

$$n_{c,\phi} = \frac{1}{2} N_c m c^2 (\cos^2\phi)(\sin\phi)\mathrm{d}\phi \tag{3-6}$$

Since it is assumed all the molecules reflect off the surface, then integration gives the pressure on the surface as:

$$P = \frac{1}{3} Nm\overline{c^2} \tag{3-7}$$

Combining (3-7) and (3-1) produces:

$$\overline{c^2} = \frac{3}{\rho_1} \tag{3-8}$$

where, at constant temperature and P=1 dyne/cm^2:

$$\rho_1 = \frac{\rho}{P} \tag{3-9}$$

Using the universal gas constant, equation (3-8) is rewritten as:

$$\overline{c^2} = \frac{3R_o T}{M} \tag{3-10}$$

According to Maxwell's law of the distribution of velocities [164], equation (3-10) can be rewritten as:

$$\frac{1}{3}\overline{c^2} = \frac{\pi}{8}\left(\bar{c}\right)^2 \tag{3-11}$$

Which from (3-7) would also make the pressure equal to:

$$p = \frac{\pi}{8} Nm\bar{c}^2 \tag{3-12}$$

Therefore, if

$$G = nm = \frac{1}{4} Nm\bar{c} \tag{3-13}$$

then substituting (3-10) and (3-11) into (3-13) yields the equation for the mass flow hitting a unit surface during a unit time.

$$G = \frac{1}{\sqrt{2\pi}}\sqrt{\rho_1} \cdot P = \frac{P}{\sqrt{2\pi R}}\sqrt{\frac{M}{T}} \tag{3-14}$$

3.3 Molecular Effusion

Now this equation is applied to the problem of molecular effusion. Assume two chambers at different pressures are separated by an ideally thin membrane (Figure 3-3). A single aperture is located in the center of the membrane with area A.

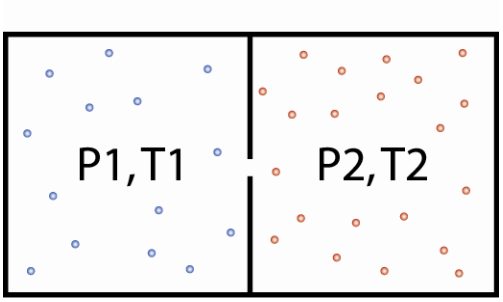

Figure 3-3: Molecular Effusion

From equation (3-14), the mass flow [132] through the aperture is:

$$G \cdot A = \frac{1}{\sqrt{2\pi}} \sqrt{\rho_1} \left(P_2 - P_1\right) A = \frac{\left(P_2 - P_1\right) A}{\sqrt{2\pi R}} \sqrt{\frac{M}{T}} \tag{3-15}$$

where $T=T_1=T_2$. If Q is equal to the volume of gas flowing through the aperture at 1 dyne/cm^2, then:

$$Q = \frac{G \cdot A}{\rho_1} \tag{3-16}$$

since GA is the product of the volume and pressure. Now we define the conductance

$$U = \frac{Q}{P_2 - P_1} \tag{3-17}$$

and combine this with equations (3-15) and (3-16) to get:

$$U = \frac{1}{\sqrt{2\pi}} \frac{1}{\rho} A \tag{3-18}$$

It was shown experimentally by Knudsen that the conductance "decreased with decreasing pressures to a specific asymptotic value" as would be expected from Poiseuille's law. In regimes where the diameter of the aperture was much smaller than the mean free path of the gas, he found the conductance to be proportional to the mass of the gas, inversely proportional to the square root of the temperature, and completely independent of the pressure. This phenomenon he termed molecular effusion.

This equation can be used to determine the gas flow between the two reservoirs with the following assumption. If ρ_1 is replaced in equation (3-15) by:

$$\rho_1 = \frac{\rho_0 \cdot 273}{T_1} = \frac{M}{R_o T} \tag{3-19}$$

where ρ_0 is the specific gravity at 273° and 1 dyne/cm^2, then the mass of gas flowing from a reservoir to a vacuum per unit time is:

$$G_1 = \frac{1}{\sqrt{2\pi}} \sqrt{\frac{M}{R_o T_1}} A \cdot P_1 \tag{3-20}$$

To determine the mass flow of a two reservoir system at different temperatures and pressures yields:

$$G_1 - G_2 = \frac{A}{\sqrt{2\pi}} \sqrt{\frac{M}{R_o}} \left(\frac{P_1}{\sqrt{T_1}} - \frac{P_2}{\sqrt{T_2}} \right) \tag{3-21}$$

Even if the pressures in the system are equal there would still be a change of mass due to the temperature difference. In a closed system, the system would eventually

reach an equilibrium where $G_1=G_2$. The relation between the temperature and pressure would then become:

$$\frac{P_1}{\sqrt{T_1}} - \frac{P_2}{\sqrt{T_2}} = 0 \quad \text{or} \quad \frac{P_1}{P_2} = \sqrt{\frac{T_1}{T_2}} \tag{3-22}$$

3.4 Cosine Law

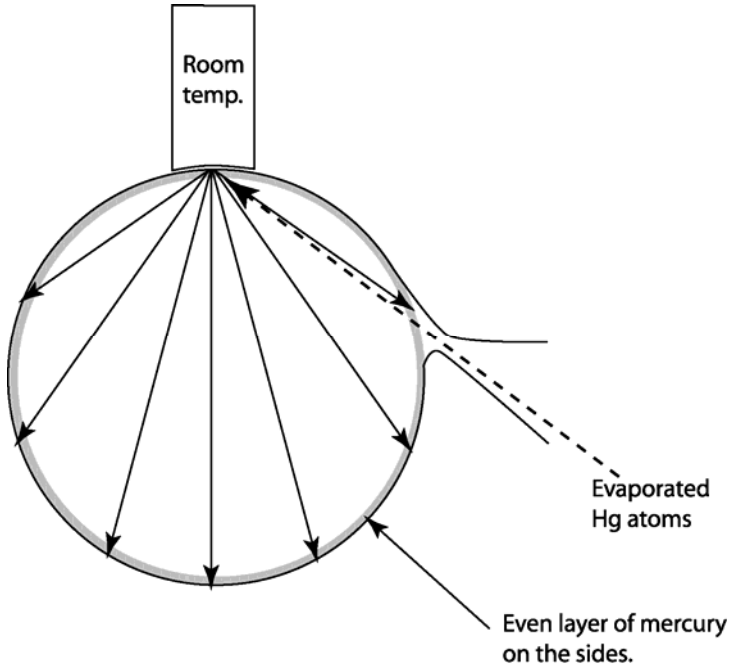

Figure 3-4: Knudsen's Cosine Law Experiment

Before the flow theory mentioned above can be extended to flow through tubes, an important law must be described called the cosine law. Martin Knudsen [128] was the first to introduce the cosine law of diffuse scattering which describes the impingement and scattering of molecules off tube walls or surfaces. The cosine law

states, under free molecular conditions, the direction of an individual molecular reflection off of a surface is independent of the impinging direction and is thus diffusely scattered. In other words, the incidence angle and reflection angle are independent of each other. This is in contrast with specularly reflected molecules whose impingement and reflected angle with the surface are the same. This theory is equivalent to Lambert's law on optical and thermal radiation.

To prove his theory, Knudsen devised an ingenious experiment (Figure 3-4), where he took a glass sphere attached to two tubes (one inside the other) whose separation was filled with mercury. The top of the sphere was kept at room temperature while the rest of the sphere was cooled. As molecules evaporated some of them would enter the sphere and impinge on the room temperature portion of the sphere. They would then reflect in all directions equally creating a uniformly condensed layer of

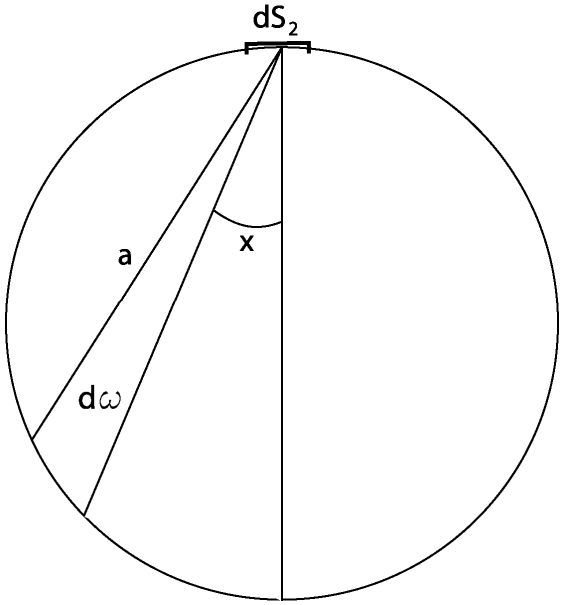

Figure 3-5: The Cosine Law

mercury through out the sphere.

To understand why this works consider the sphere with radius R and an area at its top, dS_1 (Figure 3-5). The number of molecules, dn, that leave dS_1 in a solid angle, $d\omega$ is given by:

$$\mathrm{d}n = \frac{1}{\pi} n \cdot \cos(x) \mathrm{d}\omega \tag{3-23}$$

Where x is the angle between a bisection of the sphere and the solid angle. If the area on the surface of the sphere cutout by the solid angle is dS_2 then using:

$$\iint_S \frac{\underline{n} \cdot \mathrm{d}\underline{A}}{r^2} \tag{3-24}$$

yields:

$$\mathrm{d}\omega = \frac{\mathrm{d}S_2 \cdot \cos(x)}{a^2} \tag{3-25}$$

Inserting (3-25) into (3-23):

$$\mathrm{d}n = \frac{n \cdot \cos^2(x) \cdot dS_2}{\pi \cdot a^2} \tag{3-26}$$

where

$$a = 2R \cdot \cos(x) \tag{3-27}$$

Thus

$$\mathrm{d}n = \frac{n \cdot dS_2}{4\pi R^2} \tag{3-28}$$

Thus the total number of molecules hitting a unit area of the sphere is:

$$\frac{\mathrm{d}n}{\mathrm{d}S_2} = \frac{n}{4\pi R^2} \tag{3-29}$$

Which is independent of which section of the sphere dS_2 comprises.

By applying this formula to gas scattering in a molecular flow, the following assumptions must be considered:

1. There is no absorption of the gas onto the walls.
2. There aren't any delayed effects of molecules "residing" at a surface for a period of time as described by Clausing.
3. There is no surface species diffusion
4. There aren't any chemical reactions at the walls, disassociation of polymers, etc.
5. Other Knudsen geometric effects on the molecular level are negligible.
6. The pressures of the gas are low enough so there is no velocity gradient normal to the walls. This is also true when the dimensions of the channels are small compared to the mean free path of the gas.

It is also important to mention that Knudsen's cosine law is different than the 'equilibrium cosine scattering law' which is a consequence of the 2nd law of thermodynamics. Knudsen's cosine law is only describing the diffuse reflection of individual molecules and does not incorporate the specularly reflected molecules nor the effects temperature and accommodation have on the molecules. Rather the diffuse reflection specifically deals with the post-collision direction and velocity, the latter which will have a distribution according to Maxwell's law. This does not invalidate it for use in free molecular gas flow in tubes since the molecules are not necessarily at temperature equilibrium with the surface. For those cases where the

reflection of molecules is specular, Berman and Maegley [22] proposed a modification to the law saying the molecules that are diffusely reflected comprise a portion α while the number of specularly reflected molecules are $1-\alpha$. The constant is a function of the gas type, wall material, and surface conditions of the tube.

Several authors have since studied the molecule wall interaction [113]. Shin [234], Wachman [272], Goodman [92] and Demirel [59] all described the thermal accommodation and the accommodation along with the effect of surface roughness on the energy transfer. Frederking [74], Malek [166, 167] and Murphy [188] both developed models for the effect of surface/pore roughness on the flow through tubes. It has been shown that the rougher the surface, the more the energy transfer since the molecules tend to strike the surface more than one time. Other literature [71, 112, 143, 161, 217] has described the momentum accommodation and the effect specular reflections [60] has on the flow. Albo outlined studied the effect of residence times to the surface Recent experiments [111] have shown that for very smooth walls, the flow of a gas through a channel can increase greatly even in very small pores.

3.5 Flow of Gas Through Tubes

From equation (3-5), Knudsen [127, 130] showed the number of molecules striking a cm^2 of surface per second is known. From Maxwell's distribution (3-11), as was discussed before (3.2), the number of molecules with velocities between c and $c+dc$ is:

$$N_c = \frac{4N}{\alpha^3\sqrt{\pi}} c^2 e^{\left(-\frac{c^2}{\alpha^2}\right)} \mathrm{d}c \tag{3-30}$$

where α is the most probable speed. The number of molecules with each velocity which strike a unit area per second is:

$$n = \frac{1}{4} c \mathrm{d}N_c \tag{3-31}$$

As these molecules pass through a tube they strike the wall with a longitudinal velocity, ω, which imparts a momentum to the wall. It is assumed the molecules reflect diffusely (i.e. they reside long enough on the surface to lose their history and transfer all their momentum to the wall). Thus the momentum applied to the wall by the N_c molecules is equal to:

$$nm\omega = \frac{1}{4} cm\omega N_c \tag{3-32}$$

c and ω can be related by a proportionality constant, k, to yield:

$$\frac{1}{4} kc^2 mN_c \tag{3-33}$$

By combining equations (3-30) and (3-33), the momentum sum applied to the wall for all velocities is:

$$B = \frac{1}{4} Nk \frac{4}{\sqrt{\pi}} m \int_0^\infty \frac{c^4}{\alpha^3} e^{\left(-\frac{c^2}{\alpha^2}\right)} \mathrm{d}c \tag{3-34}$$

Simplifying

$$B = \frac{3}{8} Nkm\alpha^2 \tag{3-35}$$

The value α is now be replaced by:

$$\alpha = \frac{\bar{c}\sqrt{\pi}}{2} \tag{3-36}$$

to give:

$$B = \frac{3\pi}{32} Nkm\bar{c}^2 \tag{3-37}$$

If the flow is in the molecular regime (with no collisions between molecules) the velocity gradient normal to the tube walls is assumed to be zero. Therefore the bulk velocity, *v*, of the gas flow is defined as:

$$v = \frac{\sum \omega}{N} = \frac{\sum kc}{N} = \frac{\sum w}{N} = k\bar{c} \tag{3-38}$$

Substituting (3-38) into (3-37) gives the bulk momentum as:

$$B = \frac{3\pi}{32} Nm\bar{c}v \tag{3-39}$$

Substituting (3-1). in for *Nm* gives:

$$B = \frac{3\pi}{32} \rho \cdot \bar{c}v \tag{3-40}$$

Knudsen applied this momentum to a differential length of a cylindrical tube defined, *dl*, with a cross-section, A and circumference, *O*:

$$B = \frac{3\pi}{32} Nm\bar{c}vO\mathrm{d}l\mathrm{d}t \tag{3-41}$$

Combining this with (41) results in:

$$B = \frac{3}{8}\sqrt{\frac{\pi}{2}}\rho\sqrt{\frac{p}{\rho}}vO\mathrm{d}l\mathrm{d}t \tag{3-42}$$

which when combined with (3-9) is:

$$B = \frac{3}{8}\sqrt{\frac{\pi}{2}}\rho\sqrt{\frac{1}{\rho_1}}vO\mathrm{d}l\mathrm{d}t \tag{3-43}$$

For molecular flow with the following conditions

1. There is no temperature jump
2. dl is sufficiently small
3. The tube is long enough so that end effects are negligible

it can be assumed the entire momentum is caused by the pressure difference between the two ends of dl. Thus for dt=1 sec.:

$$\frac{3}{8}\sqrt{\frac{\pi}{2}}\rho\sqrt{\frac{1}{\rho_1}}vO = -A\frac{\mathrm{d}p}{\mathrm{d}l} \tag{3-44}$$

To find the mass flow through dl, we use the equation:

$$G = Av\rho = -\frac{8}{3}\sqrt{\frac{2\rho_1}{\pi}}\frac{A^2}{O}\frac{\mathrm{d}p}{\mathrm{d}l} \tag{3-45}$$

Integrating (3-45) the whole length of the tube gives:

$$G\int_0^L \frac{O}{A^2}dl = -\frac{8}{3}\sqrt{\frac{2\rho_1}{\pi}}\mathrm{d}p \tag{3-46}$$

so that:

$$G = \frac{4}{3}\sqrt{2\pi\rho_1}\frac{R^3}{L}\left(p_1 - p_2\right) \tag{3-47}$$

Substituting for ρ_1 gives the mass flux for a long cylindrical tube:

$$\boxed{G = \frac{4}{3}\sqrt{2\pi}\sqrt{\frac{M}{R_o}}\frac{R^3}{L}\left(\frac{p_1}{\sqrt{T_1}} - \frac{p_2}{\sqrt{T_2}}\right)} \tag{3-48}$$

In the case where the tube is short enough so that end effects must be considered then (3-44) becomes:

$$\frac{3}{8}\sqrt{\frac{\pi}{2}}\rho\sqrt{\frac{1}{\rho_1}}vO = -A\frac{\mathrm{d}p}{\mathrm{d}l} - v\rho\frac{\mathrm{d}v}{\mathrm{d}l} \tag{3-49}$$

where the last term is from the kinetic energy of the gas leaving the tube. Once again, using the first expression in (3-45) with (3-49):

$$\frac{3}{8}\sqrt{\frac{\pi}{2}}\sqrt{\frac{1}{\rho_1}}\frac{O}{A^2}G = -\frac{\mathrm{d}p}{\mathrm{d}l} - \frac{G^2}{A^2\rho_1}\frac{\mathrm{d}}{\mathrm{d}l}\left(\frac{1}{p}\right) \tag{3-50}$$

and integrating over the length of the tube:

$$\frac{3}{8}\sqrt{\frac{\pi}{2}}\sqrt{\frac{1}{\rho_1}}G\int_0^L\frac{O}{A^2}\mathrm{d}l = \left(p_1 - p_2\right) - \frac{G^2}{A^2\rho_1}\left(\frac{p_1 - p_2}{p_1 p_2}\right) \tag{3-51}$$

For simplification, let

$$Z = \frac{3}{8}\sqrt{\frac{\pi}{2}}\int_0^L\frac{O}{A^2}\mathrm{d}l \tag{3-52}$$

so that (3-51) becomes

$$\boxed{G = \left(p_1 - p_2\right)\frac{\sqrt{\rho_1}}{Z}\frac{1}{1 + \dfrac{G\left(p_1 - p_2\right)}{A^2 Z\sqrt{\rho_1}\left(p_1 p_2\right)}}} \tag{3-53}$$

For cases where the end effects are negligible, the term on the right hand side of the denominator is much less than one, which after integrating W, reduces to (3-47). Looking at just this term:

$$U = \frac{1}{A^2 Z^2}\frac{\left(p_1 - p_2\right)^2}{p_1 p_2} \tag{3-54}$$

Integrating this yields

$$U = \frac{32}{9\pi}\frac{R^2}{L^2}\frac{(p_1 - p_2)^2}{p_1 p_2} \tag{3-55}$$

It is of note that this term is dependant on *R/L* so that the longer the tube with respect to the radius, the less the end effects have on the mass flow even when the pressure difference is great. To determine the volumetric flow rate of a long tube, divide (3-47) by ρ_1 to give:

$$Q = \frac{4}{3}\sqrt{\frac{2\pi}{\rho_1}}\frac{R^3}{L}(p_1 - p_2) \tag{3-56}$$

Finally, substitute (3-19) into (3-56) and assume a temperature difference across the tube length to give Knudsen's thermal transpiration equation for tubes:

$$\boxed{Q = \frac{4}{3}\sqrt{2\pi}\frac{R^3}{L}\sqrt{\frac{R_o T}{M}}(p_1 - p_2)} \tag{3-57}$$

Note that this equation is an approximate solution that assumes the temperature in the tube is uniform throughout the tube.

3.6 V. Smoluchowski

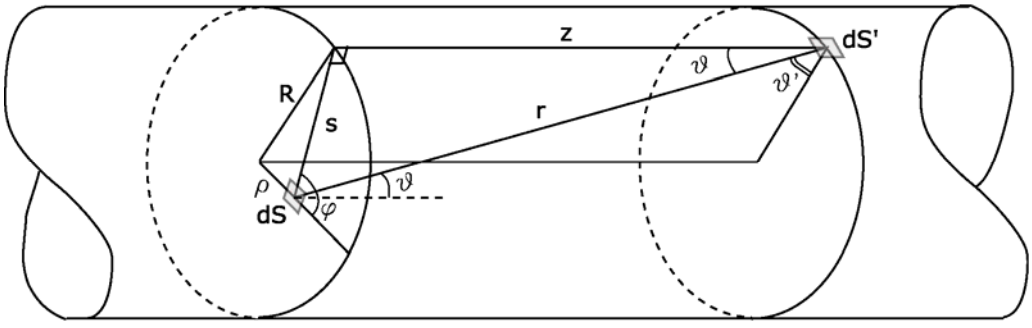

Figure 3-6: Coordinate System of Free Molecular Tube Flow

Although Knudsen thought his equation was valid for all flows and channel cross-section shapes, von Smoluchowski (from here identified as VS) [129, 250-252] revealed some errors in Knudsen's derivation. In reality, Knudsen's solution was only valid for circular cross-sections and long channels. VS derived an expression for molecular flow that was valid for flows through tubes with any cross-section. The following paragraphs summarize this work in order to show the highlights of the derivation.

Knowing that the flow is calculated from the net molecular transport through the tube, an expression is derived for flow through an element of cross-section, *dS*, and then integrated over the entire tube length (Figure 3-6). The flow through *dS* is found by determining the number of molecules that reflect off the sidewall and pass in a straight line through the elemental area. Combining equations (22) and (5) give the number of molecules that reflect off a unit surface area, *dS'*, in 1 second at a particular angle, θ:

$$N\bar{v}\cos(\theta)\frac{\mathrm{d}\omega}{4\pi} \tag{3-58}$$

where N_d is the number density. The number of molecules that pass from *dS'* to *dS* per unit time is:

$$\mathrm{d}^2G = \frac{N\bar{v}\mathrm{d}S'\cos(\theta')\mathrm{d}\omega}{4\pi} \tag{3-59}$$

If a line of length r connects the centers of *dS* and *dS'*, the angles to the two normals are θ and θ'. The solid angle, $d\omega$, is found in the same way as (3-25) so that:

$$\mathrm{d}\omega = \frac{\mathrm{d}S \cdot \cos\theta}{r^2} \tag{3-60}$$

Equation (3-59) then becomes:

$$\begin{aligned} \mathrm{d}^2 G &= \frac{N\bar{v}}{4\pi} \frac{\mathrm{d}S' \cos\theta' \cos\theta}{r^2} \\ &= \frac{N\bar{v}\mathrm{d}S}{4\pi} \cos\theta \sin\theta \cdot \mathrm{d}\theta \cdot \mathrm{d}\phi \end{aligned} \tag{3-61}$$

Since the number density is an unknown function of *z*, it is assumed a small variation of density along the tube and used a Taylor series expansion around *dS'*:

$$N(z) = N(0) + z\left(\frac{\mathrm{d}N}{\mathrm{d}z}\right) + \frac{z^2}{2}\left(\frac{\mathrm{d}^2 N}{\mathrm{d}z^2}\right) + \ldots \tag{3-62}$$

Now the net flow of molecules that pass through *dS* is found by adding the molecules that pass through it from both sides of the tube. Integrating (3-61) throughout the entire range of solid angles the net flow is found to be:

$$\mathrm{d}G = \mathrm{d}G_+ - \mathrm{d}G_- = -\frac{\bar{v}dS}{4\pi} \int_0^{2\pi} \mathrm{d}\phi \int_0^{2\pi} N(z) \cdot \cos\theta \cdot \sin\theta \cdot \mathrm{d}\theta \tag{3-63}$$

Substituting (3-62) into (3-63) and knowing that:

$$r \cdot \cos\theta = s \cdot \cot\theta \tag{3-64}$$

the net flow equation is reduced to:

$$\mathrm{d}G = -\frac{\bar{v}a\mathrm{d}S}{2}\left(\frac{\mathrm{d}N}{\mathrm{d}z}\right) \int_0^{\pi/2} \sqrt{\left(1 - \rho'^2 \sin^2\phi\right)} \mathrm{d}\phi \tag{3-65}$$

where:

$$\rho' = \rho / R \tag{3-66}$$

The integral in equation (3-65) is an elliptic integral, *E(ρ'),* which can be rearranged into the net molecular flux per unit area:

$$\frac{\mathrm{d}G}{\mathrm{d}S} = -\frac{\bar{v}R}{2} E(\rho') \frac{\mathrm{d}N}{\mathrm{d}z} \tag{3-67}$$

It is important to note that when ρ'=0 (along the center axis of the tube), the integral reduces to *π/2* and when *ρ'=R* (along the outer circumference of the tube), the integral reduces to 1. Therefore the net flow rate changes radially through the tube which is contrary to Knudsen's assumption [equation (3-38)]. The net flow is now obtained by integrating (3-65) through the entire cross section:

$$G = -\pi R^2 \frac{2\bar{v}R}{3} \frac{\mathrm{d}N}{\mathrm{d}z} \tag{3-68}$$

Now the velocity must be determined from the Maxwellian distribution of velocities. Combining (3-10) and (3-11) gives an equation for the velocity:

$$\bar{v} = \sqrt{\frac{8R_oT}{\pi M}} \tag{3-69}$$

so that the net flow becomes:

$$G = -\frac{2\pi R^2}{3} \left(\frac{8R_oT}{\pi M} \right)^{\frac{1}{2}} \frac{\mathrm{d}N}{\mathrm{d}z} \tag{3-70}$$

From Boyle's law:

$$N = \frac{M \cdot P}{R_oT} \tag{3-71}$$

At steady state, the mass flux will be uniform longitudinally so the last term in (3-70) can be expressed as:

$$\frac{\mathrm{d}N}{\mathrm{d}z} = \frac{M(P_1 - P_2)}{R_oTL} \tag{3-72}$$

Substituting this into (3-70) gives the total net flow equation found by Knudsen:

$$G = \frac{4}{3}\sqrt{\frac{2\pi M}{R_o T}}\frac{R^3}{L}\left(P_1 - P_2\right) \tag{3-73}$$

If the temperature is not constant through the tube then the temperature will be evaluated in the Taylor expansion as a function of z and will carry through with the density gradient term. The result will be a mass flow which matches Knudsen's equation:

$$G = \frac{4}{3}\sqrt{\frac{2\pi M}{R_o}}\frac{R^3}{L}\left(\frac{P_1}{\sqrt{T_1}} - \frac{P_2}{\sqrt{T_2}}\right) \tag{3-74}$$

3.7 Flow resistance

Knudsen's equations (3-52) through (3-54) use the variable Z which he termed the flow resistance in a tube. Carrying out the integration of (3-51) for a cylindrical tube with length L and radius R:

$$Z = \frac{3}{8}\sqrt{\frac{2}{\pi}}\frac{L}{R^3} \tag{3-75}$$

This resistance has a parallel in electrical resistance calculations and can even follow Kirchoff's laws of branched circuits to find a flow resistance in a complicated set of tubes. VS later determined a flow resistance based on the derivation above equal to:

$$Z = \sqrt{\frac{8}{\pi}}\frac{L}{I} \tag{3-76}$$

where I is equal to:

$$I = \int_S \int_{\frac{-\pi}{2}}^{\frac{\pi}{2}} \frac{1}{2} \rho^2 \cos\theta \cdot \mathrm{d}\theta \cdot \mathrm{d}S \tag{3-77}$$

Carrying out the integrals for a circular tube gives the same result as that of Knudsen [equation (3-75)].

Dushman [63, 64] was the first to propose a solution to the problem of flow through short tubes, however, his derivation used the idea of entrance and exit resistances which Clausing [48] proved was not a good conclusion for all cases (especially when discussing flow into a vacuum). While his derivation was good where $L<R$ and when L/R approached infinity, it was not good in the intermediate regions. The Dushman resistance:

$$Z = \frac{3}{4\sqrt{2\pi}} \frac{L}{R^3} \sqrt{\rho_o} + \frac{\sqrt{2}}{\pi} \frac{1}{R^2} \sqrt{\rho_o} \tag{3-78}$$

thus comes to the same conclusion as the Knudsen resistance and is only regarded as an approximation to the flow in short tubes.

3.8 Conductance And Transmission Probabilities

To study the relationship between flowrates and the pressure gradient across the tube, Knudsen created the following relation:

$$Q_P = U\left(P_1 - P_2\right) \tag{3-79}$$

where Q_P is a measure of pressure*volumetric flowrate and U is the conductance of the flow. The conductance is defined as:

$$U = \frac{1}{Z\sqrt{\rho_1}} \tag{3-80}$$

Thus for Knudsen's solution for flow through long tubes, the conductance is:

$$U = \frac{8}{3}\sqrt{\frac{\pi R_o T}{2M}}\frac{R^3}{L} \tag{3-81}$$

While the conductance equation has value in understanding the problem of flow through tubes, Clausing and his successors chose to use a method based on a slightly different derivation than their predecessors. Rather than using flow resistance, he assumed the net flow could be calculated using a transmission probability. In essence, the net flow is determined from the difference of the two directional probabilities:

$$G = (n_1 A_1 - n_2 A_2)W \tag{3-82}$$

where *nA* is the incident rate of molecules entering the tube (from each direction) and W is the probability that the molecules will pass through from one side to the other. As an example, if the opening between the two chambers were an ideal orifice, all the molecules would pass from one side to the next, thus *W*=1. The transmission probability for Knudsen's formulation can be found by assuming P_2=0 (which is the situation for effusion). Equation (3-82) then becomes:

$$G = n_1 A_1 W \tag{3-83}$$

The molecules entering from the chamber are:

$$G_0 = n_1 A = \frac{N_1 \bar{v} A}{4} \tag{3-84}$$

Combining (3-18) and (3-82) results in:

$$U = \frac{G_0}{N_1} \cdot W = \frac{n_1 A}{N_1} = U_0 W \tag{3-85}$$

where U_0 is the entrance conductance. Now using (3-81), (3-84) and (3-85) the transmission probability for Knudsen's derivation is:

$$W_{Knudsen} = \frac{8R}{3L} \tag{3-86}$$

It is easily seen that the formula breaks down when $L<<R$ thus the equation only holds for long tubes. Dushman's solution:

$$W_{Dushman} = \frac{1}{1 + \frac{3L}{8R}} \tag{3-87}$$

results in a more accurate result for long tube flows because he adds an entrance conductance to the long tube conductance, i.e.:

$$\frac{1}{W_{Dushman}} = 1 + \frac{1}{W_o} \tag{3-88}$$

where W_o is $W_{Knudsen}$. While this formula gives reasonable results for long tubes, as mentioned above, it only provides a general approximation of conductance through short tubes. Thus, Clausing [48, 106] uses the following derivation to determine the flow conductance through tubes of any ratio of r/L.

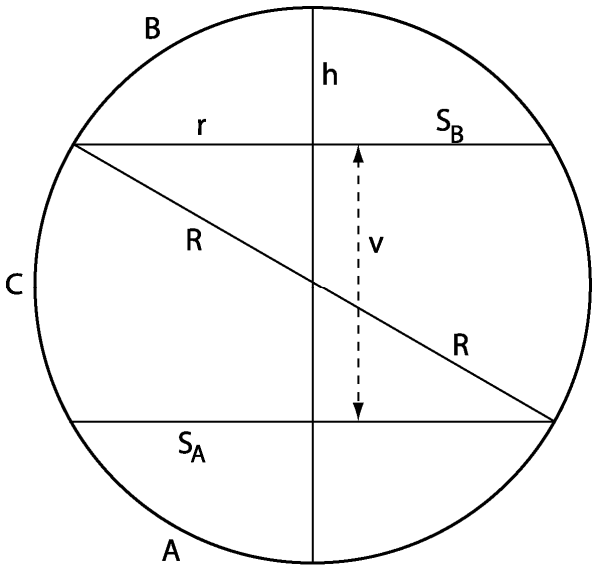

Figure 3-7: Clausing's Derivation

Clausing divides a tube into three sections using two planes perpendicular to the tube axis. He assumes the resulting rings cut out by the planes have a width dv and are separated by a distance *v*. Following the cosine law, he defines the following probabilities:

1. $W_{rr}(v)dv$: Probability that a molecule will leave the first ring and strike the second.
2. $W_{rs}(v)dv$: Probability that a molecule will leave the first ring and pass through the area cut out by the second ring.
3. $W_{sr}(v)dv$: Probability that a molecule will leave the area cutout by the first ring and strike the second ring.
4. $W_{ss}(v)dv$: Probability that a molecule will leave the area cut out by the first ring and pass through the area cut out by the second ring.

It can be shown through the cosine law that the number of molecules that pass through surface B is related to those that pass through C in proportion to their two surface areas (Figure 3-7). Using this along with other geometric relations yields analytic solutions for the probabilities mentioned above:

$$W_{ss}(v) = \frac{1}{2r^2}\left[v^2 - v\left(v^2 + 4r^2\right)^{\frac{1}{2}} 2r^2 \right] \tag{3-89}$$

$$W_{rs}(v) = \frac{1}{4r}\left[\left(v^2 + 4r^2\right)^{\frac{1}{2}} + \frac{v^2}{\left(v^2 + 4r^2\right)^{\frac{1}{2}}} - 2v \right] \tag{3-90}$$

$$W_{rr}(v) = \frac{1}{4r}\left[2 + \frac{v^2}{\left(v^2 + 4r^2\right)^{\frac{3}{2}}} - \frac{3v}{\left(v^2 + 4r^2\right)^{\frac{1}{2}}} \right] \tag{3-91}$$

$$W_{sr}(v) = \frac{1}{2r^2}\left[\left(v^2 + 4r^2\right)^{\frac{1}{2}} + \frac{v^2}{\left(v^2 + 4r^2\right)^{\frac{1}{2}}} - 2v \right] \tag{3-92}$$

He combined these into a single equation for the transmission probability:

$$W_{Clausing} = \int_0^L W_{sr}(x) \cdot w(x) dx + W_{ss}(L) \tag{3-93}$$

where

$$w(x) = \int_0^L W_{rr}(\xi - x) d\xi \cdot w(\xi) + W_{rs}(L - x) \tag{3-94}$$

is the "escape probability". Clausing determined approximate solutions for the transmission probability by substituting escape probabilities averaged over the length of the tube to yield:

$$W_{\text{Clausing}} = \frac{1-\left(\frac{8r}{3L}\right)}{3r^2L}\left[4r^3 + \left(L^2 - 2r^2\right)\left(L^2 + 4r^2\right)^{\frac{1}{2}} - L^3\right] + \left(\frac{4r}{3L}\right) + \frac{1-\left(\frac{4r}{3L}\right)}{2r^2}\left[L^2 - L\left(L^2 + 4r^2\right)^{\frac{1}{2}} + 2r^2\right] \tag{3-95}$$

If $r<<L$ then this equation gives the Knudsen result above and for $r>L$ gives an approximate solution satisfying flow through short tubes. An addendum to this work stipulates that for very short or infinitely long tubes, a simpler transmission probability is:

$$W_{Clausing} = \frac{8}{3L + 8r} \tag{3-96}$$

Since Clausing did not provide any error assessment of his equations, many of his contemporaries criticized the validity of his equations. DeMarcus and Hopper [57] re-examined his work and determined his results had an error of 0.1 percent. Their work was numerical and bounded the solution in what they termed a "squeezing" method. Since their results did not contain analytic solutions, Berman [22] later derived asymptotic expansions (for long tubes) and series expansions (for short tubes) to Clausing's integral (3-93):

$$R \geq L \qquad W_{D\&B} = 1 - \left(\frac{L}{2R}\right) + \left(\frac{L^2}{4R^2}\right) + \left(\frac{5L^3}{48R^3}\right) + \left(\frac{L^4}{32R^4}\right) + \ldots \tag{3-97}$$

$$R << L \qquad W_{D\&B} \approx \left(\frac{8R}{3L}\right) - \left(\frac{2R^2 \ln\left(L/R\right)}{L^2}\right) - \left(\frac{91R^2}{18L^2}\right) + \left(\frac{32R^2 \ln\left(L/R\right)}{3L^3}\right) + \left(\frac{8R^3}{3L^3}\right) - \left(\frac{8R^4\left[\ln\left(L/R\right)\right]^2}{L^4}\right) + O\left(\frac{R^4}{L^4}\right) \tag{3-98}$$

Others developed solutions and bounds to Clausing's integral [183, 178, 70], however, some the best results were achieved by Cole and Pack [50] who were able to achieve results with errors no greater than 8.6×10^{-2} %. Tao [261, 262] introduced the "dusty gas model" as a method to solve the thermomolecular pressure difference. Santeler [219, 220] later derived transmission probabilities for rectangular tubes whereas Bassanini [18] and Steckelmacher [247, 249] looked at rectangular and elliptical cross-sections.

CHAPTER 4 THE BOLTZMANN DISTRIBUTION

While many papers are devoted to the well known problem of free molecular flow through a tube, a true analytic solution is still not available when intermolecular collisions are present. It is clear that the transmission probability method is not suited for a complete analysis in the transition regime and a new approach is needed which adds a collision model. The Boltzmann equation includes such a model and makes it possible to look at the macroscopic quantities derived from the individual motion of the each molecule. This section outlines this method and builds a foundation for the numerical/statistical technique called Direct Simulation Monte Carlo.

4.1 The Boltzmann Equation

To this point, this dissertation has used an average value to describe the velocities of molecules. This assumes the mean is representative enough of the gas to be able to determine the state of the gas which is not totally accurate. A fundamental idea behind kinetic theory is the molecular distribution law which says a gas is comprised of a set of molecules at a distribution of velocities and locations. In equilibrium, the number of molecules having certain velocity should remain the same. Rather than trying to calculate the state variables for each molecule, the derivation of the Boltzmann distribution [102] below follows Bird's [29] method to show how the macroscopic quantities of the distribution is determined as a representation of the entire gas.

Consider the phase space shown in Figure 4-1. The volume shown represents a molecule with velocity components between u and $u+du$, v and $v+dv$, and w and $w+dw$ where u, v, and w represent the velocities along the x, y, and z axes. The velocity vector, **c**, is drawn from point O to the volume element and represents all molecules with velocities in that geometric volume. Assuming the molecules follow the distribution law, the number of molecules, dN, lying in the volume is

$$dN = Nf(\mathbf{c})dudvdw \tag{4-1}$$

where N is the total number of molecules and $f(c)$ is the velocity distribution function which gives the fraction of molecules with a particular velocity. This equation can also be written as:

$$dN = Nf(\mathbf{c})d\mathbf{c} \tag{4-2}$$

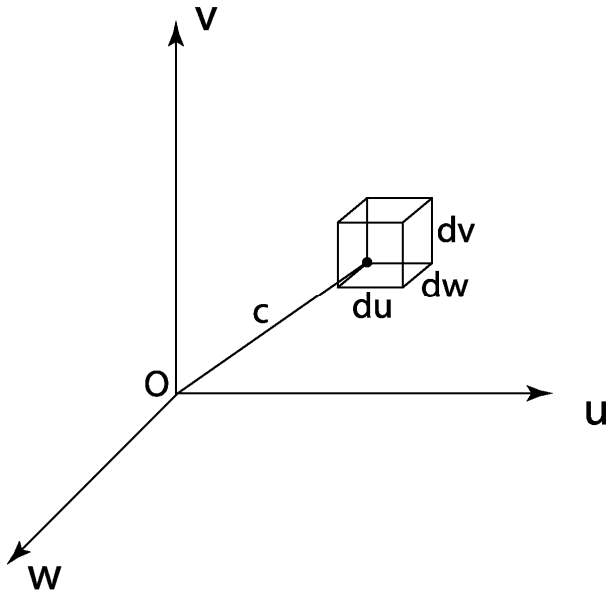

Figure 4-1: Velocity Space

since dc is the same volume element as *dudvdw*. *f(c)* can now be simplified to f and calculated for all velocities

$$\int_{-\infty}^{\infty}\int_{-\infty}^{\infty}\int_{-\infty}^{\infty} f\mathrm{d}u\mathrm{d}v\mathrm{d}w = \int_{-\infty}^{\infty} f\mathrm{d}\mathbf{c} = 1 \tag{4-3}$$

It should be noted that the distribution function cannot be negative and it has finite bounds. For most problems it is important to have the distribution determined by position which would make the overall state of the molecule be described by a 6N phase space. Within the velocity space described above a position vector and volume element can also be introduced using the variables ***r*** and ***dr***. Equation (4-2) would then become

$$\mathrm{d}N = \mathcal{F}(\boldsymbol{c},\boldsymbol{r},\boldsymbol{t})\mathrm{d}\mathbf{c}\mathrm{d}\mathbf{r} \tag{4-4}$$

where $\mathcal{F}$ represents a single particle distribution in phase space. Knowing that the number density n=N/d***r*** the following identity can be rewritten as

$$nf = nf(\boldsymbol{c},\boldsymbol{r},\boldsymbol{t}) = \mathcal{F}(\boldsymbol{c},\boldsymbol{r},\boldsymbol{t}) \tag{4-5}$$

This function can be applied to multiple particles, gas mixtures, and gases of various densities. For the context of this dissertation the focus is on dilute gases of a single species. While monatomic gases like Argon fit into these parameters, any diatomic or polyatomic molecules must include internal degrees of freedom.

Now assuming the volume element above doesn't change with time, the rate of change of the number of molecules in that volume space is

$$\frac{\partial}{\partial t}(nf)\mathrm{d}\boldsymbol{c}\mathrm{d}\boldsymbol{r} \tag{4-6}$$

In the absence of outside forces, the only other processes that contribute to the number of molecules within d$\boldsymbol{c}$d$\boldsymbol{r}$ are:

1) The motion of molecules across the surface surrounding $d\boldsymbol{r}$ with a single molecular velocity, $\boldsymbol{c}$. In this case the physical and velocity spaces are kept separate which allows the two variables to be treated independently.
2) The change of velocity of molecules caused from binary intermolecular collisions. In this case the collisions affect only the velocity of the particles while the position vector remains the same.

The conservation of molecules through surface d$\boldsymbol{r}$ with velocity $\boldsymbol{c}$ is given by the equation

$$\int_{S_\mathbf{r}} nf(\mathbf{c}\cdot\mathbf{e}_r)\mathrm{d}S_r\mathrm{d}\boldsymbol{c} \tag{4-7}$$

where $\boldsymbol{e}_r$ is the normal unit vector across the surface, S_r. Gauss' theorem converts this from a surface to a volume integral

$$-\int_{d\mathbf{r}} \nabla\cdot(nf\mathbf{c})\mathrm{d}r\mathrm{d}\boldsymbol{c} = -\nabla\cdot(nf\mathbf{c})\mathrm{d}r\mathrm{d}\boldsymbol{c} \tag{4-8}$$

which can be simplified to

$$\mathbf{c}\cdot\frac{\partial}{\partial\mathbf{r}}(nf)\mathrm{d}\boldsymbol{c}\mathrm{d}\boldsymbol{r} \tag{4-9}$$

If we assume there are no molecular collisions (item 2) then the description of molecules in $d\boldsymbol{r}d\boldsymbol{c}$ becomes:

$$\frac{\partial}{\partial t}(nf)\mathrm{d}\boldsymbol{c}\mathrm{d}\boldsymbol{r} + \mathbf{c}\cdot\frac{\partial}{\partial \mathbf{r}}(nf)\mathrm{d}\boldsymbol{c}\mathrm{d}\boldsymbol{r} = 0 \tag{4-10}$$

Finally, solving this for the entire position and velocity space gives the Collisionless Boltzmann Equation:

$$\frac{\partial}{\partial t}(nf) + \mathbf{c}\cdot\frac{\partial}{\partial \mathbf{r}}(nf) = 0 \tag{4-11}$$

Including collisions, Boltzmann's equation would be

$$\frac{\partial}{\partial t}(nf)\mathrm{d}\boldsymbol{c}\mathrm{d}\boldsymbol{r} + \mathbf{c}\cdot\frac{\partial}{\partial \mathbf{r}}(nf)\mathrm{d}\boldsymbol{c}\mathrm{d}\boldsymbol{r} = Q\left(ff^*\right) \tag{4-12}$$

where Q(ff^*) is he collision integral. In order to determine this integral we only consider binary collisions and the velocities of these molecules both before ($\boldsymbol{c}$, $\boldsymbol{c_1}$) and after ($\boldsymbol{c}^*$, $\boldsymbol{c_1}^*$) the collision. The collision cross sectional area is defined as

$$\sigma = \pi d^2 \tag{4-13}$$

where d is the diameter of molecule. It can be assumed that one molecule is stationary and another is moving at a velocity, c_r, which in reality is the relative velocity of $\boldsymbol{c_1}$ to $\boldsymbol{c}$. In three

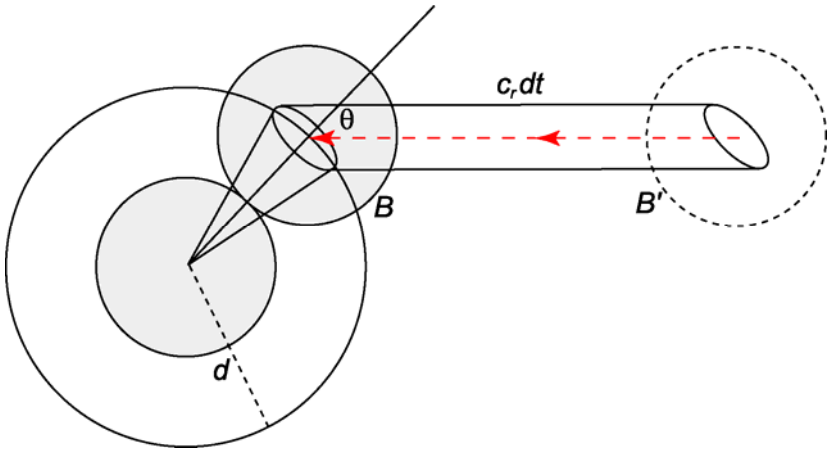

Figure 4-2: Collision area

dimensional space, the cross-sectional collision area is $\sigma d\omega$. For molecules with velocity, c_r, the number of molecules that a single molecule collides with per unit time is:

$$nf_1 c_r \sigma \mathrm{d}\omega \mathrm{d}c_1 \tag{4-14}$$

For the unit element, there are $nf\mathrm{d}\boldsymbol{c}\mathrm{d}\boldsymbol{r}$ molecules with velocity $\boldsymbol{c}$, so the total number of c-c_1 collisions is:

$$Q\left(ff^*\right)_{c,c_1\to c^*,c_1^*} = n^2 ff_1 c_r \sigma \mathrm{d}\omega \mathrm{d}\boldsymbol{c}_1 \mathrm{d}\boldsymbol{c}\mathrm{d}\boldsymbol{r} \tag{4-15}$$

This equation gives the number of molecules that scatter *out of* the phase space element $\mathrm{d}\boldsymbol{c}\mathrm{d}\boldsymbol{r}$ due to pre-collision To calculate the molecular collisions that move molecules *into* the element due to collisions, inverse collisions are used. This produces the following:

$$Q\left(ff^*\right)_{c,c_1\leftarrow c^*,c_1^*} = n^2 f^* f_1^* c_r^* \left(\sigma d\omega\right)^* \mathrm{d}\boldsymbol{c}_1^* \mathrm{d}\boldsymbol{c}^* \mathrm{d}\boldsymbol{r} \tag{4-16}$$

The rate of increase of molecules with velocity, $\boldsymbol{c}$, is found by subtracting the number of molecules leaving the element from the number of molecules entering the element.

$$Q\left(ff^*\right)_{dcdr} = n^2\left[f^* f_1^* c_r^* \left(\sigma d\omega\right)^* \mathrm{d}\boldsymbol{c}_1^* \mathrm{d}\boldsymbol{c}^* - ff_1 c_r \sigma \mathrm{d}\omega \mathrm{d}\boldsymbol{c}_1 \mathrm{d}\boldsymbol{c}\right]\mathrm{d}\boldsymbol{r} \tag{4-17}$$

If momentum is conserved in the collision, the collision term becomes the following:

$$Q\left(ff^*\right)_{dcdr} = n^2\left(f^* f_1^* - ff_1\right)c_r \sigma \mathrm{d}\omega \mathrm{d}c_1 \mathrm{d}\boldsymbol{c}\mathrm{d}\boldsymbol{r} \tag{4-18}$$

Since this integral only comprises a single phase element, it must be integrated over the entire velocity and positions space:

$$Q\left(ff^*\right)=\int_{-\infty}^{\infty}\int_{0}^{4\pi}n^2\left(f^*f_1^*-ff_1\right)c_r\sigma\mathrm{d}\omega\mathrm{d}c_1\mathrm{d}\boldsymbol{c}\mathrm{d}\boldsymbol{r} \tag{4-19}$$

Substituting this back into equation (4-12) and dividing by d***c***d***r*** gives the Boltzmann Equation (BE) for a dilute gas.

$$\frac{\partial}{\partial t}\left(nf\right)+\mathbf{c}\cdot\frac{\partial}{\partial\mathbf{r}}\left(nf\right)=\int_{-\infty}^{\infty}\int_{0}^{4\pi}n^2\left(f^*f_1^*-ff_1\right)c_r\sigma\mathrm{d}\omega\mathrm{d}\boldsymbol{c}_1 \tag{4-20}$$

4.2 Moment Equations

Now that the BE is defined, it can now be used to determine the macroscopic properties of interest. Let's take a molecular quantity Q whose mean is

$$\overline{Q}=\frac{1}{N}\int_{N}Q\mathrm{d}N \tag{4-21}$$

This quantity can be related to the distribution function using equation (4-2).

$$\overline{Q}=\frac{1}{N}\int_{-\infty}^{\infty}Qf\left(c\right)N\mathrm{d}\boldsymbol{c}=\int_{-\infty}^{\infty}Qf\left(c\right)\mathrm{d}\boldsymbol{c} \tag{4-22}$$

Macroscopic properties are referred to as moments of the distribution function since, as shown above, they quantity is set as a moment to the function. The same can be performed on the BE (equation (4-20) which will allow us to determine the property change within the system:

$$Q\frac{\partial}{\partial t}\left(nf\right)+Q\mathbf{c}\cdot\frac{\partial}{\partial\mathbf{r}}\left(nf\right)=Q\int_{-\infty}^{\infty}\int_{0}^{4\pi}n^2\left(f^*f_1^*-ff_1\right)c_r\sigma\mathrm{d}\omega\mathrm{d}\boldsymbol{c}_1 \tag{4-23}$$

The first term on the left can be rewritten as

$$Q\frac{\partial}{\partial t}(nf)=\int_{-\infty}^{\infty}\frac{\partial}{\partial t}(Qnf)\mathrm{d}\boldsymbol{c} \tag{4-24}$$

since Q and f are functions of the molecular velocity. This can then be simplified using (4-22) to

$$Q\frac{\partial}{\partial t}(nf)=\frac{\partial}{\partial t}(\overline{Q}n) \tag{4-25}$$

The second term uses a similar process to bring Q into the equation knowing that both Q and $\boldsymbol{c}$ are independent of position and time in this portion of the equation.

$$Q\mathbf{c}\cdot\frac{\partial}{\partial \mathbf{r}}(nf)=\int_{-\infty}^{\infty}\nabla\cdot(\boldsymbol{c}Qnf)\mathrm{d}\boldsymbol{c} \tag{4-26}$$

This can be simplified to

$$Q\mathbf{c}\cdot\frac{\partial}{\partial \mathbf{r}}(nf)=\nabla\cdot(\overline{\boldsymbol{c}Q}n) \tag{4-27}$$

The right hand side of the equation is changed by bringing Q inside the equation:

$$\Delta Q(ff^*)=Q\int_{-\infty}^{\infty}\int_{0}^{4\pi}n^2\left(f^*f_1^*-ff_1\right)c_r\sigma\mathrm{d}\omega\mathrm{d}\boldsymbol{c}_1=\int_{-\infty}^{\infty}\int_{-\infty}^{\infty}\int_{0}^{4\pi}Qn^2\left(f^*f_1^*-ff_1\right)c_r\sigma\mathrm{d}\omega\mathrm{d}\boldsymbol{c}_1\mathrm{d}\boldsymbol{c} \tag{4-28}$$

Substituting (4-25), (4-27) and (4-28) into (4-23) gives the Boltzmann Transfer Equation.

$$\frac{\partial}{\partial t}(\overline{Q}n)+\nabla\cdot(\overline{\boldsymbol{c}Q}n)=\int_{-\infty}^{\infty}\int_{-\infty}^{\infty}\int_{0}^{4\pi}Qn^2\left(f^*f_1^*-ff_1\right)c_r\sigma\mathrm{d}\omega\mathrm{d}\boldsymbol{c}_1\mathrm{d}\boldsymbol{c} \tag{4-29}$$

This equation describes the change of a macroscopic property Q as it changes with position, time and in the presence of intermolecular collisions. The right hand side of the equation can be rewritten to show the change in quantity Q from inverse collisions is the same as the change in Q from direct collisions (Bird).

$$\frac{\partial}{\partial t}\left(\overline{Q}n\right)+\nabla\cdot\left(\overline{\mathbf{c}Q}n\right)=\frac{1}{4}\int_{-\infty}^{\infty}\int_{-\infty}^{\infty}\int_{0}^{4\pi}n^2\left(Q+Q_1-Q^*-Q_1^*\right)\left(ff_1-f^*f_1^*\right)c_r\sigma\mathrm{d}\omega\mathrm{d}\mathbf{c}_1\mathrm{d}\mathbf{c} \tag{4-30}$$

Assuming there is a conservation of the property Q (i.e. Q is mass, momentum or energy), then

$$Q+Q_1=Q^*-Q_1^* \tag{4-31}$$

which is the definition of a summational invariant [102]. Q could then be written in its most general form:

$$Q=A\frac{1}{2}mc^2+\mathbf{B}\cdot m\mathbf{c}+C \tag{4-32}$$

4.3 Equilibrium

The significance of the H theorem lies not only in its application to the distribution law, but more importantly, H describes an irreversible change in entropy despite underlying reversible gas dynamics. To understand this, let's simplify equation (4-20). Assuming spatial uniformity of the gas, the 2nd term in the equation can be eliminated which then becomes:

$$\frac{\partial f}{\partial t}=n\int_{-\infty}^{\infty}\int_{0}^{4\pi}\left(f^*f_1^*-ff_1\right)c_r\sigma\mathrm{d}\omega\mathrm{d}\mathbf{c}_1 \tag{4-33}$$

Now H is defined as

$$H=\overline{\ln\left(nf\right)} \tag{4-34}$$

which can also be written as

$$H=\int_{-\infty}^{\infty}f\ln\left(nf\right)\mathrm{d}\mathbf{c} \tag{4-35}$$

Substituting ln(*nf*) into (4-33) and using the form of the collision term from (4-30) we get

$$\frac{\partial H}{\partial t} = \frac{n}{4}\int_{-\infty}^{\infty}\int_{-\infty}^{\infty}\int_{0}^{4\pi}\left(\ln f + \ln f_1 - \ln f^* - \ln f_1^*\right)\left(ff_1 - f^* f_1^*\right)c_r \sigma \mathrm{d}\omega \mathrm{d}\boldsymbol{c}_1 \mathrm{d}\boldsymbol{c} \tag{4-36}$$

This can be simplified to

$$\frac{\partial H}{\partial t} = \frac{n}{4}\int_{-\infty}^{\infty}\int_{-\infty}^{\infty}\int_{0}^{4\pi}\ln\left(\frac{ff_1}{f^* f_1^*}\right)\left(ff_1 - f^* f_1^*\right)c_r \sigma \mathrm{d}\omega \mathrm{d}\boldsymbol{c}_1 \mathrm{d}\boldsymbol{c} \tag{4-37}$$

This equation can only have a negative or zero result which means *H* will always decrease in value:

$$\frac{\partial H}{\partial t} \le 0 \tag{4-38}$$

Now let's assume $\partial H/\partial t$=0. This would mean

$$ff_1 - f^* f_1^* = 0 \quad or \quad \ln(f) + \ln(f_1) = \ln(f^*) + \ln(f_1^*) \tag{4-39}$$

which is equivalent to the summational invariant shown in (4-31). Equation (4-39) is the definition of equilibrium which states the velocity distribution does not vary with time. Now, using (4-32) we can write ln(*f*) as

$$\ln(f) = A\frac{1}{2}mc^2 + \mathbf{B}\cdot m\mathbf{c} + C \tag{4-40}$$

Let's now introduce a new parameter called the peculiar velocity:

$$c' = c - c_o \tag{4-41}$$

where c is the total velocity and c_o is the stream or bulk velocity. Equation (4-40) can then be written in terms of its peculiar velocity

$$\ln(f) = A\frac{1}{2}m(c' + c_o)^2 + \mathbf{B}\cdot m(\mathbf{c}' + \mathbf{c_o}) + C \tag{4-42}$$

Carrying out the multiplication

$$\ln(f) = A\frac{1}{2}mc'^2 + Amc'c_o + A\frac{1}{2}mc_o{}^2 + \mathbf{B}\cdot m(\mathbf{c}' + \mathbf{c_o}) + C \tag{4-43}$$

Rearranging this into velocity components gives

$$\ln(f) = A\frac{1}{2}mc'^2 + m(A\mathbf{c_o} + \mathbf{B})\cdot\mathbf{c}' + A\frac{1}{2}mc_o{}^2 + \mathbf{B}\cdot m\mathbf{c_o} + C \tag{4-44}$$

If the gas is in equilibrium then the coefficient to ***c'*** must be zero, thus

$$-A\mathbf{c_o} = \mathbf{B} \tag{4-45}$$

Therefore,

$$\ln(f) = A\frac{1}{2}mc'^2 - A\frac{1}{2}mc_o{}^2 + C \tag{4-46}$$

Thus

$$f = \exp\left(A\frac{1}{2}mc'^2 - A\frac{1}{2}mc_o{}^2 + C\right) \tag{4-47}$$

Now we define a new constant

$$\beta^2 = -A\frac{1}{2}m \tag{4-48}$$

Substituting (4-48) into (4-47)

$$f = \exp\left(-\beta^2 c'^2 + \beta^2 c_o{}^2 + C\right) \tag{4-49}$$

Using the relation in (4-3), equation (4-49) can be rewritten as

$$\int_{-\infty}^{\infty} f d\mathbf{c} = \exp\left(\beta^2 c_o{}^2 + C\right)\int_{-\infty}^{\infty}\exp\left(-\beta^2 c'^2\right)d\mathbf{c}' = 1 \tag{4-50}$$

After evaluating the integral on the right side of the equation,

$$\left(\frac{\pi^{3/2}}{\beta^3}\right)\exp\left(\beta^2 c_o{}^2 + C\right)=1 \quad or \quad \exp\left(\beta^2 c_o{}^2 + C\right)=\frac{\beta^3}{\pi^{3/2}} \tag{4-51}$$

Substituting this back into (4-49) gives the Maxwellian Distribution for equilibrium which is the same equation as given in (1-4).

$$f_o = \frac{\beta^3}{\pi^{3/2}}\exp\left(-\beta^2 c'^2\right) \tag{4-52}$$

The average velocity can be found using the distribution equation and (4-21) where $Q=\boldsymbol{c}$

$$\bar{c} = \int_{-\infty}^{\infty} c f \mathrm{d}c \tag{4-53}$$

From (3-10) we know

$$\overline{c'^2} = 3RT \tag{4-54}$$

Thus, to get the maxwellian into its more common form we must use (4-53) and (4-54) and the relation $k=mR$

$$\overline{c'^2} = \frac{3kT}{m} = \frac{\beta^3}{\pi^{3/2}}\int c'^2 \exp\left(-\beta^2 c'^2\right)\mathbf{dc} \tag{4-55}$$

This yields

$$\beta^2 = \frac{m}{2kT} \tag{4-56}$$

Finally

$$f_o = \left(\frac{m}{2\pi kT}\right)^{3/2}\exp\left(-\frac{mc'^2}{2kT}\right) \tag{4-57}$$

Equation (4-53) showed how the macroscopic velocity of the gas could be calculated from the distribution. Here are some other properties:

Number Flux	$N = \int_{-\infty}^{\infty} f \mathrm{d}\boldsymbol{c}$	(4-58)
Temperature	$T = \frac{m}{3k} \int_{-\infty}^{\infty} \boldsymbol{c}^2 f \mathrm{d}\boldsymbol{c}$	(4-59)
Pressure	$P = \frac{nm}{3} \int_{-\infty}^{\infty} \boldsymbol{c}^2 f \mathrm{d}\boldsymbol{c}$	(4-60)
Heat Flow	$q = \frac{nm}{2} \int_{-\infty}^{\infty} c^2 \boldsymbol{c} f \mathrm{d}\boldsymbol{c}$	(4-61)

4.4 Flux

If we assume a gas flows in a particular direction with the velocity $\boldsymbol{c_o}$ then each molecule has a velocity component

$$\begin{aligned} u &= u' + c_o \cos(\theta) \\ v &= v' + c_o \sin(\theta) \\ w &= w' \end{aligned} \tag{4-62}$$

where θ is the angle between the normal of a surface element and the velocity vector $\boldsymbol{c_o}$. If the x-axis is defined as directed toward $-e_o$. Using (4-53), the (positive) flux across the surface element per unit time is given by

$$\dot{Q}_{dA} = n \int_{-\infty}^{\infty} \int_{-\infty}^{\infty} \int_{0}^{\infty} Quf \mathrm{d}u\mathrm{d}v\mathrm{d}w \tag{4-63}$$

We know from (4-52) that in equilibrium (4-63) can be written as

$$\dot{Q}_{dA} = \frac{n\beta^3}{\pi^{3/2}} \int_{-\infty}^{\infty} \int_{-\infty}^{\infty} \int_{0}^{\infty} Qu \exp\left(-\beta^2 c'^2\right) \mathrm{d}u\mathrm{d}v\mathrm{d}w \tag{4-64}$$

Dividing $\boldsymbol{c}$' into its components gives

$$\dot{Q}_{dA} = \frac{n\beta^3}{\pi^{3/2}} \int_{-\infty}^{\infty}\int_{-\infty}^{\infty}\int_{0}^{\infty} Qu \exp\left[-\beta^2\left(u'^2 + v'^2 + w'^2\right)\right] du\,dv\,dw \tag{4-65}$$

Now substitute (4-62) in for the velocities to get the flux in terms of the peculiar velocities.

$$\dot{Q}_{dA} = \frac{n\beta^3}{\pi^{3/2}} \int_{-\infty}^{\infty}\int_{-\infty}^{\infty}\int_{-c_o\cos(\theta)}^{\infty} Q\left[u' + c_o\cos(\theta)\right]\exp\left[-\beta^2\left(u'^2 + v'^2 + w'^2\right)\right] du'\,dv'\,dw' \tag{4-66}$$

If we want the number flux across the surface element, use (4-58) where Q=1.

$$\dot{N}_{dA} = \frac{n\beta^3}{\pi^{3/2}} \int_{-\infty}^{\infty}\int_{-\infty}^{\infty}\int_{-c_o\cos(\theta)}^{\infty} \left[u' + c_o\cos(\theta)\right]\exp\left[-\beta^2\left(u'^2 + v'^2 + w'^2\right)\right] du'\,dv'\,dw' \tag{4-67}$$

We can now separate the integral into individual independent variables

$$\begin{aligned}\dot{N}_{dA} = \frac{n\beta^3}{\pi^{3/2}} &\left[\int_{-\infty}^{\infty} \exp\left(-\beta^2 w'^2\right) dw'\right] \times \left[\int_{-\infty}^{\infty} \exp\left(-\beta^2 v'^2\right) dv'\right] \\ &\times \left[\int_{-c_o\cos(\theta)}^{\infty} \left[u' + c_o\cos(\theta)\right]\exp\left(-\beta^2 u'^2\right) du'\right]\end{aligned} \tag{4-68}$$

The integrals can then be solved to give

$$\dot{N}_{dA} = \frac{n}{\beta}\left[\frac{\exp\left(-c_o{}^2\beta^2\cos^2(\theta)\right) + \pi^{1/2} c_o\beta\cos(\theta)\left[1 + erf\left(c_o\beta\cos(\theta)\right)\right]}{2\pi^{1/2}}\right] \tag{4-69}$$

The relation $\boldsymbol{c_o\beta}$ is an important relation in this equation. It shows the relationship between the most probable molecular velocity, $\boldsymbol{c_m'}$ and the bulk velocity, $\boldsymbol{c_o}$. It can be shown that

$$c_m' = \frac{1}{\beta} \tag{4-70}$$

Therefore substitution gives us the molecular speed ratio.

$$c_o \beta = \frac{c_o}{c'_m} \tag{4-71}$$

Replacing β with (4-56) we can also find its relation to the temperature

$$\frac{c_o}{c'_m} = c_o \sqrt{\frac{m}{2kT}} \tag{4-72}$$

For a stationary gas, $\boldsymbol{c_o}$ is equal to zero which means (4-69) reduces to

$$\dot{N}_{dA} = \frac{n}{2\pi^{1/2}\beta} \tag{4-73}$$

If we substitute β once again we get

$$\dot{N}_{dA} = n\sqrt{\frac{RT}{2\pi}} \tag{4-74}$$

which is the same result Knudsen found for his effusion calculation in (3-5).

4.5 Solution Methods

It can be seen that in the free molecular regime the Boltzmann equation is much easier to solve since the collision integral is zero. For flow in the transition regime, there are effects of both continuum (hydrodynamic) flow as well as molecular flow, so in these instances it is difficult to solve the BE through analytical techniques so other methods [25, 255, 282] must be used. Below are some of most common solutions being used to analyze microflows today.

4.5.1 Moment Method (Grad's method)

In near hydrodynamic regimes, there are two analytical solutions which are generally used. The first is the Moment Method which assumes the distribution function is a series function:

$$f(t,r,v) = f_{loc}^{M}\left(a^{(0)}H^{(0)} + a_{\alpha_1}^{(0)}H_{\alpha_1}^{(0)} + ... + \frac{1}{N!}a_{\alpha_1...\alpha_N}^{(N)}H_{\alpha_1...\alpha_N}^{(N)} + ...\right) \tag{4-75}$$

where:

$$f_{loc}^{M}(n,T,\mathbf{u}) = n(t,\mathbf{r})\left[\frac{m}{2\pi k_b T(t,\mathbf{r})}\right]^{\frac{3}{2}} \times \exp\left[-\frac{m\left[\mathbf{v}-\mathbf{u}(t,\mathbf{r})\right]^2}{2k_b T(t,\mathbf{r})}\right] \tag{4-76}$$

and $H_{\alpha 1}^{(N)}$ are the Hermite polynomials defined as:

$$H_{\alpha_1...\alpha_N}^{(N)} = (-1)^N\left(\frac{k_b T}{m}\right)^{\frac{N}{2}}\exp\left(\frac{mV^2}{2k_b T}\right) \times \frac{\partial^N}{\partial V_{\alpha_1}...\partial V_{\alpha_N}}\exp\left(-\frac{mV^2}{2k_b T}\right) \tag{4-77}$$

The coefficients (α_N) can then be expressed using the moments of the distribution function which in turn are used to describe the macrocharacteristics of the gas. Since the distribution function assumes a condition of being continuous for all velocities, it has the limitation of being used only in lower number transition regimes.

4.5.2 Chapman-Enskog

The second set of analytical solutions is the Chapman-Enskog method. This solution is expanded into a power series where:

$$f = f^{(0)} + Kn \cdot f^{(1)} + Kn^2 \cdot f^{(2)} + ... \tag{4-78}$$

Assuming the distribution function is only dependant on the number density n(t,**r**), the spatial velocity **u**(t,**r**), and temperature T(t,**r**), then after substituting f into the BE:

$$f^{(0)} = f_{loc}^{M} \tag{4-79}$$

The second solution $f^{(N)}$ is found using the previous one $f^{(N-1)}$. As with the Moment Method this solution is limited to near hydrodynamic regimes since the perturbation assumption is for small Knudsen numbers.

4.5.3 BGK – Isothermal Gas Flows

Two solutions called the Model Kinetic equations are used to determine flow characteristics for arbitrary Knudsen numbers. The main concept for this type of technique is to modify the collision integral in the BE in order to simplify it enough to derive an exact solution. The first type of method is one of the most widely used and is called the Bhatnagar, Gross, and Krook (BGK) method.

The BGK method assumes:

$$Q_{BGK}(ff_*) = \nu\left[f_{loc}^{M} - f\right] \tag{4-80}$$

Where ν is the collision frequency and is assumed to be independent of the molecular velocity. There are three different methods for choosing ν. The first is to use the Chapman-Enskog method which says:

$$\nu = \frac{v_T}{\lambda} = \frac{4}{\pi}\frac{P(r,t)}{\mu(T)} \tag{4-81}$$

where v_T is the average thermal velocity, μ is the viscosity, and λ is the mean free path. This value doesn't give an accurate result according to the Chapman-Enskog model, so a solution considered more accurate is:

$$v = \frac{P(r,t)}{\mu(T)} \tag{4-82}$$

The third equation for the collision frequency is:

$$v = \frac{5k_b}{2m}\frac{P(r,t)}{k(r,t)} = \frac{2}{3}\frac{P(r,t)}{\mu(T)} \tag{4-83}$$

where k is the thermal conductivity coefficient, and k_b is Boltzmann's constant.

Loyalka [149-158] has used the BGK method to describe thermal transpiration in cylindrical tubes, parallel plates, and rectangular channels as well as the slip and velocity profiles. His most expansive work was developing the kinetic theory for thermal transpiration and the mechanocaloric effect. In addition, both he and Sone [242-245] described temperature jump flows and temperature gradient profiles within channels. Sharipov [230] expanded this work by removing lateral wall effects in his analysis of rarefied gas flows in rectangular channels. A limitation to the BGK method, however, is it produces the wrong Prandtl number and without modification should only be used for isothermal flows with small perturbations. Alexeenko [8] produced a comparison of DSMC and BGK in thermal creep problems which yielded a good comparison, however there is disagreement over whether or not the BGK method is best suited for this sort of problem.

4.5.4 Sharipov's S-model

The second model equation which does provide the correct Prandtl number is the S-Model. This method is used for any linear, non-isothermal gas flows. The collision integral is assumed to be:

$$Q_S(ff_*) = \frac{P}{\mu}\left\{ f_{loc}^M \left[1 + \frac{2m}{15n(k_b T)^2} q \cdot V \left(\frac{mV^2}{2k_b T} - \frac{5}{2} \right) \right] - f \right\} \tag{4-84}$$

Sharipov [227-229, 231] used this method to describe gas flows at any temperatures and flows through a slit and circular channels. His most comprehensive work which reported results for channel flows in all dilutes regimes is presented in [232]. It is generally used in conjunction with a linearized Boltzmann equation which is described next.

4.5.5 Linearized BE – Weakly non-equilibrium

Linearization of the Boltzmann Equation is performed by one of two modifications of the distribution function. The first modification is to write the function in terms of the absolute Maxwellian, f_o:

$$f(\mathbf{r}, \mathbf{v}, t) = f_o(n_o, T_o)\left[1 + h(\mathbf{r}, \mathbf{v}, t)\right] \tag{4-85}$$

which uses the equilibrium number density n_o and the equilibrium temperature T_o. The absolute Maxwellian is defined as:

$$f_o^M(n, T, \mathbf{u}) = n_o \left[\frac{m}{2\pi k_b T_o} \right]^{\frac{3}{2}} \times \exp\left[-\frac{mv^2}{2k_b T_o} \right] \tag{4-86}$$

The linearized BE then becomes:

$$\frac{\partial h}{\partial t} + v \cdot \frac{\partial h}{\partial r} = Qh \tag{4-87}$$

where:

$$Qh = \int f_o^M w(v, v_*; v, ' v_*') \times (h' + h_*' - h - h_*) dv_* dv_*' dv' \tag{4-88}$$

From this the macroscopic characteristics can be determined as:

$$n = n_o + (1, h) \tag{4-89}$$

$$n_o u = (v, h) \tag{4-90}$$

$$T = T_o + \frac{m}{3k_b n_o}(v^2, h) - \frac{T_o}{n_o (1, h)} \tag{4-91}$$

The other modification to linearize the BE is to use the local Maxwellian instead of the absolute Maxwellian. This equation is:

$$f(\mathbf{r}, \mathbf{v}, t) = f_{loc}^M (n, T, 0)\left[1 + h(\mathbf{r}, \mathbf{v}, t)\right] \tag{4-92}$$

This yields the linearized version of the BE:

$$\frac{\partial h}{\partial t} + v \cdot \frac{\partial h}{\partial \mathbf{r}} = Qh - \mathbf{v} \cdot \left[\frac{1}{n} \frac{\partial n}{\partial \mathbf{r}} + \left(\frac{mv^2}{2k_b T} - \frac{3}{2} \right) \frac{1}{T} \frac{\partial T}{\partial \mathbf{r}} \right] \tag{4-93}$$

Several authors have reported on the use of the BE to solve the thermal transpiration problem. Siu [238] used a modified form to determine the pressure limits of thermal transpiration. In 1978, Storvick [254] used the BGK solution method to compare his experimental results for the thermomolecular pressure difference for a variety of gases. Recently Takata [259] derived a method to separated gases using the BGK solution, however, he reports the model gives erroneous results. The gas separation idea was originally submitted 40 years earlier by Gilliland [91] who

performed Reynold's experiments through porous solids. Ohwada [195] and Chen [42] derived a solution to thermal transpiration using the linearized BE for highly rarefied gases. Bahukudumbi [15] also used the linearized BE to predict lubrication in air resistance slider bearings.

CHAPTER 5 DIRECT SIMULATION MONTE CARLO

5.1 Introduction

Direct Simulation Monte Carlo (DSMC) [7] is emerging as the favored analysis tool for the study of rarefied gases. When compared to other numerical solutions of mathematical models, DSMC has an advantage in that numerical instabilities are absent because the model simulates the physics of the real gas. The drawback to using DSMC is the exaggerated scatter caused from the model using simulated molecules to represent a large number of real molecules. In order to achieve accurate results in the continuum regime, a large number of particles would be needed which would drive the computational cost to levels which might not justify the method. However, when the critical dimension is small and/or the Knudsen number is large, the number of simulated molecules approaches the actual number of real molecules in the system. This leads to higher accuracy and can even simulate fluctuations present in the real flow.

Thermal transpiration (or thermal creep) demonstrates this situation because the phenomenon occurs when the channel size is on the order of the mean free path of the gas. Thermal transpiration is the unique phenomenon of gas molecules flowing through a channel from a cold region to hot region and creating a thermomolecular pressure difference (pressure difference caused only by the thermal gradient along a channel). The only requirement is the gas must be rarefied enough so that wall collisions are more dominant than inter-molecular collisions.

Bird's DS2V program uses the DSMC method and can be applied to a variety of gas flow situations. It has the added advantage that it can be run on a single computer which makes it available to all groups of users. DS2V employs the use of separate sampling and collision cells to evaluate the flow and has an adaption method to adjust the collision elements based on the density of particles. Presented below are the results of the DS2V simulations showing the pressure distributions along the channels at various levels of rarefaction in the slip-flow, transition, and free molecular regimes. Mass flux data under no pressure gradient is also given as a function of Kn.

5.2 DSMC – A Review

Monte Carlo is one of many computational simulation techniques used to study physical systems. It derives its name from the Italian city where the 'games of chance' have a similar characteristic of random behavior. It is this unique characteristic that separates Monte Carlo from other methods. The simulation process is stochastic meaning each successive step is randomly determined by taking a sample from a probability distribution. Other methods are typically deterministic whereas Monte Carlo is probabilistic.

The first use of a Monte Carlo technique in small tube flows was done by Davis [56, 40] to calculate rarefied molecular flow rates through pipes of various shapes and sizes. He described a method of calculating flow rates in complicated connectors in

vacuum systems, which were not complicated by the difficulties of evaluating complicated integrals introduced by Clausing and Lorentz.

Seven years later, Ward [276] developed a Knudsen cell and studied the vapor emission distribution from it. The results from both experiments and the Monte Carlo calculations were in agreement with the cosine law/distribution. Beijerinck et. al. [19] used the same method to study the random walks of molecules under free molecular flow in tubes. Their work compared favorably with the cubic approximations of DeMarcus and gave approximations of the wall collision rates, transmission probabilities and angular distributions. Adamson [2] used the test-particle method to look at thermal molecular beams. Bird [27, 28] was the first to introduce what would eventually be called Direct Simulation Monte Carlo (DSMC) in 1963 as a method to study the velocity changes of gas approaching a state of equilibrium. His values agreed favorably with the work of Alder and Wainwright.

DSMC solves the Boltzmann equation [190, 273] for fluids by using individual simulated particles (or molecules) to model the behavior of thousands of real molecules. These simulations are very useful due to their simplicity and great speed. One of the key components for this method to work involves de-coupling the motion and collisions of the molecules. This procedure is outlined in greater detail below.

DSMC began to emerge as a prominent component of gas simulation in the late 1980s and early 1990s. While, the initial demand was primarily for rarefied gas dynamics as it relates to hypersonic flows [44] and shock waves [186, 67], two concurrent factors began to draw the attention to other areas. The first was the growing interest and development of microfluidic systems and nanotechnology. Within a short time the scale lengths of fluidic channels were on the order of the mean free path of the gas which introduced new phenomenon as well as new problems to solve. In 1992, Piekos [208] outlined the viability of using DSMC for MEMS analysis by simulating microchannel flows in the slip-flow and transition regimes as well as through a micro-nozzle. His work was based on the work of Arkilic [12-14] who studied slip-flow problems through silicon microchannels. The second factor spurring the growth of DSMC was the improved speed of personal computers which opened the door for simulations of continuum flow (and the associated large number of molecules). Oran [202] presented a good summary of many other applications of DSMC in the early and late 1990s. In the decade since that time, DSMC has been used to study all types of gas flows including gas mixing, chemical reactions, flow through nozzles, aerosols, filters, vapor depositions, shock, hypersonic flows, air bearings [80], etc.

In the arena of micro-flows, Gallis, Rader, and Torczynski [83-84] reported on thermophoresis in rarefied gas flows. Their work studied both monatomic and diatomic gases and the forces applied to the particles by the thermal gradient created between two plates at different temperatures. They later extended this work by

determining the velocity distribution of molecules in near continuum conditions under Fourier and Couette flow conditions. Park [206] also studied Couette flow under time-periodic oscillatory conditions. In 2001, Wu and Tseng [282] ran simulations on low Knudsen number flow through tubes, t-channels, and along surfaces such as those on a hard drive. Sun [256] also performed similar work with a focus on the effects of compressibility, rarefaction, and surface roughness. He presented axial pressure distributions, velocity profiles, and friction coefficients as a comparison to experimental data. His DSMC simulations confirmed that rarefaction didn't affect the pressure distribution but changed the slip at the wall in slip-flow and transition regime flows. Aoki [11] presented an analysis of the flow induced between two coaxial elliptic cylinders. Wang [275] also studied micro-geometries of low-Kn flow with the addition of Poiseuille flow through orifices and around corners as did Shinigawa [235]. A similar work was performed by Alexeenko [7] who studied how flow rates and pressure losses were impacted by constrictions in the micro-channels. She validated her results to Arkilic's analytical expression for mass flow rate in slip-flow. It is her conclusion that Navier–Stokes equations may be used with reasonable accuracy if the surface velocity-slip conditions are appropriately modified. In Prasanth's review [212], however, he argues that as the rarefaction increases and flow go into the transition regime, the Navier-Stokes equations yield poor approximations to the physics of gas dynamics as they relate to transport terms for mass, diffusion, viscosity, and thermal conductivity.

It is this area (transition and free molecular regimes) which is of primary interest and more specifically the simulations of micro-channel flows under a thermal gradient. In 1997, Mavriplis [172] conducted a study of heat transfer in short microchannels. Using pressure boundaries at each end of the channels, he determined the temperature gradient and heat flux in the channel for various wall temperatures. In one simulation, he divided the wall into alternating segments of temperature jumps. This was possibly the first DSMC study of a non-isothermal flow through a microchannel and was performed on a personal computer. In 1998, Wong [280, 281] performed a preliminary study of thermal transpiration. While not a complete discourse on the subject, it showed that DSMC was a feasible option for studies of this type of flow. Nishizawa [193] performed a DSMC analysis of thermal transpiration of a capacitive diaphragm gauge. For his system the cosine law distribution was insufficient to describe the real effects as it produced a high pressure area along the central axis of the channel. Alexeenko [8] studied thermal transpiration in microchannels using the SMILE DSMC code. She chose 5 Knudsen numbers between 0.05 and 50 to study the effect of a single pressure ratio and multiple temperature ratios on the flow. For the solely temperature driven case, she used both step-wise, linear, and non-monatonic temperature gradients on the walls. While the difference between the step-wise and linear was negligible in terms of overall pressure difference, there was an expected temperature jump on the step-wise interface. Her work presented another preliminary study of thermal transpiration, however, the mass flux results presented were for a single Knudsen value of 0.2. Her equivalent 2D number flux was 6.8E19 molecules/s.

Papadoupoulos [205] and Masters [170] both looked at thermal driven flows, however, their results are for enclosures and couette systems only and do not deal with flow through channels. This current work presents a DSMC analysis of the mass flux and pressure ratios resulting from thermal transpiration in short microchannels at a wide range of Knudsen numbers.

5.3 DSMC Procedure

There have been several new modifications [202, 162] and techniques developed recently in the DSMC method, however the basic principle remains the same. Our simulations used Bird's technique and it was his expertise and advice that enabled us to obtain the results shown below. Now, Direct Simulation Monte Carlo (DSMC) Technique involves four main steps:

1. Motion of the particles
2. Indexing and cross-referencing particles
3. Simulating collisions
4. Sampling macroscopic characteristics of the flow

The flow field is divided into small cells similar to a finite-volume method of analysis. The cell size should be on the order of 1/3 the mean free path and the time step is about half that of the mean collision time. The analysis involves a simulation of particle motion rather than mimicking the real motion.

The first step is to move the particles. During this step there will be interactions with the boundary so boundary conditions must be known which include accommodation coefficients. At this time it is necessary to include any outside

forces and other physical phenomena included the analysis. The second step is the key step in the DSMC method. Molecules have moved since the last position so these individual positions must be indexed. Since the number of particles is extremely high, it is important to efficiently record the motion of particles into and out of each individual cell in the flow field.

The third step is to simulate the particle collisions using a probabilistic method. This is typically a collision model called the no-time-counter technique which calculates collision rates within the cells and collision pairs within subcells. This method improves accuracy by ensuring the collisions occur between cell neighbors. The fourth step is to calculate the macroscopic properties of the flow at each cell center. Steady flow conditions can be time and space averaged and unsteady flow characteristics can be obtained by ensemble averaging independent calculations.

There are a few limitations and errors associated with the DSMC method:

1. Finite Cell Size: The size of the cell should be around 1/3 that of the mean free path. If the cell is larger then there develops unusually high viscosity in the analysis due to undeveloped diffusion parameters. If the cell size is too small then many of the cells will not have particles in them and the statistical results will be skewed.
2. Finite Time Step: The time step must be sufficiently small to assure particles do not go through more than one cell at each step, otherwise, collisions could be missed.

3. Ratio of simulated particles to the Real Molecules: Typically each particle represents 10^{14} to 10^{18} molecules. This can be too high if there are any sort of complicated dynamics. If the ratio of simulated particles becomes too high, then the statistical scatter of the solution is increased.
4. Boundary Condition Treatment: The inflow and outflow boundary conditions are especially important. Typically the number density, temperature and average velocity should be provided at both the inlet and the outlet. This will significantly reduce the undesired numerical boundary layers at these regions. Also, for high Knudsen numbers, it is important to determine the influence a body in the flow has with relation to particles in the inlet or outlet.

5.4 A comparison of Methods

There has been much discussion over the best method to analyze gas flows in microchannels especially gases that are dilute. Proponents of Navier-Stokes (NS) [5, 34, 68, 218, 271, 278], Molecular Dynamics (MD), the Boltzmann Equation (BE) solutions (i.e. BGK, S-Model, etc.) and Direct Simulation Monte Carlo (DSMC) tend to champion their method while outlining in detail the short-comings of opponent methods. It has become apparent to the author that there is not a single method for all gas dynamic solutions. There is therefore not a need to rigorously align oneself to a single method but to understand each method and apply it to the application which suits it best. Since the focus of this work concerns DSMC, we will begin with an analysis of this method and explain why it is probably the best method to characterize thermal transpiration in microchannels.

As mentioned above, DSMC traces and calculates the motion of hundreds of thousands of particles to determine the macroscopic quantities of the gas. While similar to MD, it is different in that a single particle represents many molecules instead of the one-to-one relationship in MD [46, 47, 26, 6]. Since MD is based on classical mechanics and Newtonian physics it is valid for all flow regimes, however it can become impractical for many flows due to the number of simulated molecules. DSMC, on the other hand, brings a reduction in the total number of particles and reduces the computational time, however, it can still be computationally intensive compared to some methods and the particle-to-molecule ratio introduces a statistical scatter.

For dilute flows, the Boltzmann equation is often a good options since it is based on a physical interpretation of a real gas and can be solved with great speed. The problem lies in the nonlinear collision integral which is difficult to solve for all but the simplest problems. The way to solve the Boltzmann equation then is to linearize or modify the collision integral. The most common approach is to apply the Bhatnagar-Gross-Krook modification, which is based on an expansion of 1/Kn. The BGK equation is thus most accurate for problems in which perturbations are small and boundary conditions are prescribed in terms of equilibrium distributions. One drawback with the BGK method is it doesn't represent highly non-linear problems and it doesn't accurately represent flows with both viscous and thermal forces. This results in a predicted Prandtl number of 1, rather than a value close to

2/3 appropriate for a monoatomic gas. It is thus important to take great care when calculating flows involving heat transfer as in the case of thermal transpiration. The S-model modification to the BE collision integral seems to have fixed the thermal/viscous problem however it is still too rigorous of a calculation to solve the integral for anything other than simple geometries.

The linearized Boltzmann equation is often used when the flow is somewhere between the free molecular and slip regime. In the slip regime the Knudsen layer is limited to the region of the wall typically within the distance of a mean free path. While the Navier-Stokes equation models the bulk flow away from the walls the model breaks down in the "slip" layer [97, 295]. Thus, the solution is often derived using a dual-solution method where a Navier-Stokes technique is used in conjunction with a kinetic boundary layer "correction". In this case the solution can be obtained using asymptotic approaches for the linearized BE. It is important to note that the solution leads to an "effective" boundary condition [24, 241] that opponents to the NS method for this regime call a "correction factor" [4].

Now, several sources have determined the criterion for failure of the continuum regime to be Kn>0.05. Thus, as the gas becomes more dilute and moves from the slip regime to the transition/free molecular regimes, the Navier–Stokes equations break down even more since there are more manifestations of temperature jump and velocity-slip. The reason for this is that the constitutive equations that relate the shear stress and heat transfer to other variables break down. More specifically, the

linear transport terms for mass, diffusion, viscosity, and thermal conductivity in the partial differential equations are no longer valid. Thus, the flow of a dilute gas require a kinetic-theory description/method which points to DSMC as one of the most likely candidates.

DSMC is widely used when macroscopic gradients can no longer be considered small in comparison to the mean free path. The first advantage of DSMC is it brings a physical model of the gas itself which lacks any numerical instabilities that occur in other numerical solutions of a mathematical models. Second, it also has a simple enough algorithm which allows for straightforward incorporation of higher-order physical models and for application to complex geometries. While it avoids the difficulties involved with the collision integral in the BE, it has been proven to be equivalent to solving the Boltzmann equation for a monatomic gas undergoing binary collisions (since this is the limit of the BE) [190]. Opponents of DSMC identify some concerns with statistical scatter, random walks, and other types of errors unique to this method so these are now discussed in greater detail.

5.5 Errors in DSMC

Because of the stochastic nature of DSMC, there are statistical errors that make the method less attractive. These errors depend on the selection of numerical parameters such as the time step, cell size, number of samples and the total number of simulated particles. Both the cell size and time step [87] should be suitably chosen so individual particles do not pass completely through a cell in a time step so as to miss

a possible collision with another particle. Care should also be taken to avoid repeated collisions within a cell since studies have shown that the fraction (>20%) of repeated collisions is a reliable indicator of deviation of simulation [212]. Bird introduced the ratio between the mean collision separation (mcs) and the mean free path (mfp) as the key parameter to determine the quality of a simulation which in turn stipulates the time step and cell size. As long as mcs/mfp << 1 the calculation should be accurate. This ratio can be reduced by adding more simulated molecules assuming cells are small enough to maintain the "nearest-neighbor" collision. Another consideration to the cell size is with regard to sampling. If macroscopic properties are sampled for every cell the database becomes cumbersome. For most applications the sampling resolution doesn't need to be this fine so separate "Sampling" and "Collision" cells are used conjunctively and are completely independent of each other.

While this is an advantage of DSMC, care must be taken because a particle is often sampled several times with the same property in one cell before it collides with another and changes its properties. The collision rate thus can be one measure of the statistical error in the simulation. However, the collision rate can vary greatly in a flow field, so it is more difficult to analyze the statistical error. This is also complicated by the fact that statistical errors also depend on the models employed for intermolecular interaction. Chen [43] reported that the errors are the smallest for hard sphere interaction, since this model produces the highest collision rate. This

error is altogether eliminated in collisionless flows where the only error is due to the number of molecules used for averaging.

To find a solution for the DSMC method, the macroparameters of a flow are obtained by averaging particle properties over a certain number of time steps. The source of the statistical errors is the process of taking a sample average in a finite volume. Since they represent different moments of the distribution function, it is expected that the density (the zeroth moment), Temperature and Pressure (second-order moments), and other parameters will show different forms of fluctuation and errors. Still, the errors have an asymptotic behavior so that as the contribution of each cell is accumulated and averaged over time the correct solution should be achieved as the sample size goes to infinity (which some have termed "convergence").

One example of this error has been well documented in analysis of low-speed flows [86, 98, 265, 69]. From above, we know the velocity can be divided into two components, the peculiar velocity and the bulk velocity. It is entirely possible that the error in the peculiar velocity of a flow could be greater than the velocity of the bulk flow even to many orders of magnitude. This signal-to-noise ratio would be much less than 1 which is unacceptable. This error is inversely proportional to the sample size, and can be reduced by increasing the sample size by either increasing the number of particles in the computational domain or increasing the number of time steps used in the sample. If we look at a low-velocity flow with a high number

density it would take an enormous number of timesteps for a particle to make one complete pass through the entire computational domain so the only course of action would be to increase the total number of particles.

This leads to a discussion of the number of particles used in a simulation or more specifically, the particle-to-molecule (ptm) ratio. The statistical scatter from the ptm ratio is assumed to follow the Poisson distribution with a standard deviation on the order of the inverse square root of the sample. The advantage of using DSMC with microflows is that even with dense flows, the size scales of the channels are typically such that the ptm ratio approaches 1. In this setting, the scatter and errors in other simulation techniques are numerical, however with particle based methods (like DSMC) ,Garcia [85] proved it is a physical phenomenon. Fluctuations in the simulation proved to be an accurate model of real fluctuations in the actual gas. Because of this, we see that in regard to thermal transpiration in microchannels, DSMC goes beyond the capability of the NS and the BE.

CHAPTER 6 2-D DSMC SIMULATIONS AND RESULTS

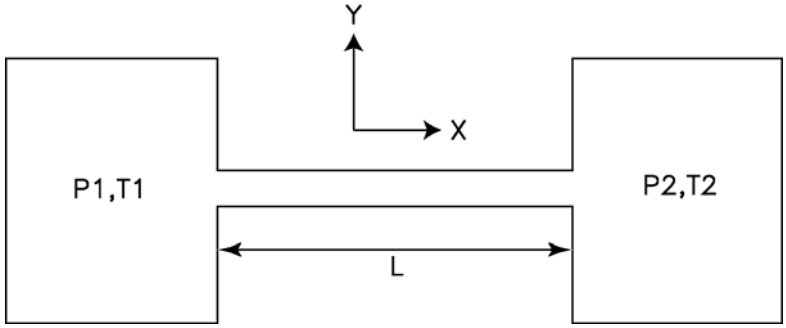

Figure 6-1: Channel Layout

Figure 6-1 shows the geometry used for all of the DSMC simulation studies. We use a modified form of Bird's DS2V program which is for use on a personal computer. All simulations were run using a processor ranging from a 3.1GHz dual core to a 4.0GHz quad core where each simulation took between 24 hours to approximately 7 days to achieve sufficient samples. The channel size is 500nm long and 100nm wide. The channel is divided into sampling and collision cells so there are approximately 8 particles per collision cell and 8-15 particles per sampling cell.

Symmetry was used to reduce the computational time of the model so the centerline of the channel is used as the axis of symmetry. At the cold (left) end of the channel is a reservoir of molecules at temperature T_1 and another reservoir at the hot end at temperature T_2. Diffuse reflection on the wall is used for the surface interaction calculations and the wall has a continuous gradient along the channel wall from T_1 to T_2.

The molecular velocity distributions are based on Argon using the VHS collision model. The values for reference diameter (4.17E-10m) and molecular mass (6.65E-26kg) were taken from Bird (Bird 1994).

The first set of simulations performed concerned closed system cases. The walls in each reservoir were kept at constant temperature and the temperature gradient boundary condition along the channel walls is incremented in 1% steps. The Knudsen number is entered as an initial condition for the entire flow by iterating on the number density.

A closer look shows that the Knudsen number is a ratio of the channel width to the mean free path of the gas.

$$Kn = \frac{\lambda}{d} \tag{6-1}$$

Thus, only one of these parameters needs to be changed in order to vary the flow conditions. For simulation purposes, the former value is more difficult to iterate because it requires a new geometry and mesh for each simulation. It is important to use a sufficient number of divisions within the geometry since the collision and samplings cells are derived from the divisions. By varying the mean free path, only the initial number density needs to be changed which is a much simpler process upon which to iterate.

The second set of simulations involve an open system with constant pressure boundaries at both ends. An imaginary boundary line of constant x is placed at the middle of the channel. This line divides the flowfield into two distinct sections each with their own initial conditions. The molecular flux in the channel is determined by calculating the net molecular flux across this boundary. The reservoir walls at the extreme ends of the x-axis are kept at a constant pressure which maintains the initial pressure value. At these walls new molecules are introduced/removed at the same rate as those crossing the middle discontinuity. The remaining reservoir walls are kept at constant temperature so neither a temperature nor pressure gradient in the reservoir can effect the flow in the channel.

As with the closed system, the Knudsen number is varied using the number density initial condition. In the open system, however, the average number density of the two sides of the channel is kept constant. This allows the number density on each side of the boundary to be varied creating a set of pressure ratios and pressure differences for a single Knudsen number.

The output from the DSMC simulation is in the form ASCII delimited text files. The text files consist of either macroscopic state data for every sampling cell in the flowfield or the surface properties of each surface cell. Surface plots of the flowfield data and linear property profiles (i.e. pressure, number density, x-velocity, etc.) taken from two points in the flow can also be created and exported. With the exception of the flowfield plots, the data was taken from the surface and flowfield

output files. Scripts were used to compile the data from multiple simulations and plot the results.

6.1 Results

6.1.1 Closed System

The results from the closed system show a nice flowfield translation temperature distribution (Figure 6-2). The temperature divisions are uniform across the width of the channel. If we look at how the pressure ratios vary with Knudsen number (Figure 6-3) the

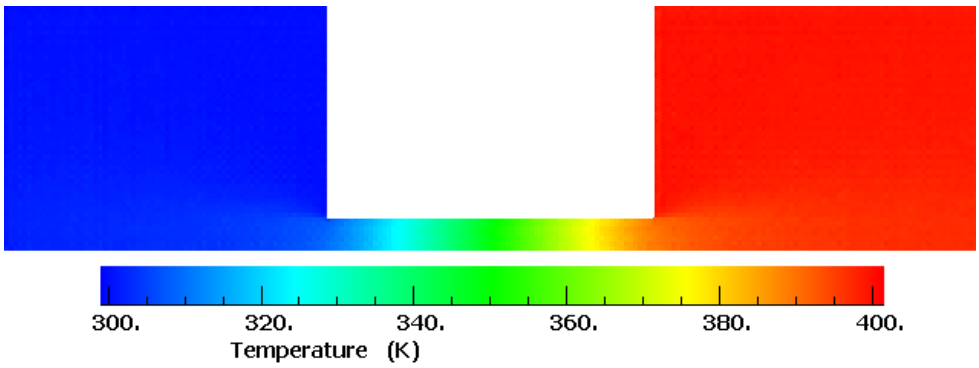

Figure 6-2: Closed Flowfield Temperature Distribution (T=300K thru 400K)

lower data points represent a temperature gradient from 300K to 400K and the upper ones 300K to 600K. As the Knudsen number approaches a continuum (denser) flow the

pressure ratio approaches unity where there is no change in pressure across the channel. It is this area where molecules are sufficient in number to transfer energy through the channel via inter-molecular interactions. As the rarefaction increases

(Kn approaches infinity) the pressure ratio approaches an asymptote equal to the square root of the

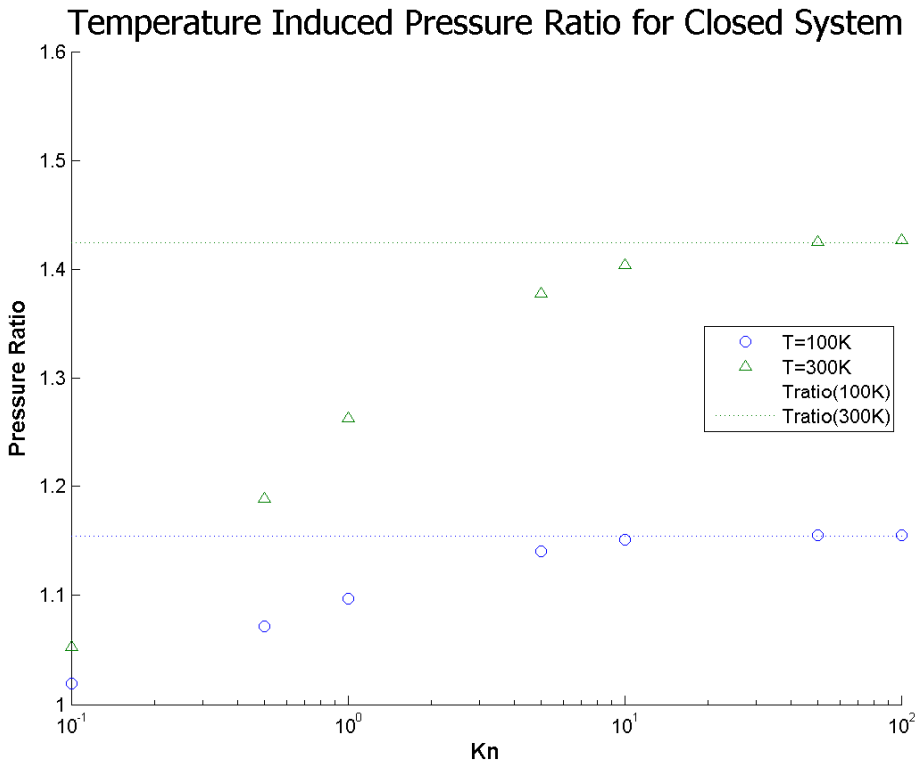

Figure 6-3: DSMC Simulation: Closed System Pressure Ratio for Various Knudsen Numbers

temperature ratio (represented by the horizontal lines).

$$\frac{P_1}{P_2} = \sqrt{\frac{T_1}{T_2}} \qquad \textbf{(6-2)}$$

This equation is commonly used to quantitatively describe the pressure increase when referring to thermal creep and was first derived by Knudsen. This maximum value has some inherent conditions. First, the rarefaction must be such that the mean free path is greater than 10 times the characteristic width of the channel and second the flowfield must be closed. As was mentioned above, the greater the rarefaction, the greater the thermomolecular pressure. Regarding the latter criteria,

any outside influence causing a change in an intrinsic property changes the pressure ratio. Should the flowfield be opened, the pressure ratio would decrease due to the transmission of molecules through the channel.

While the pressure ratio is the most common way describe the thermomolecular pressure change, a more useful view is to look at the pressure difference (Figure 6-4). The log-log plot shows a plateau in the denser regions and a continual drop as the rarefaction increases. In this view, both temperature profiles run in parallel with the same slope in the regions of higher Knudsen number.

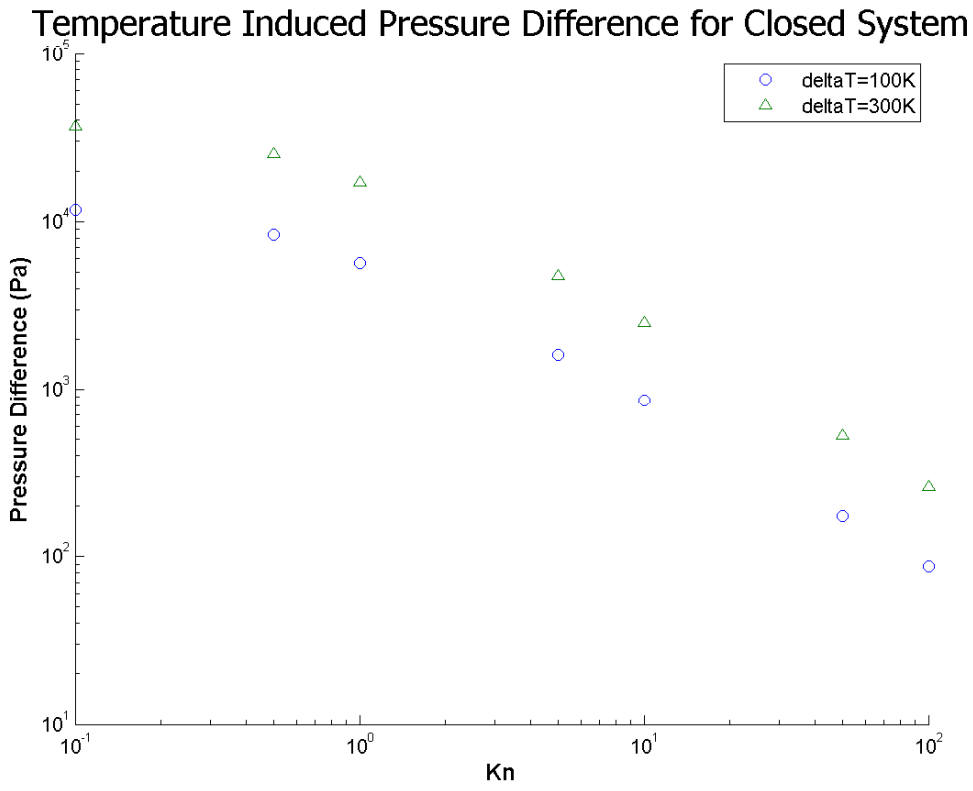

Figure 6-4: DSMC Simulation: Closed System Pressure Difference for Various Knudsen Numbers

6.1.2 Open System

The second set of results deals with this open system of channels. As mentioned above the reservoir boundaries were set as constant pressure boundaries which allows a transmission of the molecules. For each Knudsen number 6-10 different pressure ratios were set as initial boundary conditions. The temperature gradient was kept as a boundary condition along the length of the channel walls. Each series of simulations produced a set

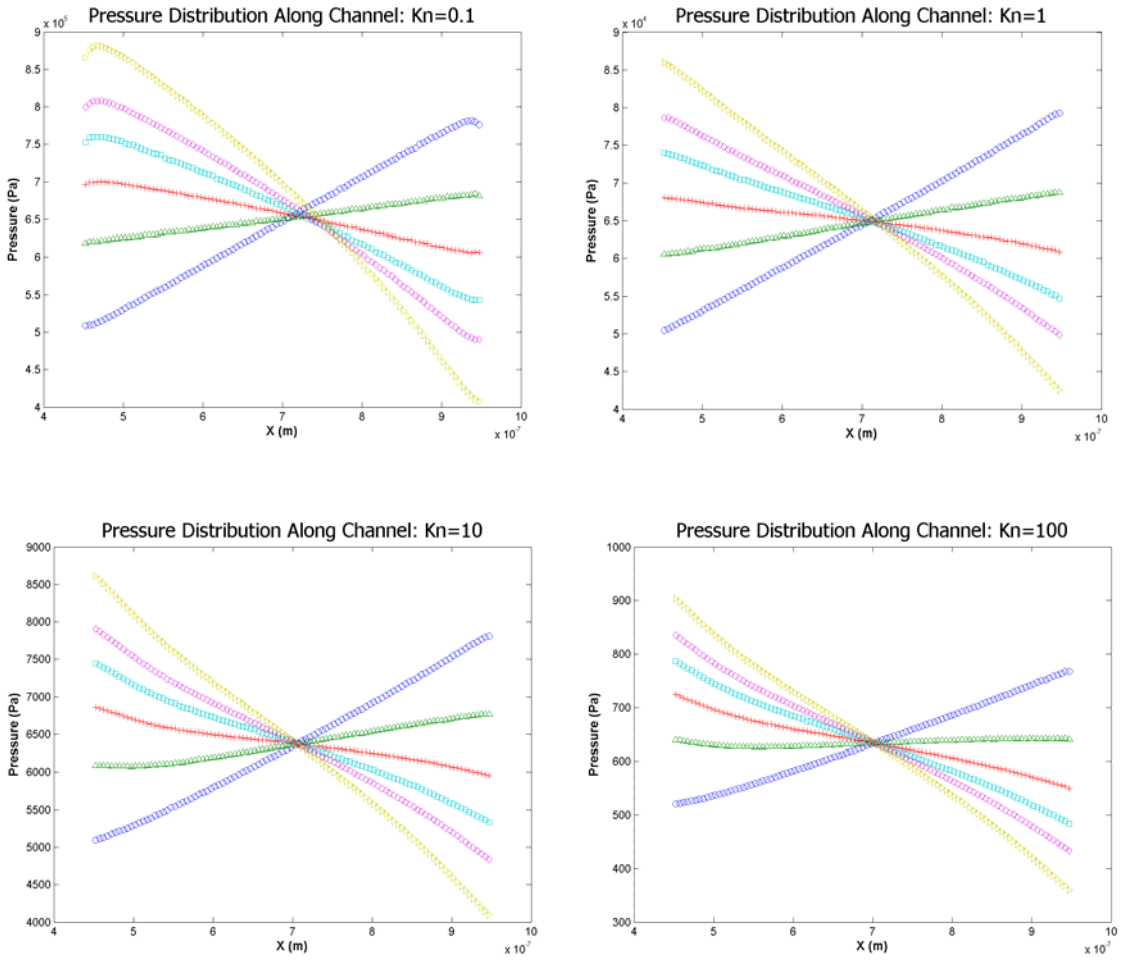

Figure 6-5: DSMC Simulation: Pressure Distributions Along Channel

of pressure curves along the length of the channel (Figure 6-5). While a larger number of simulations were run, only Kn=0.1, 1, 10, 100 are shown. A closer look at the plot shows

how each curve intersects at P_{avg}. There is a little bit of translation of this intercept in the lower Knudsen number plot that corresponds to a slight shift due to the motion of the flow through the channel. This does not result in a change in average Knudsen number, just a minor change in the location of the average pressure. The stream pressures also contribute to the slight curve at the channels ends where the stream returns to the steady state of the reservoir. We believe these are the first DSMC simulation results with both pressure and temperature differences between the two channels.

Figure 6-6 and Figure 6-7 show the velocity profiles for the channels at a variety of pressure ratios between the two reservoirs. The first shows the profile for a Knudsen number equal to 0.1 which is at the edge of the slip-flow and transition regimes. The velocity profiles are well characterized although there is a greater scatter at the lower speed flows. This is caused by the error described in section 5.5 where the lower speed flows have a greater scatter due to the signal-to-noise ratio of the peculiar velocity compared to the bulk velocity. There is also contribution of the scatter due to the high ratio of simulated particles to real molecules. Compared to the free molecular regime, the number of molecules is increased by at least 2 orders of magnitude.

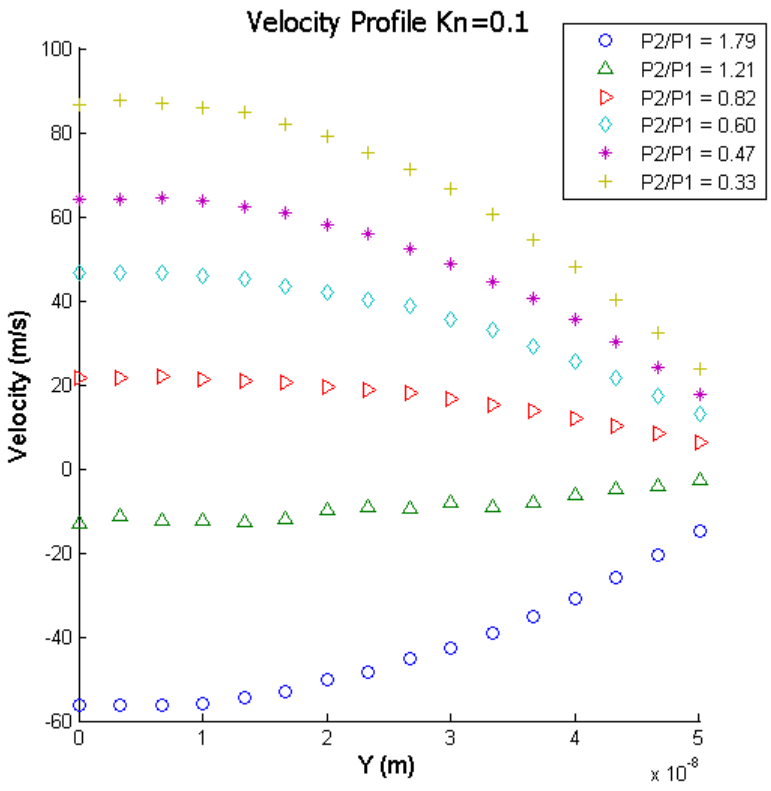

Figure 6-6: DSMC Simulation Results: Velocity Profile for Kn=0.1

Figure 6-6 shows the velocity profile for a Knudsen number of 10 where the gas is more dilute. Notice the increased scatter compared to the previous profile. The rarefaction of the gas contributed to this scatter since there are fewer molecular interactions but there is also the contribution of the peculiar velocity. The way to increase the accuracy of this result is to 1) increase the number of molecules to reduce the particle-to-molecule ratio and 2) run the simulation longer to collect more samples.

Data for the net flux of molecules crossing the middle boundary was also collected for each of these simulations. These data points were plotted versus the pressure difference

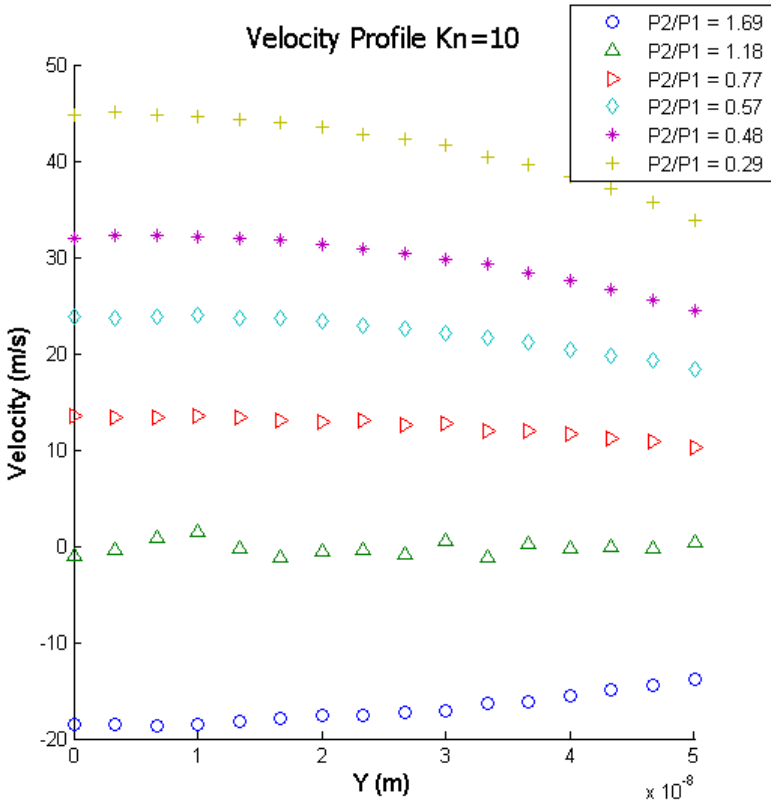

Figure 6-7: DSMC Simulation Results: Velocity Profile for Kn=10

across the channel (Figure 6-8). The pressure difference was chosen rather than the pressure ratio because the response of the molecular flux to the pressure difference could be determined using a simple linear regression.

It is important to note that the line going through these plots is linear and does not go through the origin. The origin denotes a zero pressure differential and zero flux. The offset in these plots signifies the contribution of the temperature gradient to the

flow. It should also be noted that the offset increases with Knudsen number which supports the conclusions made with regard to the closed system.

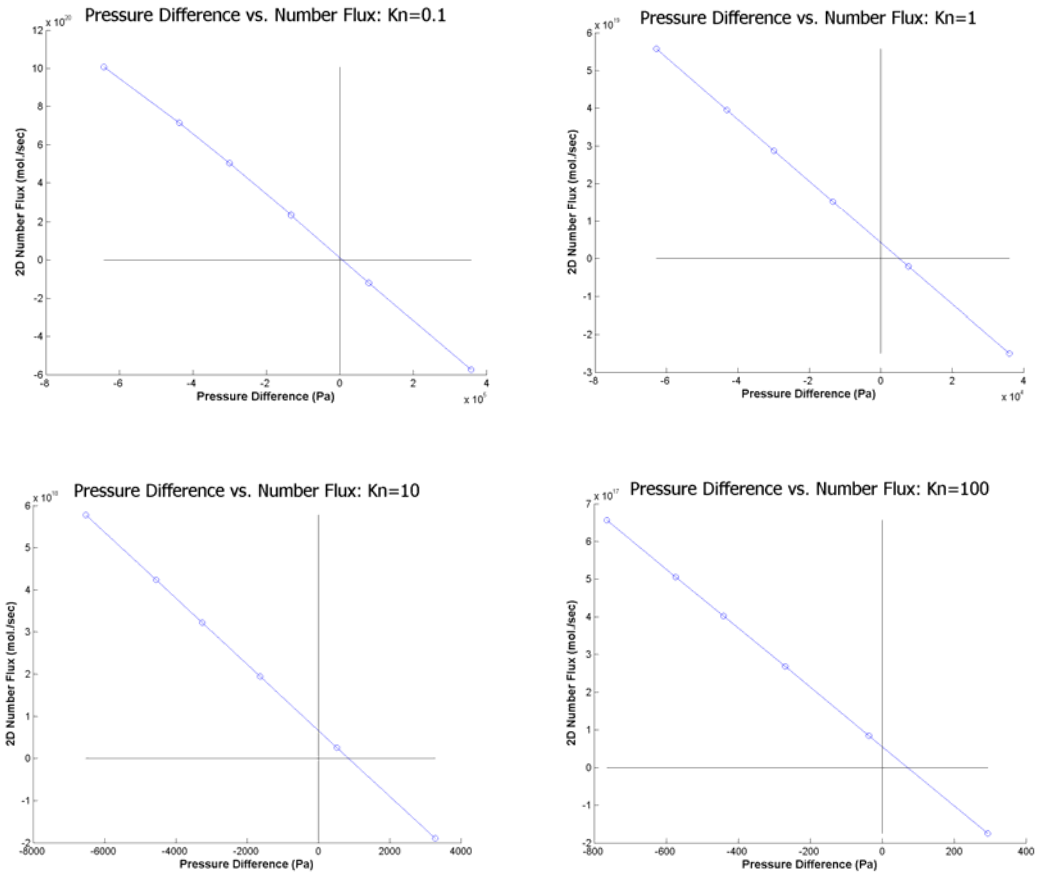

Figure 6-8: DSMC Simulation Results: Number Flux vs. Pressure Differential

The two key points on this plot are the intersections with each axis (x and y). The y-axis

is the molecular flux and the x-axis is the pressure differential. The y-intercept is the thermal molecular flux contribution when there is no pressure difference. This is the

maximum flux contribution from the thermal gradient that can be achieved. Any flux greater than this value has a pressure contribution. The intersection with the x-axis is the pressure differential for zero flux. This value would correspond to the pressure difference in a closed system. Now, the y-intercepts from the plots in Figure 6-8 are plotted for all Knudsen numbers in Figure 6-9.

Figure 6-9 shows the thermomolecular flux contributions when there is no pressure difference across the channel where each data point is representative of several simulation runs. All curves have the same channel width, however, they each have a different aspect ratio (2.5, 5.0 and 10.0). The maximum flux occurs around the transition between slip flow and the transition regime. As the rarefaction increases the number flux decreases which is expected since the number of total molecules in the system also decreases. Note the difference between the aspect ratios. The shorter channel (aspect ratio = 2.5) has a marked increase in flux. This can be attributed to a lower chance of molecular interactions and lower occurrence of molecules reflecting off the channel walls and back from the direction they came. While an aspect ratio of 5:1 is considered a short channel, as the channel length decreases the flux value approaches the effusion case where the pore has a zero length (assuming the flow is in the free molecular regime). The 10:1 aspect ratio is considered the transition from short channels to long channels. Under this aspect

ratio, end effects become more pronounced as the channel shortens. DSMC provides a great tool to include these effects to the flow without having to provide a special case for the inlet and outlet.

The thermal creep phenomenon has been described as the result of a "shear force" of molecules acting on the surface due to a change in temperature. Loyalka[157] reported that the tangential momentum accommodation coefficient (α_p) had no effect on the flow and the energy accommodation coefficient (α_E)had a slight effect on the flow. Our results show a slight increase in flow with a change in α_p while keeping α_E=1. Figure 6-10 shows the effect of slight (α=0.8) specular accommodation in a channel. In terms of momentum, full specular reflection should acts more like the effusion model since the walls will

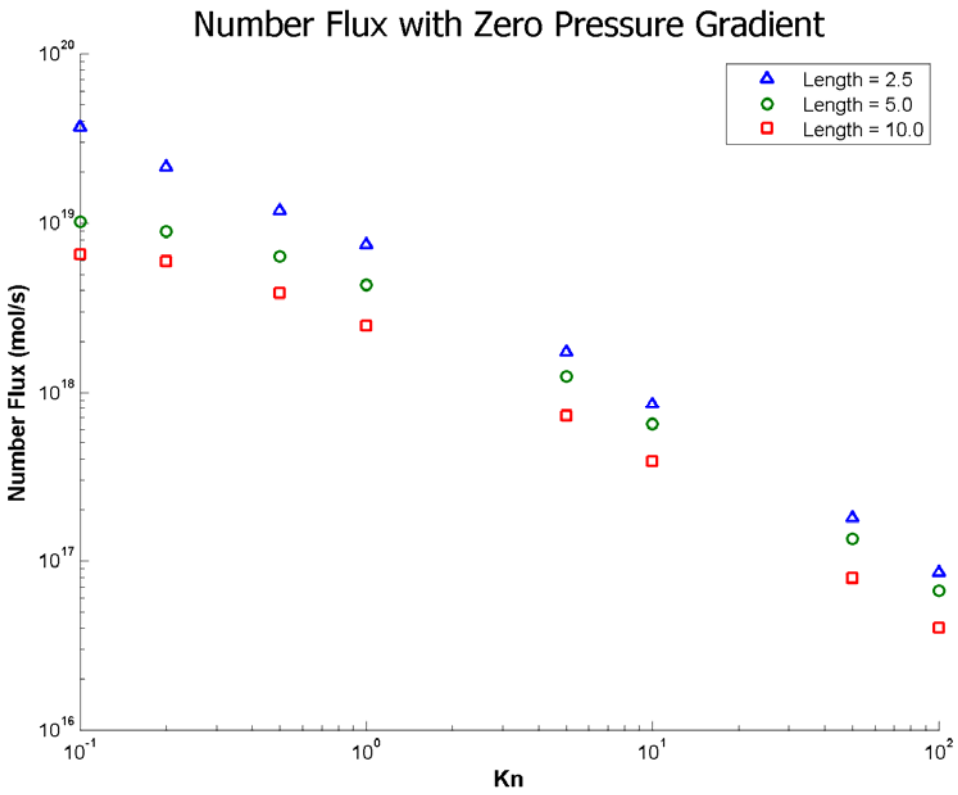

Figure 6-9: DSMC Simulation: Number Flux with Zero Pressure Gradient

create a change in tangential velocity to the molecule. Under the conditions below the majority of walls impacts result in diffuse reflection; the rest are specularly reflected which are the collisions contributing to the increase in flux. These results show the effect of the walls declines in the denser regimes.

Another plot of interest is the pressure difference when there is no number flux as shown in Figure 6-11. This would occur in a closed system where molecules could not enter or exit. Once again the maximum is near the boundary between the

transition and slip-flow regimes although it is slightly more rarefied. This graph is important because it shows the region where the highest pressure would occur.

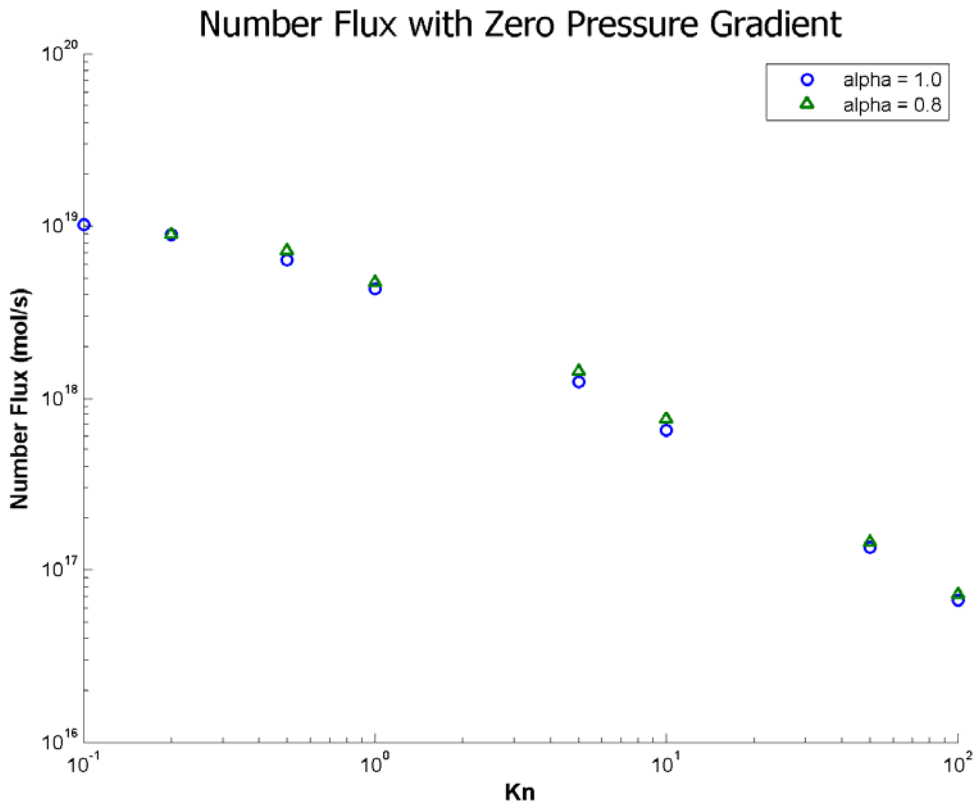

Figure 6-10: DSMC Simulation: Number Flux with Zero Pressure Gradient and Different Accommodation Coefficients

To put our results into a context with existing results in literature we have plotted (Figure 6-13) the reduced mass flux values with BGK and S-model results from Loyalka [150] and Sharipov [232] and Sone [187]. In order to compare the results, the number flux results from the DSMC simulations were multiplied times the mass of a molecule to get the mass flux. The average values for pressure were determined by using the Knudsen

number to find the mean free path. The mean free path relates to the number

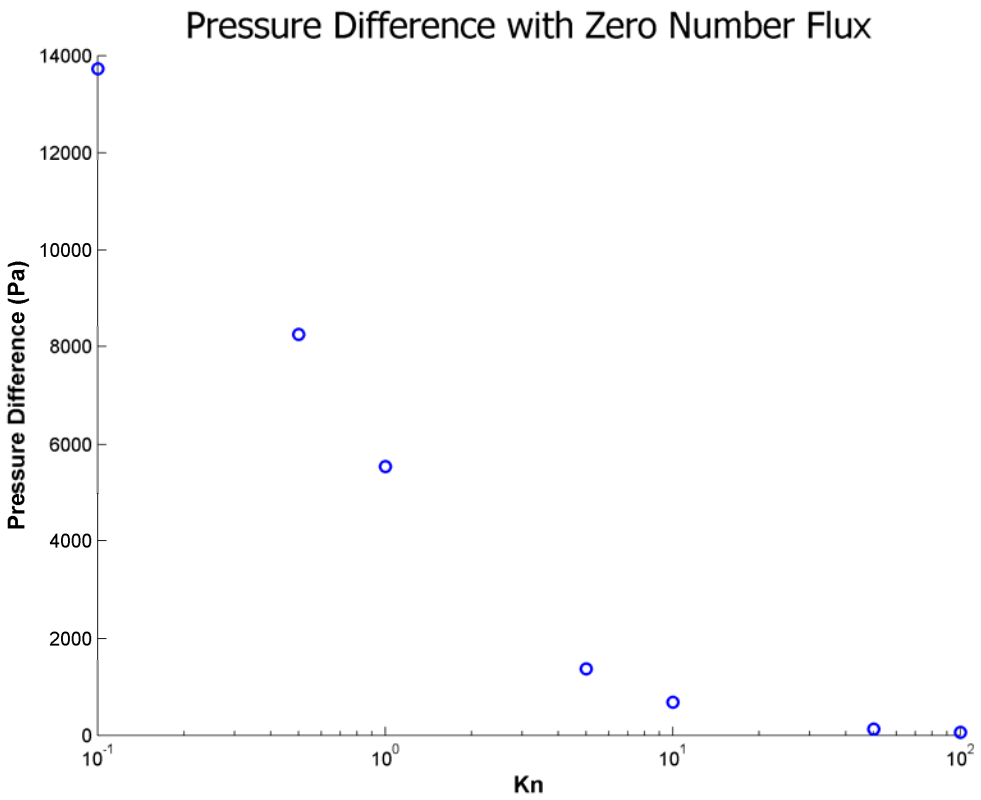

Figure 6-11: Pressure Difference with Zero Number Flux

density

which has a direct correlation to the pressure using Boyle's law. We took values for average pressure and temperature, width, molecular mass and length and substituted them into the following dimensionless equation [232, 187]:

$$G = G_{pressure} + G_{thermal} = \frac{1}{2} P_0 wA \left(\frac{2kT_o}{m} \right)^{-\frac{1}{2}} \left[\left(\frac{1}{P_o} \frac{dP}{dl} \right) Q_P + \left(\frac{1}{T_o} \frac{dT}{dl} \right) Q_T \right] \quad \textbf{(6-3)}$$

For a purely temperature induced flow the differential pressure component of the equation is equal to zero so only the terms on the right side of the brackets remain. Now, Solving for Q_T gives:

$$Q_T = \frac{2GT_o L}{P_0 wA\Delta T}\left(\frac{2kT_o}{m}\right)^{\frac{1}{2}} \qquad \textbf{(6-4)}$$

This gives the reduced thermomolecular mass flux, Q_T, which is independent of channel dimensions, pressure difference and temperature difference. In (6-4), P_0 is the average pressure, w is the width of the channel, A is the cross sectional area of the channel, k is Boltzmann's constant, m is the reference mass of the gas molecule, T_0 is the average temperature in the channel, Q_P is the pressure induced dimensionless mass flux and Q_T is the thermally induced dimensionless mass flux. The area value we use for our conversion is the channel width since the in-plane channel depth is unity. My values are shown in Table 6-1.

Kn	0.1	0.5	1	5	10	50	100
Q_T	.087	.236	.312	.456	.504	.546	.547

Table 6-1: Dimensionless 2D DSMC QT Values

The Both authors presented their results in the form of tabulated dimensionless mass flux values (Table 6-2 and Table 6-3). Loyalka's values were calculated using the BGK (Bhatnagar, Gross and Krook) solution to the Boltzmann equation and diffuse scattering along the walls (i.e. α=1). Sharipov used an improvement on the BGK model called the S-model solution. The S-model corrects the problems of the BGK

solution which cannot correctly calculate the viscosity and heat conductivity simultaneously.

The results shown in Figure 6-12 show a closer correlation to Sharipov than Sone and Loyalka. The discrepancy with Sharipov could be due to the decrease in particle-to-molecule ratio or the lack of sufficient samples.

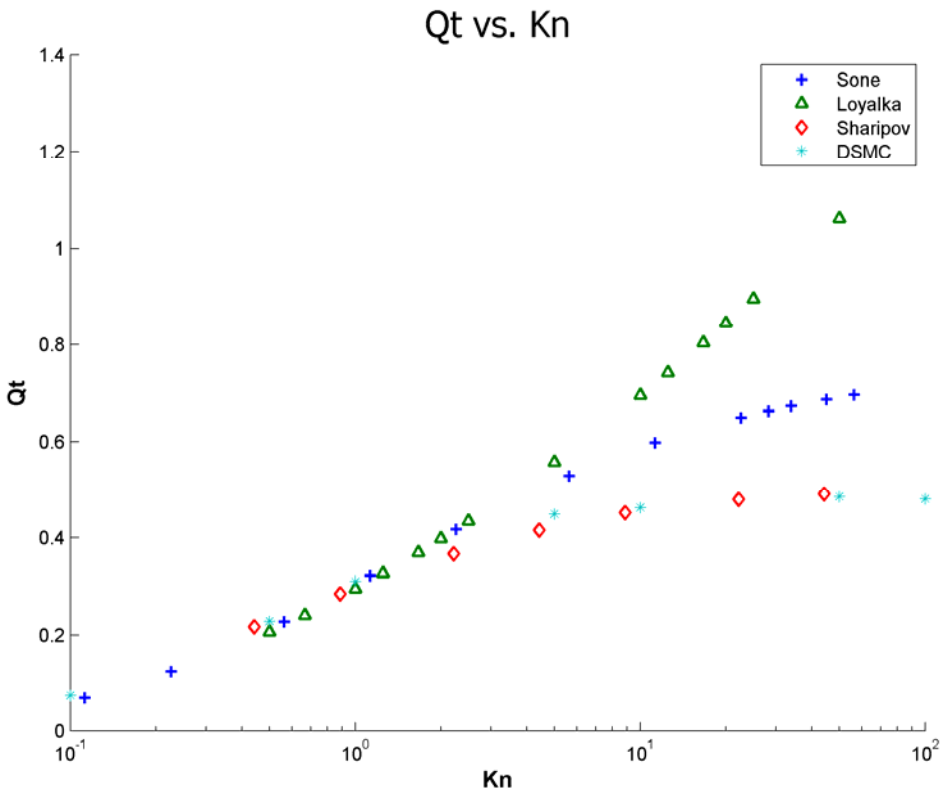

Figure 6-12: DSMC Simulation results: Reduced Thermo-molecular Flux Contribution (Q_T)

Loyalka's and Sone's results were for long tubes where end effects are negligible compared to the channel. These two curves were added because other authors have used them to validate simulation data through short channels. Based on my results, the other models do not predict the short channel flow sufficiently and only

correlate well to the intended model. Sharipov's results, however, are for short channels with fully diffuse reflection. Both the S-model and DSMC show a comparable response, the difference

Kn	**Q_T**	**Kn**	**Q_T**	**Kn**	**Q_T**
0.0564	0.0363	1.128	0.3217	28.209	0.663
0.0846	0.053	2.257	0.4171	33.851	0.6729
0.1125	0.0686	5.642	0.5294	45.135	0.6867
0.2257	0.1222	11.284	0.5975	56.419	0.696
0.5642	0.2272	22.568	0.6495	112.84	0.7179

Table 6-2: Dimensionless Q_T values from Loyalka's BGK solution

possibly being due to end effects of the channel flow. In some cases the differences arise based on the location where the Knudsen number is derived.

Kn	**Q_T**	**Kn**	**Q_T**
.44	.217	8.86	.452
.886	.285	22.12	.48
2.22	.367	44.3	.491
4.43	.416		

Table 6-3: Dimensionless Q_T values from Sharipov's S-Model

At this point it is important to note one area which initially gave erroneous results. The curves from the initial set of DSMC results presented Figure 6-12 represent two sets of simulation runs. The first set doesn't compare well at all with the results shown above.

One obvious discrepancy is the disparity in the slopes of the curves which suggests a problem with the DSMC flowfield. Figure 6-14 shows the flowfield for the simulation at two different Knudsen numbers and explains the reason for the disparity. In both cases the temperature gradient along the channel walls goes from 300K to 400K.

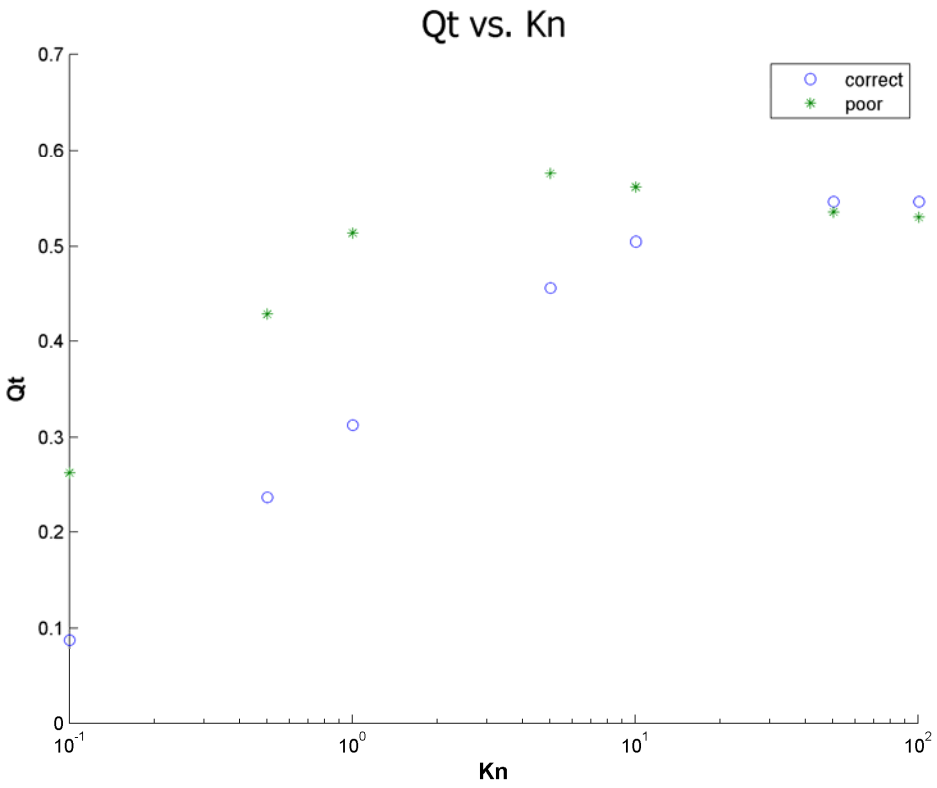

Figure 6-13: DSMC Simulation results: Error in Reduced Thermo-molecular Flux Contribution (Q_T)

Figure 6-14a shows the flow field for a Knudsen number of 0.2 with flow moving from left to right. The temperature gradient in the fluid is nearly a full 100K through the channel for this case. This is in contrast to Figure 6-14b which shows a lower gas temperature gradient for a Knudsen number equal to 50. The gradient in this case is closer to 50K which would explain the lower flux and pressure ratio values for the more rarefied flows.

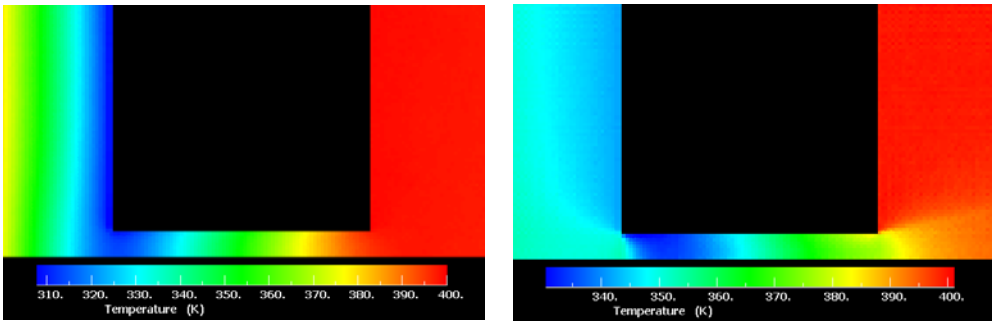

Figure 6-14: Flowfield Temperature a) Kn=50; b) Kn=0.2

The difference between the two is caused by an insufficient supply of molecules from the reservoir at the correct temperature. In Bird's DSMC program, the number of new molecules entering the stream is equal to the number of molecules crossing the imaginary boundary line in the channel. The temperature of the molecules entering the flowfield is equal to the initial flowfield temperature which is the average temperature. Where the pressure is higher (and thus more molecules), there is sufficient inter-molecular interaction to carry the surface temperature through the entire reservoir. In the more rarefied cases, the molecules don't interact enough to maintain the reservoir temperature.

While the dense case maintains a temperature gradient close to what is desired, it is unclear what affect this will have on the flux.

To prove this explanation, Q_T values of the DSMC data were calculated using equation (6-3) along with the geometric and state data. The flux values came from the DSMC results shown in Figure 6-9, however, rather than using the temperature gradient from the wall (100K), the flowfield gradient was uses. These values were extracted from the channel centerline for each simulation and listed in Table 6-4. When these results

Kn	**ΔT**	**Kn**	**ΔT**
0.09	90	1	70
0.1	90	5	50
0.2	90	10	45
0.5	80	50	38
0.9	70	100	36

Table 6-4: Actual Temperature Values for Flux Experiments

are plotted with Loyalka's and Sharipov's dimensionless fluxes, the results (Figure 6-13) are comparable and show the validity of the DSMC solution.

Since we desire consistent flux values for a 100K temperature gradient we need to ensure the correct gas temperature at the channel inlet and outlet. The solution to

this problem was to increase the size of the reservoir and the distance between the inlet boundary and entrance to the channel. A flowfield image demonstrating this change for Kn= 50 is shown in Figure 6-15. The flow has reached a fully developed state and the gas maintains the full temperature gradient. For this case, the reservoir size was increased and the top surface was brought closer to the symmetry line so the walls would have greater influence on the flow temperature. Finally, a boundary was added to the top of the reservoir with a specified temperature so the only molecules entering the stream are from the sides boundaries. The results of this modification gave the correct values shown in the plots above and are the basis of all the design calculations.

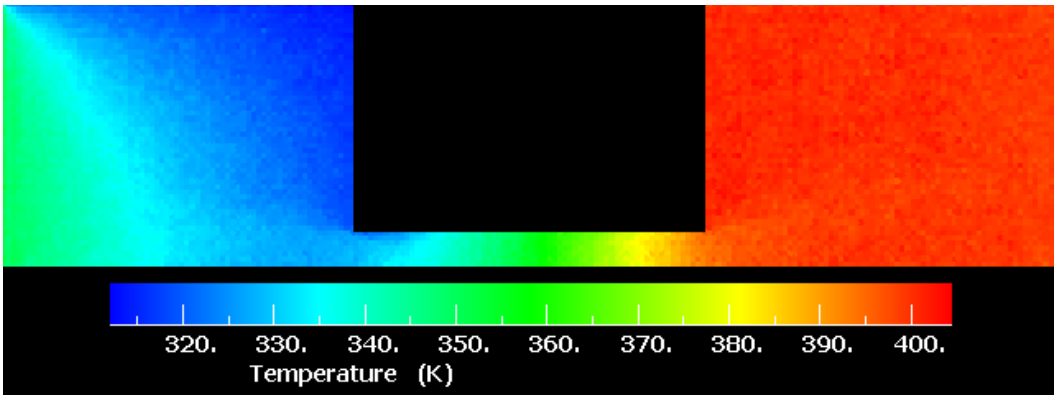

Figure 6-15: DSMC Simulation: Increased reservoir simulation for Kn=50.

Knudsen pump designers can maximize the pressure difference by changing the characteristic width of their channels (pores) to achieve a transition regime Knudsen number based on the operating pressure for the pump. Designers more interested in maximizing the flux should use Figure 6-9. These results, however, could be somewhat deceiving since those results are for a single channel whereas most designs use an array of channels where the density of channels per unit area becomes important. Below are some design examples where the simulation results are applied to design.

7.1 Design #1

Find: Maximum number flux for a $1cm^2$ array of pores with a 5:1 aspect ratio

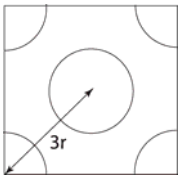

Figure 7-1: Pore packing arrangement

A unit section of the pore array in the arrangement shown in Figure 7-1 would contain 2 pores and comprises an area:

$$A_{pore} = 18r^2 \tag{7-1}$$

Where r is the radius of the pore and each unit section contains two pores. The total number of pores in a $1cm^2$ area is found using:

$$\mathrm{N}_{\mathrm{pores}} = 2\left(\frac{1cm^2}{A_{pore}}\right) \tag{7-2}$$

The number flux for all Knudsen numbers is found in Figure 6-9. These are simulation results for a 2-D model with a unit width. To determine the 3-D flux consider the following. The reduced mass flux values from my simulations were determined using (6-4). Muntz used that equation to calculate values for flow through a circular tube whereas Sharipov used the same equation to calculate the reduced flowrate in a 2D channel. We know the Q_T values carry the cross-sectional shape in them, however, for the following the examples we won't specifying the particular form for the capillary cross sections when calculating the flowrates [187]. Now, our area value was the channel width times unity. If we want to convert our dimensionless data to 3 dimensions, we use the three dimensional pore area instead of our 2-D value. The ratio between the 2D cross-sectional "area" and the 3D area is:

$$\frac{A_{3D}}{A_{2D}} = \frac{\pi\left(\frac{w}{2}\right)^2}{w} = \frac{\pi w}{4} \tag{7-3}$$

Therefore, the number flux for a single pore is:

$$\dot{N}_{\mathrm{pore}} = \dot{N}_{2-D}\left(\frac{\pi w}{4}\right) \tag{7-4}$$

This result is shown in Figure 7-2.

Next, the total array flux is found by multiplying the flux results times the total number of pores.

$$\dot{N}_{\text{TOTAL}} = \dot{N}_{pore} N_{pores} \tag{7-5}$$

This plot is shown in Figure 7-4. The maximum flux occurs in the region of higher Knudsen number. Eventhough the maximum flux through a single pore occurs when the gas is in the transition regime, the higher density of pores in the free molecular regime dominates and allows for more total flow. It becomes more apparent that as the ability to fabricate smaller and smaller pores increases that the total volume of flow can grow with it. As with most pumping mechanisms there is an inherent inverse relationship between pressure drop and flowrate. Whether the desired goal is to achieve maximum flow or

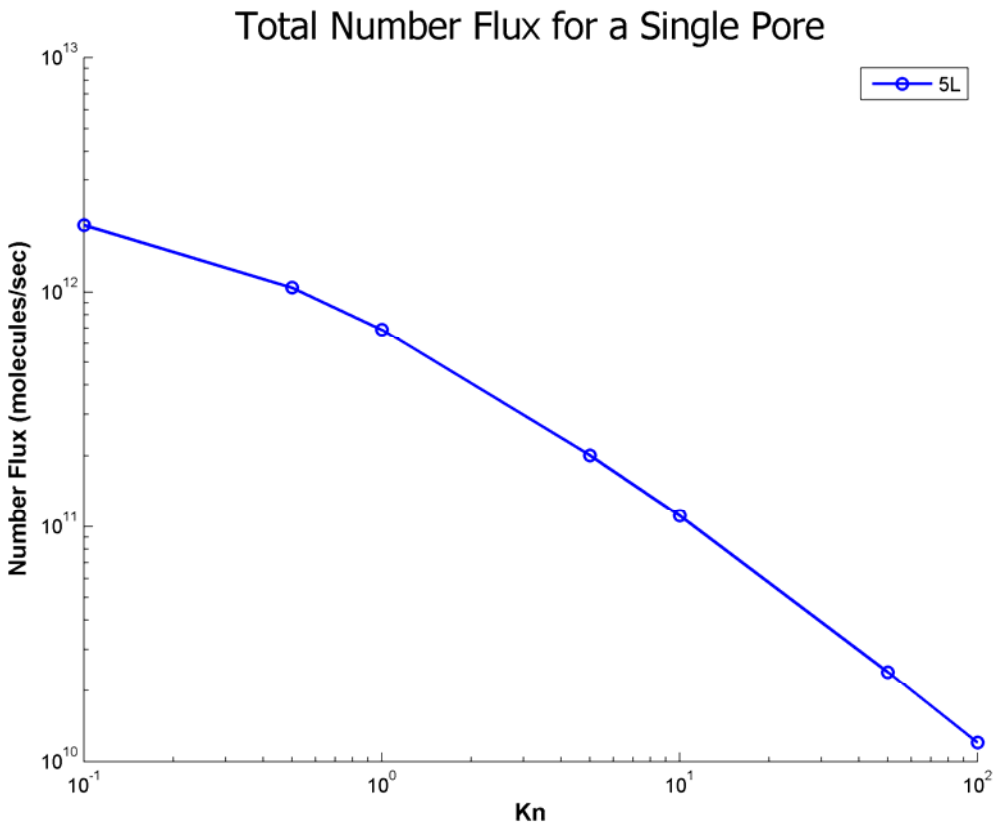

Figure 7-2: Single Pore Number Flux

maximum pressure drop, it is important to develop very thin membranes with low conductivity to maximize the thermomolecular performance.

7.2 Design #2

Find: The pressure ratio for closed system with channel width = 100nm and atmospheric pressure. The temperature gradient is 300K (300K to 400K).

The mean free path is found using:

$$\lambda = \frac{k_b T}{\pi d^2 P \sqrt{2}} \tag{7-6}$$

Figure 7-3 shows the relationship between mean free path and pressure. From this plot

we can determine the mean free path at atmospheric pressure (and an average temperature of 350K) is approximately 82nm. Using (6-1) we know the Knudsen number is then equal to 0.82. To determine the pressure ratio across the channel we use Figure 6-11 which gives a 600 Pa (~0.006atm) drop in pressure from the hot side to the cold side. While these results are from an open system, the data shown is for zero number flux which is the same condition as if the system were closed. The pressure ratio is then determined using Figure 6-3 which gives $P_2/P_1 \approx 1.14$.

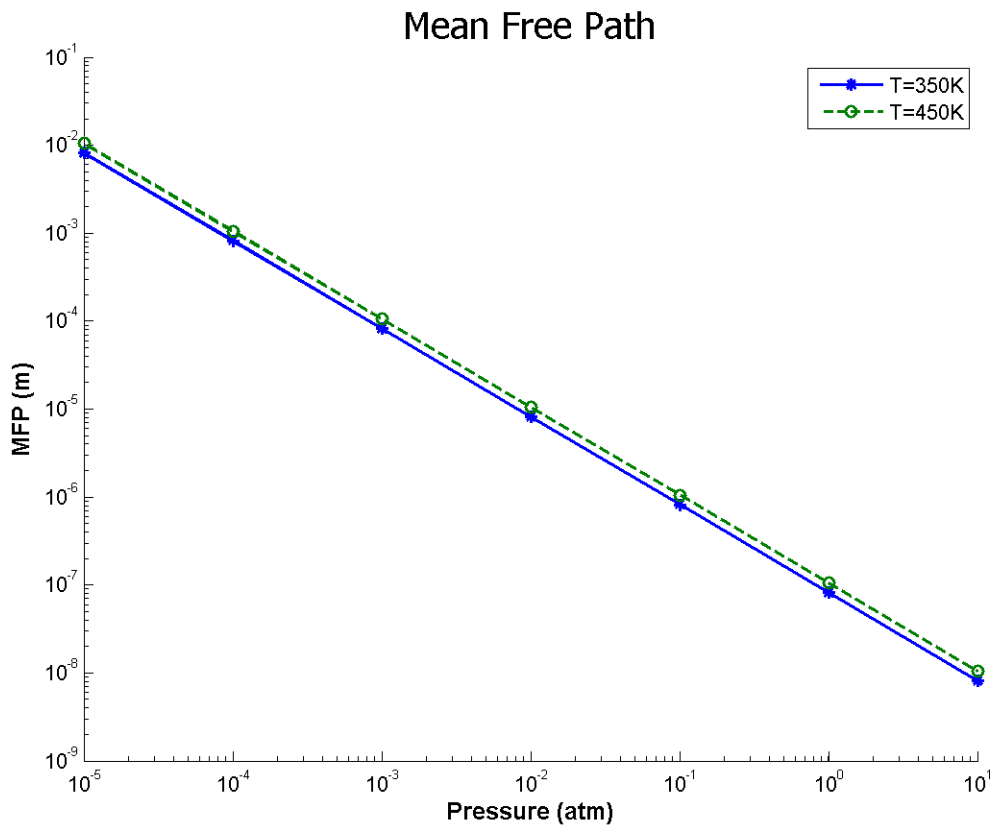

Figure 7-3: Mean Free Path vs. Pressure

7.3 Design #3

Find: The size of pore needed to achieve an arrayed flux = 1.5×10^{19} molecules/s at 10^{-3} atm and a 100K temperature difference for a 5.0 aspect ratio. The array size is $1 mm^2$.

First, the mean free path of an argon molecule at 10^{-3} atmospheres is found using Figure 7-3: λ=8.2µm. Next, the Knudsen number for the given flux are determined using Figure 7-4: Kn = 0.63. These values are now divided into the mean free path to give the pore sizes: d = 13.02µm

7.4 Design #4

Find: The pressure where a 100K temperature gradient will create a volumetric flowrate of 0.12sccm through a 1mm^2 array of 100nm pores.

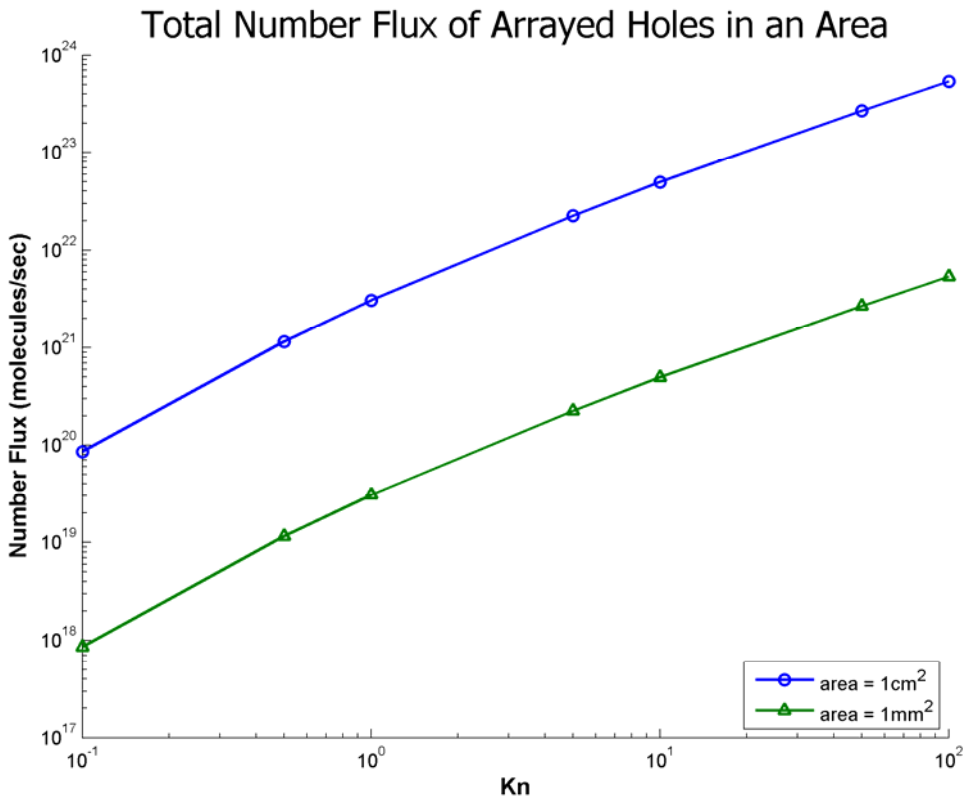

Figure 7-4: Total Molecular Flux for an Array of Holes

The volumetric flowrate can be found by multiplying the arrayed number flux (Figure 7-4) times the mass of an argon molecule and dividing this result by the density. The density values we will use will be the average density values in the channel (as a function of Knudsen number). A plot showing the volumetric flowrate is shown in Figure 7-5.

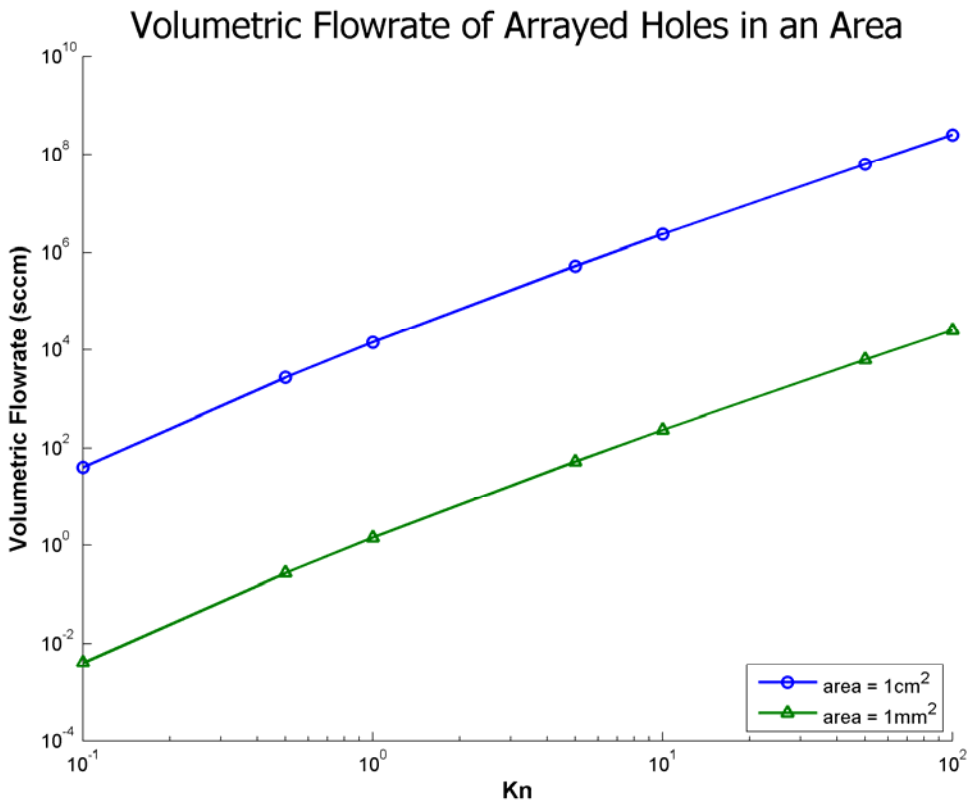

Figure 7-5: Volumetric Flowrate for an Array of Pores

The desired flowrate corresponds to a Knudsen number of 0.5 so the mean free path must be 50nm. Once again we use Figure 7-3 to determine our needed pressure: 2atm.

We now compare the performance results from our DSMC simulations to the gas pumps listed in section 2.5. Figure 7-6 shows the maximum volumetric flowrate and pressure difference results from our simulations as functions of Knudsen number. Data for both a $1cm^2$ area and a $1mm^2$ area are shown to highlight the potential performance of a

Knudsen pump. It should be emphasized here that the performance is based on the pore density described in section 7.1. The increased flowrate performance is highly dependant on the density of pores, length of the channels, accommodation coefficient and temperature gradient. We understand there are numerous issues regarding pore fabrication and power consumption, however these problems are out of the scope of this work. Our goal was simulate the thermal transpiration effect for a subset of channel and flowfield characteristics and present them in a meaningful structure for the designer.

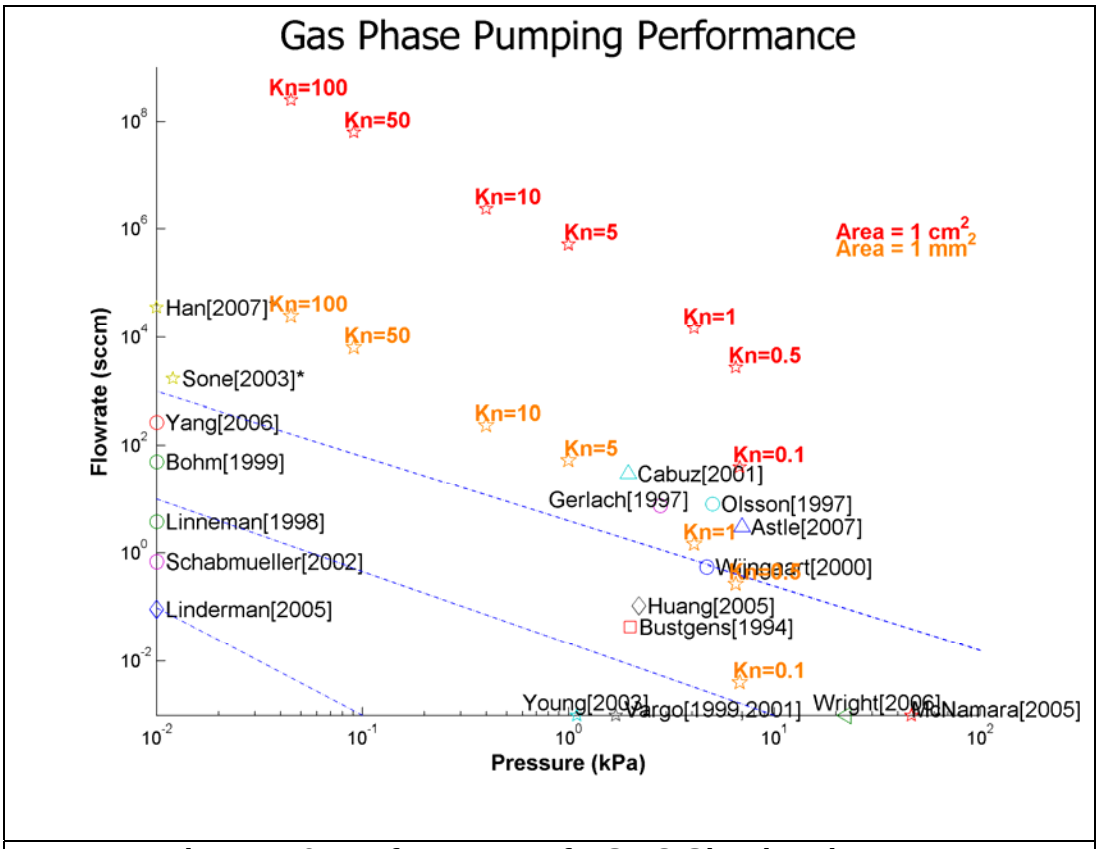

Figure 7-6: Performance of DSMC Simulated Pump

CHAPTER 8 CONCLUSION

In this dissertation, we have presented the thermal transpiration results of over 300 Direct Simulation Monte Carlo simulations which represents over 10000 hours of computational time. For each flux data point, 6-10 simulations were run under various pressure ratios. We have introduced the first set of DSMC results for gas flow with both thermal and multiple pressure differences along the channel at many Knudsen numbers within the transition ($0.1 < Kn < 10$) and free molecular regime ($Kn > 10$). From these results we were able to derive the velocity profiles for a wide range of flows as well as derive the maximum flux, pressure difference, and pressure ratio values throughout that same range of Knudsen numbers. We also presented similar data for varying channel lengths and accommodation coefficients.

We have also included simulation data of closed system thermal transpiration with only temperature gradients. From these simulations we were able to characterize the maximum pressure drop achievable using the thermomolecular pumping effect at linear temperature gradients of 100K and 400K. We presented the data in terms of both pressure differences and pressure ratios and show how the pressure ratios approach Knudsen's *P-T* ratio as the gas becomes more rarefied. Through design examples we have shown the performance of an $1cm^2$ array of holes at a 100K temperature difference could produce a maximum pressure difference of 7 kPa and a maximum flowrate of over 1×10^8 sccm. Based on both the open and closed data included in this dissertation, we believe we have compiled the most comprehensive set of DSMC simulations of thermal transpiration found in literature to date.

Of key importance to this problem is the underlying kinetic theory and DSMC method. First, we outlined some of the basic concepts of kinetic theory and used them to derive the effusion equation. The complexity of surface impacts was then added to the problem which clarified the difficulty in modeling thermal transpiration in anything outside of the Knudsen regime. Second we presented various methods used to model thermal transpiration including analytical, numerical, and simulated solutions. We included a derivation of the Boltmann equation in this section and outlined how to extract macroscopic properties from the velocity distribution. Third, we illustrated the DSMC procedure and highlighted the features that made the technique the most advantageous tool for this type of problem.

To provide a clearer understanding of the problem, we have also included an historical review describing the works that led to Knudsen's discovery of thermomolecular pressure. This includes an in depth examination of the Knudsen pump and the attempts to utilize this unique phenomenon over the last century. As part of the assessment we also present an overview of current micropump design and performance and highlight what role the Knudsen pump can fill in this context.

The potential applications of the Knudsen pump are numerous, however, the author suggests that the most reasonable situation would be where a thermal gradient already exists (i.e. electronic cooling). The most likely candidate would seem to be in a space application since the temperature extremes are great. In this situation, the

pump would not only have zero moving parts but the heat is supplied by the environment (i.e. passive pump).

BIBLIOGRAPHY

1. Accoto, D.; Carrozza, M.C.; Dario, P. "Modelling of Micropumps Using Unimorph Piezoelectric Actuator and Ball Valves." *J. Micromech. Microeng.* 10 (2000): 277-281.

2. Adamson, S.; O'Carroll, C.; McGilp, J.F. "The Angular Distribution of Thermal Molecular Beams Formed by Single Capillaries in the Molecular Flow Regime." *Vacuum*, 38 (6) (1988): 463-467.

3. Ahn, S. H., and Kim, Y. K. "Fabrication and Experiment of a Planar Micro Ion Drag Pump." *Sens. Actuators* A, 70, (1998): 1–5.

4. Aktas, O.; Aluru, N.R. "Application of a Parallel DSMC Technique to Predict Flow Characteristics in Microfluidic Filters." *J. of MEMS* 10 (4) (2001): 538-549.

5. Al-Ghoul, M.; Eu, B.C. "Generalized Hydrodynamics and Microflows." *Physical Review* E 70, 016301 (2004): 1-16.

6. Albo, S.E.; Broadbelt, L.J.; Snurr, R.Q. "Multiscale Modeling of Transport and Residence Times in Nanostructured Membranes." *AIChE Journal* 52 (11) (2006): 3679-3687.

7. Alexander, F.J.; Garcia, A.L. "Direct Simulation Mote Carlo Method, The." *Computers in Physics* 11 (6) (1997): 588-593.

8. Alexeenko, A.A.; Gimelshein, S.F.; Muntz, E.P.; Ketsdever, A.D. "Kinetic Modeling of Temperature Driven Flows in Short Microchannels." *Proc. Intl. Conf. Microchannels and Minichannels*, June 2005, Toronto, Canada : 483-491.

9. Annis, B.K. "Thermal Creep in Gases." *J. of Chemical Physics*, Vol. 57, No. 7 (1972): 2898-2905.

10. Annis, B.K.; Malinauskas, A.P. "Temperature Dependance of Rotational Collision Numbers from Thermal Transpiration." *J. of Chemical Physics*, Vol. 54, No. 11 (1971): 4763-4768.

11. Aoki, K.; Sone, Y.; Waniguchi, Y. "A Rarefied Gas Flow Induced by a Temperature Field: Numerical Analysis of the Flow Between Two Coaxial Elliptic Cylinders with Different Uniform Temperature." *Computers Math. Applic.* Vol. 35, No. 1/2, (1998): 15-28.

12. Arkilic, E.B.; Breuer, K.S.; Schmidt, M.A. "Mass Flow and Tangential Momentum Accomodation in Silicon Micromachined Channels." *J. Fluid Mech.* 437 (2001): 29-43.

13. Arkilic, E.B.; Schmidt, M.A.; Breuer, K.S. “Gaseous Slip Flow in Long Microchannels.” *J. MEMS*. 6 (2) (1997):167-178.

14. Arkilic. E.B. “Measurement of the Mass Flow and Tangential Momentum Accomodation Coefficient in Silicon Micromachined Channels.” Doctoral Dissertation, Massachusetts Institute of Technology (MIT), FDRL TR 97-1.

15. Astle, AA ; Kim, HS ; Bernal, LP ; Najafi, K ; Washabaugh, PD. "Theoretical and Experimental Performance of a High Frequency Gas Micropump" *Sensors and Actuators A - Physical* 134 (1) (2007): 245-256.

16. Bahukudumbi, P.; Beskok, A. “A Phenomenological Lubrication Model for the Entire Knudsen Regime.” *J. Micromech. Microeng.* 13 (2003): 873-884.

17. Bart, S. F., Tavrow, L. S., Mehregany, M., and Lang, J. H. “Microfabricated Electrohydrodynamic Pumps.” *Sens. Actuators* A, 21–23, : 193–197, 1990.

18. Bassanini, P.; Cercignani, C.; Sernagiotto, F. “Flow of a Rarefied Gas in a Tube of Annular Section.” *Physics of Fluids*, 9 (6) (1966): 1174-1178.

19. Beijerinck, H.C.W.; Stevens, M.P.J.M; Verster, N.F. “Monte-Carlo Calculation of Molecular Flow Through a Cylindrical Channel.” *Physica* 83C (1976): 209-219.

20. Benard, W.L.; Kahn, H.; Heuer, A.H.; Huff, M.A. “Thin-Film Shape-Memory Alloy Actuated Micropumps.” *J. of MEMS*, Vol. 7, No. 2, June 1998.

21. Berg, J.M.; Anderson, R.; Anaya, M.; Lahlouh, B.; Holtz, M.; Dallas, T. “A Two-Stage Discrete Peristaltic Micropump.” *Sensors and Actuators* A 104 (2003): 6-10.

22. Berman, A.S. “Free Molecule Transmission Probabilities.” *J. Appl. Phys.* 10 (1965) p.3356.

23. Bernoulli, D. “Hydrodynamics (in Latin).” Section 10, p.200.

24. Beskok, A.; Karniadakis, G.E. “A Model for Flows in Channels, Pipes, and Ducts at Micro and Nano Scales.” *Microscale ThermoPhysical Eng*ineering 3 (1999): 43-77.

25. Beylich, A.E. “Solving the Kinetic Equation for All Knusden Numbers.” *Phys. of Fluids* 12 (2) (2000): 444-465.

26. Bhattacharya, D.K.; Lie, G.C. “Nonequilibrium Gas Flow in the Transition Regime: A Molecular-Dynamics Study.” *Physical Review* A, 43 (2) (1991): 761-767.

27. Bird, G.A. “Forty Years of DSMC, and Now?.” AIP Conference Proceedings - *Rarefied Gas Dynamics*: 22nd International Symposium - 585 (2001): 372-380.

28. Bird, G.A. “Approach to Translational Equilibrium in a Rigid Sphere Gas.” *Phys. of Fluids* 6 (1963): 1518-1519.

29. Bird, G.A. *Molecular Gas Dynamics and the Direct Simulation of Gas Flows*, Oxford Engineering Science Series, vol. 42, The Clarendon Press Oxford University Press, New York, (1995).

30. Bohm, S.; Olthuis, W.; Bergveld, P. “A Plastic Micropump Constructed with Conventional Techniques and Materials.” *Sensors and Actuators* 77 (1999): 223-228.

31. Bourouina, T.; Bosseboeuf, A.; Grandchamp, Jean-Paul “Design and Simulation of an Electrostatic Micropump for Drug-Delivery Applications.” *J. Micromech. Microeng.* 7 (1997): 186-188.

32. Boyle, R. “Robert Boyle and His Data.” *J. College Sci. Teaching* (May 1992): 363-365.

33. Branton, G.R.; Ryce, S.A. “A Kinetic Model of the Accomodation Pumping Phenomenon.” *Can. J. Chem*. 52 (1974): 2073-2076.

34. Brenner, H. “Navier-Stokes Revisited.” *Physica* A 349 (2005): 60-132.

35. Brown, G.P.; DiNardo, A.; Cheng, G.K.; Sherwood, T.K. “Flow of Gases in Pipes at Low Pressures.” *J. Applied Phys*. 17 (1946): 802-813.

36. Bureau, A.J.; Laslett, J.; Keller, J.M. “Pumping Speed of a Circular Aperture in a Diaphragm Across a Circular Tube.” *Rev. Scientific Instrum*. 23 (12) (1952): 683-686.

37. Bustgens, B.; Bacher, W.; Menz, W.; Schomburg, W.K. “Micropump Manufactured By Thermoplastic Molding.” Conference*: IEEE Micro Electro Mechanical Systems An Investigation of Micro Structures, Sensors, Actuators, Machines and Robotic Systems*, 25-28 Jan. 1994, Oiso, Japan.

38. Cabuz, C.; Cabuz, E.I.; Ohnstein, T.R.; Neus, J.; Maboudian, R. “Factors Enhancing the Reliability of Touch-Mode electrostatic Actuators.” Sensors and Actuators A-Physical. 79 (3) (2000): 245-250.

39. Cabuz, C.; Herb, W.R.; Cabuz, E.I.; Son Thai Lu “The Dual Diaphragm Pump.” Proceedings: IEEE MEMS Workshop (2001): 519-522.

40. Carette, J.D.; Pandolfo, L.; Dube, D. “New Developments in the Calculation of the Molecular Flow Conductance of a Straight Cylinder.” *J. Vac. Sci. Technol.* A 1 (2) (1983): 143-146.

41. Cercignani, C.; Sernagiotto, F. “Cylindrical Poiseuille Flow of a Rarefied Gas.” *Physics of Fluids* 9 (1) (1966): 40-44.

42. Chen, C.C.; Chen, I.K.; Liu, T.P.; Sone, Y. “Thermal Transpiration for the Linearized Boltzmann Equation.” *Communications on Pure and Applied Mathematics*, Vol. LX, (2007): 0147–0163.

43. Chen, G.; Boyd, I.D. “Statistical Error Analysis for the Direct Simulation Monte Carlo Technique.” *J. of Comp. Phys.* 126 (1996): 434-448.

44. Cheng, H.K.; Emanuel, G. “Perspective on Hypersonic Equilibrium Flow.” *AIAA Journal* 33 (3) (1995): 385-400.

45. Chuan-Hua Chen; Shulin Zeng; Mikkelsen, J.C., Jr.; Santiago, J.G. “Development of a Planar Elektrokinetic Micropump.” Stanford Microfluidics Laboratory, 2000.

46. Cieplak, M.; Koplik, J.; Bavanar, J. “Applications of Statistical Mechanics in Subcontinuum Fluid Dynamics.” *Physica* A 274 (1999): 281-293.

47. Cieplak, M.; Koplik, J.; Bavanar, J. “Molecular Dynamics of Flows in the Knudsen Regime.” *Physica* A 287 (2000): 153-160.

48. Clausing, P. “Flow of Highly Rarefied Gases Through Tubes of Arbitrary Length.” *J. Vac. Sci. Technol.* 8 (5) (1971): 636-646.

49. Clausius, R. “Ueber die Art der Bewegung welche wir Wärme nennen.” Annalen der Physik 100, 353-380 (1857); translation published in *Philosophical Magazine* 14, 108-127 (1857).

50. Cole, R.J. “Transmission Probability of Free Molecular Flow Through a Tube.” Paper 11 at the *10th Intl. Symp. On Rarefied Gas Dyn*., Aspen, Colo., July 19-23, 1976, : 261-272.

51. Colgate, E.; Matsumoto, H. “An investigation of electrowetting-based microactuation.” *J. of Vac. Sci. Tech.* A (Vacuum, Surfaces, and Films); July-Aug. 1990; vol.8, no.4, p.3625-33.

52. Copic, D.; Brehob, E.; McNamara, S. “Theoretical Efficiency of a Microfabricated Knudsen Pump.” *IEEE* (2008): 107-110.

53. Creutz, E.S.; Zumwalt, L.R. “A New Semiempirical Equation for Gas Flow Through Capillaries.” *J. Applied Phys*. 33 (9) (1962): 2883-2888.

54. Darabi, J.; Ohadi, M.M.; DeVoe, D. "An Electrohydrodynamic Polarization Micropump for Electronic Cooling." *J. of MEMS*, Vol. 10, No. 1, March 2001.

55. Davies, C.M.; Lucas, C.B. "The Failure of Theory to Predict the Density Distribution of Gas Flowing Through a Tube Under Free Molecular Conditions." *J. Phys. D: Appl. Phys*., 16 (1983): 1-16.

56. Davis, D.H. "Monte Carlo Calculation of Molecular Flow Rates Through A Cylindrical Elbow and Pipes of Other Shapes." *J. of Applied Phys.* 31 (7) (1960): 1169-1176.

57. DeMarcus, W.C.; Hopper, E.H. "Knudsen Flow Through a Circular Capillary." *J. Chem. Phys.* 23 (7) (1955): 1344-1345.

58. Debar, M.; Liepmann, D. "Steady-state microscale pumping using the Marangoni effect: A model problem*." Bull. Am. Phys. Soc.* 45 (2000) p.126.

59. Demirel, Y.; Saxena, S. "Heat Transfer in Rarefied Gas at a Gas-Solid Interface." *Energy* Vol. 21, No. 2, (1996): 99-103.

60. Deryagin, B.V.; Fedyakin, N.N. "Complete Specular Reflection of Molecules at Low Angles of Incedence and Its Effect on the Molecular Flow of Gases Through Very Narrow Capillaries*." Progress in Surface Science* 43 (1-4) (1993): 290-301.

61. *Dielectrophoresis*, University of Texas - MD Anderson Cancer Center, Feb. 2, 2004, http://www.dielectrophoresis.org.

62. Dong Xu, Li Wang, Guifu Ding, Yong Zhou, Aibing Yu, Bingchu Cai "Characteristics and Fabrication of NiTi/Si Diaphragm Micropump." *Sensors and Actuators* A 93 (2001): 87-92.

63. Dushman, S. "Recent Advances in the Production and Measurement of High Vacuum." *J. Franklin Inst.* 211 (6) (1931): 689-750.

64. Dushman, S. "Development of High Vacuum Technique." *Industrial and Engineering Chemistry* 40 (5) (1948): 778-780.

65. Edmonds, T.; Hobson, J.P. "Study of Thermal Transpiration Using Ultrahigh-Vacuum Techniques." *J. Vac. Sci. Technol.* 2 (4) (1965): 182-197.

66. Elwenspoek, M.; Lammerink, T.S.J.; Miyake, R.; Fluitman, J.H.J. "Towards Integrated Microliquid handling Systems." *J. Micromech. Microeng.* 4 (1994): 227-245.

67. Erwin, D.; Pham-Van-Diep, G.; Muntz E.P. “Nonequilibrium Gas Flows.1. A Detailed Validation of Monte Carlo Direct Simulation for Monatomic Gases.” *Phys. of Fluids* A - *Fluid Dynamics* 3 (4) (1991): 697-705.

68. Eu, B.C. “Generalized Hydrodynamics Appraoch to the Knudsen Problem.” *Physical Review* A, 40 (11): 6395-6402.

69. Ewart, T.; Firpo, J.L.; Graur, I.A.; Perrier, P.; Meolans, J.G. “DSMC Simulation: Validation and Application to Low Speed Gas Flows in Microchannels.” *J. of Fluids Engineering* (2009) Vol. 131/014501 : 1-6.

70. Feng, Yu-Guo “Problem, of the Approximate Calculation for Molecular Conductance, The.” *Vacuum* 31 (7) (1981): 319-324.

71. Feres, R.; Yablonsky, G. “Knudsen's Cosine Law and random Billiards.” *Chemical Engineering Science* 59 (2004): 1541-1556.

72. Ferziger, J.H. “Flow of a Rarefied Gas Through a Cylindrical Tube.” *Physics of Fluids* 10 (7) (1967): 1448-1453.

73. Folta, J.A.; Raley, N.F.; Hee, E.W. “Design, fabrication and testing of a miniature peristaltic membrane pump.” Technical Digest. *IEEE Solid-State Sensor and Actuator Workshop*, 22-25 June 1992, Hilton Head Island, SC, USA.

74. Frederking, T.H.K.; Hepler, W.A.; Khandhar, P.K. “Slip Effects Associated with Knudsen Transport Phenomena in Porous Media.” *Cryogenics* 28 (1988): 110-114.

75. Fryer, G.M. “A Theory of Gas Flow Through Capillary Tubes.” *Proc. Royal Soc. London Series A - Math. Phys. Sci.* 293 (1434) (1966): 329-341.

76. Fuhr, G. “From Micro Field Cages for Living Cells to Brownian Pumps for Submicron Particles.” *Proc. of IEEE Micro Mechatronics and Human Scie*nce 97, : 1–4. 1997.

77. Fuhr, G., Hagedom, R., Mueller, T., Benecke, W., and Wagner, B. “Pumping of Water Solutions in Microfabricated Electrohydrodynamic Systems.” *IEEE* 5th Int. Workshop on MEMS (MEMS’92), (1992): 25–30.

78. Fuhr, G., Hagedorn, R., Mueller, T., Benecke, W., and Wagner, B. “Microfabricated Electrohydrodynamic (EHD) Pumps for Liquids of Higher Conductivity.” *J. of MEMS*, 1, No. 3, (1992): 141–145.

79. Fuhr, G., Schnelle, T., and Wagner, B. “Travelling Wave-Driven Microfabricated Electrohydrodynamic Pumps for Liquids.” *J. MEMS* 4, : 217–226. 1994.

80. Fukui, S.; Yamane, K. “DSMC/MGL Comparisons of Stresses on Slider Air Bearing with Nanometer Spacings.” *IEEE Transactions on Magnetics* 38 (5) (2002): 2153-2155.

81. Furuya, A., Shimokawa, F., Matsuura, T., and Sawada, R., “Fabrication of Fluorinated Polyimide Microgrids Using Magnetically Controlled Reactive Ion Etching (DRIE) and Their Applications to an Ion Drag Integrated Micropump.” *J. Micromech. Microeng.*, 6, : 310–319. 1996.

82. Furuyama, S. “Measurement's of the Thermal Transpiration Effects of NO at 90K and of CO, N2, O2, CH4, and He at 77K.” B*ulletin Che. Soc. Japan* 50 (10) (1977): 2797-2798.

83. Gallis, M.A.; Rader, D.J.; Torczynski, J.R. “Calculations of the Near-Wall Thermophoretic Force in Rarefied Gas Flow.” *Physics of Fluids*, Vol. 14, No. 12, December 2002, : 4290-4301.

84. Gallis, M.A.; Rader, D.J.; Torczynski, J.R. “Thermophoresis in Rarefied Gas Flows.” *Aerosol Science and Technology* 36 (2002): 1099-1117.

85. Garcia, A.L. “Estimating Hydrodynamic Quantities in the Presence of microscopic Fluctuations.” Comm. A: Math. and Comp. Sci. 1 (1) (2006): 53-78.

86. Garcia, A.L.; Alder, B.J. “Generation of Chapman-Enskog Distribution.” *J. of Comput. Phys.* 140 (1998): 66-70.

87. Garcia, A.L.; Wagner, W. “Time step truncation error in direct simulation Monte Carlo.” *Physics of Fluids* 12 (10) (2000): 2621-2633.

88. Gass, V.; van der Schoot, B.H.; Jeanneret, S.; de Rooij, N.F. “Integrated flow-regulated silicon micropump.” *Sensors and Actuators* A (*Physica*l); May 1994; vol.A43, no.1-3, p.335-8.

89. Gerlach, T. “Pumping gases by a silicon micro pump with dynamic passive valves.” International Solid State *Sensors and Actuators* Conference (Transducers '97), 16-19 June1997, Chicago, IL, USA.

90. Gerlach, T.; Wurmus, H. “Working principle and performance of the dynamic micropump.” *IEEE Micro Electro Mechanical Systems*. 1995, 29 Jan.-2 Feb. 1995, Amsterdam,Netherlands.

91. Gilliland, E.R.; Baddour, R.F.; Engel, H.H. “Flow of Gases Through Porous Solids Under the Influence of Temperature Gradients.” *A.I.Ch.E. J.* 8 (4) (1962): 530-536.

92. Goodman, F.O. “Thermal Accommodation Coefficients.” *J. Phys. Chem.* 84 (1980): 1431-1445.

93. Graham, T. “On the Molecular Mobility of Gases.” *Philis. Trans. R. Soc. London*, XVII, (1863), : 385-405.

94. Graham, T. “On the Motion of Gases.” Philis. Trans. R. Soc. London, XXVIII, (1846), : 573-631.

95. Grosjean, C.; Xing Yang; Yu-Chong Tai “A thermopneumatic microfluidic system.” Technical Digest. *MEMS 2002 IEEE International Conference. Fifteenth IEEE International Conference on Micro Electro Mechanical Systems*, 20-24 Jan. 2002, Las Vegas, NV, USA.

96. Gruener, S.; Huber, P. “Knudsen Diffusion in Silicon Nanochannels.” *PRL* 100, 064502 (2008): 1-4.

97. Hadjiconstantinou, N.G. “Limits, of Navier-Stokes Theory and Kinetic Extensions for Describing Small-Scale Gaseous Hydrodynamics, The.” *Phys of Fluids* 18 (111301) (2006): 111301-1 - 111301-19.

98. Hadjiconstantinou, N.G.; Garcia, A.L. “Statistical Error in Particle Simulations for Low Mach Number Flows.” *Proc. of First MIT Conf. on Comput. Fluid and Solid Mech.*, Elsevier, June 2001 (2001): 1-8.

99. Han, Y.L.; Muntz, E.P. “Experimental Investigation of Micro-Mesoscale Knudsen Compressor Performance at Low Pressures.” J. Vac. Sci. Technol. B 25 (3) (2007):703-714.

100. Hanks, R.W.; Weissberg, H.L. “Slow Viscous Flow of Rarefied Gases Through Short Tubes.” *J. Appl. Phys.* 35 (1) (1964): 142-144.

101. Hanley, H.J.M.; Steele, W.A. “Low Pressure Flow of Gases*.” J. Phys. Chemistry* 68 (10) (1964): 3087-3088.

102. Harris, S. *An Introduction to the Theory of the Boltzmann Equation*. Dover Publications. (2004).

103. Harrison, D.J.; Manz, A.; Glavina, P.G. “Electroosmotic pumping within a chemical sensor system integrated on silicon.” *TRANSDUCERS '91. 1991 International Conference on Solid-State Sensors and Actuators*. Digest of Technical Papers, 24-27 June 1991, San Francisco, CA, USA.

104. Hatch, A.; Kamholz, A.E.; Holman, G.; Yager, P.; Böhringer, K.F. “A Ferrofluidic Magnetic Micropump.” *J. MEMS*, 10 (2), JUNE 2001.

105. Hayamizu, S.; Higashino, K.; Fujii, Y.; Sando, Y.; Yamamoto, K. “Development of a Bi-Directional Valve-less Silicon Micro Pump Controlled by Driving Waveform.” *Sensors and Actuators* A 103 (2003): 83-87.

106. Helmer, J.C. “Solution of Clausing's Integral Equation for Molecular Flow.” *J. Vac. Sci. Tech.* 4 (6) (1967): 360-363.

107. Hiby, J.W.; Pahl, M. “Influence of Binary Gas Collisions on Molecular Gas Flow.” *Physical Review* 88 (2) (1952) p.414.

108. Hobson, J.P. “Concerning an Analytic Expression for the Thermal Transpiration Ratio.” *Vacuum* 15 (11) (1965): 543-544.

109. Hobson, J.P. “Accomodation Pumping - A New Principle for Low Pressures.” *J. Vac. Sci. Technol.* 7(2) 1969, : 351-357.

110. Hobson, J.P., Salzman, D.B. “Review of Pumping By Thermal Molecular Pressure.” *J. Vac. Sci. Technol.* 18(4), Jul/Aug 2000, : 1758-1765.

111. Holt, J.K.; Park, H.G.;Wang, Y.; Stadermann, M.; Artyukhin, A.B.; Grigoropoulos, C.P.; Noy, A.; Bakajin, O. “Fast Mass Transport Through Sub–2-Nanometer Carbon Nanotubes.” *Science* 312, 1034 (2006):1-6.

112. Holt, T.E.; Smith, D.M. “Surface Roughness Effects on Knudsen Diffusion.” *Chem. Eng. Sci*. 44 (3) (1989): 779-781.

113. Horton, W.S. “Molecule-Wall Collisions in Porous Media at Low Gas Pressures.” *J. Phys. Chem.* 68 (8) (1964): 2278-2281.

114. Huang, A.B.; Stoy Jr., R.L. “Rarefied Gas Channel Flows for Three Molecular Models.” *Physics of Fluids* 9 (12) (1966): 2327-2336.

115. Huang, CW ; Huang, SB ; Lee, GB. "Pneumatic Micropumps with Serially Connected Actuation Chambers" *J. MEMS* 16 (11) (2006): 2265-2272.

116. Huggill, J.A.W. “Flow of Gases Through Capillaries, The.” *Proc. Royal Soc. London Series A - Math. Phys. Sci.* 212 (1108) (1952): 123-136.

117. Ikuta, K.; Hasegawa, T.; Adachi, T. “SMA Micro Pumps and Switching Valves for BioChemical IC Family.” *2000 Inernational Symposium on Micromechatronics and Human Science, IEEE* 2000, : 169-174.

118. Jitschin, W.; Reich, G. “Molecular Velocity Distributions at Large Knudsen Numbers.” *J. Vac. Sci. Technol.* A 9 (5) (1991): 2752-2756.

119. Joule, J.P. “Some Remarks on Heat and the Constitution of elastic Fluids.” *Memoirs of the Manchester Literary and Philosophical Society November 1851 and Philosophical Magazine* 14, 211 (1857) reprinted in William Francis Magie, ed., *A Source Book in Physics* (New York: McGraw-Hill, 1935).

120. Judy, J.W.; Tamagawa, T.; Polla, D.L. "Surface-machined micromechanical membrane pump." *IEEE Micro Electro Mechanical Systems. An Investigation of Micro Structures, Sensors, Actuators, Machines and Rob*ots, 30 Jan.-2 Feb. 1991, Nara, Japan.

121. Jun, T. K., and Kim, C.-J., "Valveless Pumping Using Traversing Vapor Bubbles in Microchannels." *J. Appl. Phys.*, 83, No. 11, : 5658–5664. 1998.

122. Junghoon Lee; Chang-Jin Kim "Surface-Tension-Driven Microactuation Based on Continuous Electrowetting." *J. MEMS*; June 2000; vol.9, no.2, p.171-80.

123. Kahn, H.; Benard, W.L.; Huff, M.A.; Heuer, A.H. "The TiNi Shape-Memory Alloy and Its Applications For MEMS." *J. Micromech. Microeng.* 8 (1998): 213-221.

124. Kataoka, T.; Tsutahara, M.; Ogawa, K.; Yamamoto, Y.; Shoji, M.; Sakai, Y. "Knudsen Pump and its Possibility of Application to Satellite Control." *Theoretical and Applied Mechanics Japan* 53 (2004): 155-161.

125. Khoo, M., Liu, C. "A Novel Micromachined Magnetic Membrane Microfluid Pump." *Proc. Of the 22nd Annual EMBS Intl. Conf.*, July 23-28, 2000, Chicago, Ill, : 2394-2397.

126. Knaff, G.; Schlunder, E.U. "Experimental Confirmation of Graham's Law of Diffusion up to Pore Diameters of 2 um." *Chem. Eng. Process*. 19 (1985): 167-173.

127. Knudsen, M. "Laws of Molecular Flow and of Inner Friction Flow of Gases Through Tubes, The." *J. Membrane Science* 100 (1995): 23-25.

128. Knudsen, M. "Das Cosinusgesetz in der kinetischen Gastheorie." *Ann. Phys.,* Lpz. 48 (1916): 1113-1121.

129. Knudsen, M. "Erwiderung an Hrn. M. v. Smoluchowski." *Ann. Phys.*, Lpz. 34 (1911b): 823-824.

130. Knudsen, M. "Thermischer Molekulardruck der Gase in Rohren." *Ann. Phys.,* Lpz. 33 (1910d): 1435-1448.

131. Knudsen, M. "Die Molekularstromung der Gase durch Offnungen und die Effusion." *Ann. Phys., Lpz*. 28 (1909b): 999-1016.

132. Knudsen, M. "Eine Revision der Gleichgewichtsbedingung der Gase. Thermische Molekularstromung." *Ann. Phys*., Lpz. 31(1910a), : 205-229.

133. Koch, M.; Harris, N.; Evans, A.G.R.; White, N.M.; Brunnschweiler, A. "A Novel Micromachined Pump Based On Thick-Film Piezoelectric Actuation." *Sensors and Actuators* A 70 (1998): 98-103.

134. Koch, M.; Harris, N.; Maas, R.; Evans, A.G.R.; White, N.M.; Brunnschweiler, A. "A Novel Micropump Design With Thick-Film Piezoelectric Actuation." *Meas. Sci. Technol*. 8 (1997): 49-57.

135. Koch, M.; Schabmueller, C.G.S.; Evans, A.G.R.; Brunnschweiler, A. "Micromachined Chemical Reaction System." *Sensors and Actuators* 74 (1999): 207-210.

136. Kurosawa, M.; Watanabe, T.; Higuchi, T. "Surface acoustic wave atomizer with pumping effect." *IEEE Micro Electro Mechanical Systems.* 1995, 29 Jan.-2 Feb. 1995, Amsterdam, Netherlands.

137. Kwang-Seok Yun; Il-Joo Cho; Jong-Uk Bu; Chang-Jin Kim; Euisik Yoon "A surface-tension driven micropump for low-voltage and low-power operations." *J. MEMS*; Oct. 2002; vol.11, no.5, p.454-61.

138. Kwang-Seok Yun; Il-Joo Cho; Jong-Uk Bu; Geun-Ho Kim; Young-Sam Jeon; Chang-Jin Kim; Euisik Yoon "A Micropump Driven by Continuous Electrowetting Actuation for Low Voltage and Low Power Operations." *MEMS 2001. 14th IEEE International Conference on Micro Electro Mechanical Systems,* 21-25 Jan. 2001, Interlaken, Switzerland : 487-490.

139. Lebowitz, J.L.; Frisch, H.L. "Model of Nonequilibrium Ensemble: Knudsen Gas." *Physical Review* 107 (4) (1957): 917-923.

140. Lemoff, A.V.; Lee, A.P. "An AC Magnetohydrodynamic Micropump." *Sensors and Actuators* B 63 (2000): 178-185.

141. Lereu, A.L.; Passian, A.; Warmacks, R.J.; Ferrell, T.L.; Thundat, T. "Effect of Thermal Variations on the Knudsen Forces in the Transitional Regime." *Applied Physics Letters* Vol. 84, No. 6 (2004): 1013-1015.

142. Li, H.Q.; Roberts, D.C.; Steyn, J.L.; Turner, K.T.; Carretero, J.A. "A High Frequency High Flow Rate Piezoelectrically Driven MEMS Micropump." *Tech. Dig. Solid-State Sensor and Actuator Workshop*,Hilton Head,2000.

143. Li, Z.; Wang, H. "Gas-Nanoparticle Scattering: A Molecular View of Momentum Accommodation Function." *PRL* 95, 014502 (2005):1-4.

144. Liang. S.C. "On The Calculation of Thermal Transpiration." *J. Chem. Phys.* 57 (1953): 910-911.

145. Liang. S.C. "Some Measurements of Thermal Transpiration." *J. Applied Phys*. 22 (2) (1951): 148-153.

146. Liepmann, D; Debar, M "Development of a microfabricated single-bubble pump." *Bull. Am. Phys. Soc.* 45 (2000): 137.

147. Linderman, R.J. ; Nilsen, O. ; Bright, V.M.. "Electromechanical and Fluidic Evaluation of the Resonant Microfan Gas Pump and Aerosol Collector" *Sensors and Actuators A - Physical* 118 (1) (2005): 162-70.

148. Linnemann, R.; Richter, M.; Leistner, A.; Woias, P. "A full-wafer mounted self-priming and bubble-tolerant piezoelectric silicon micropump." *Actuator 98 6th International Conference on New Actuators,* 17-19 June 1998, Bremen, Germany.

149. Loyalka, S.K. "Temperature Jump and Thermal Creep Slip: Rigid Sphere Gas." *Phys. of Fluids* A 1 (2) (1989), : 403-408.

150. Loyalka, S.K. "Thermal Transpiration in a Cylindrical Tube." *Phys. of Fluids* 12 (11) (1969), : 2301-2305.

151. Loyalka, S.K. "Slip in the Thermal Creep Flow." *Physics of Fluids*, 14 (1) (1971): 21-24.

152. Loyalka, S.K. "Kinetic Theory of Thermal Transpiration and Mechanocaloric Effect. I." *J. of Chem. Phys.,* 55 (9) (1971), : 4497-4503.

153. Loyalka, S.K. "Comments on "Thermal Creep of Rarefied Gas in a Circular Tube"." *Phys. of Fluids* 17 (6) (1974), p.1348.

154. Loyalka, S.K. "Comments on "Pouseuille Flow and Thermal Creep of a Rarefied Gas Between Parallel Plates"." *Phys. of Fluids* 17 (5) (1974), : 1053-1055.

155. Loyalka, S.K. "Kinetic Theory of Thermal Transpiration and Mechanocaloric Effect. II*." J. of Chem. Phys.,* 63 (9) (1975), : 4054-4060.

156. Loyalka, S.K. "Velocity Profile in the Thermal Creep Slip Problem." *Phys. of Fluids* 19 (10) (1976), : 1641-1642.

157. Loyalka, S.K.; Cipolla Jr., J.W. "Thermal Creep Slip with Arbitrary Accomodation at the Surface." *Phys. of Fluids* 14 (8) (1971), : 1656-1661.

158. Loyalka, S.K.; Storvick, T.S.; Park, H.S. "Poiseuille Flow and Thermal Creep Flow in Long, Rectangular Channels in the Molecular and Transition Flow Regimes." *J. Vac. Sci. Technol.* 13 (6) (1976), : 1188-1192.

159. Lucretius (50b.c.), translated by Williams Ellery Leonard "On the Nature of Things." http://classics.mit.edu/Carus/nature_things.1.i.html#2.

160. Ludwig Boltzmann. Wikipedia. http://en.wikipedia.org/wiki/Boltzmann#cite_ref-4.

161. Lundstrom, I.; Norberg, P.; Petersson, L.G. "Wall-Induced Effects in Gas Transport Through Micromachined Channels in Silicon." *J. Appl. Phys.* 76 (1) (1994): 142-147.

162. Macrossan, M.N. "nu-DSMC: A Fast Simulation Method for Rarefied Flow." *J. Comp. Phys* 173 (2001): 600-619.

163. Makino, E.; Kato, K.; Shibata, T. "Thermo-Mechanical Properties of TiNi Shape Memory Thin Films Formed By Flash Evaporation." *Sensors and Actuators* 75 (1999): 156-161.

164. Makino, E.; Mitsuya, T.; Shibata, T. "Micromachining of TiNi Shape Memory Thin Films For Fabrication of Micropump." *Sensors and Actuators* 79 (2000): 251-259.

165. Makino, E.; Mitsuya, T.; Shibata, T. "Dynamic Actuation Properties of TiNi Shape Memory Diaphragm." *Sensors and Actuators* 79 (2000): 128-135.

166. Malek, K.; Coppens, M.O. "Knudsen Self-and Fickian Diffusion in Rough Nanoporous Media." *J. Chem. Phys.* 119 (5) (2003): 2801-2811.

167. Malek, K.; Coppens, M.O. "Pore Roughness Effects on Self- and Transport Diffusion in Nanoporous Materials." *Colloids and Surfaces A: Physiochemical and Engineering Aspects* 206 (2002): 335-348.

168. Manz, A.; Harrison, D.J.; Fettinger, J.C.; Verpoorte, E.; Ludi, H.; Widmer, H.M. "Integrated Electroosmotic Pumps and Flow Manifolds for Total Chemical Analysis Systems." *IEEE* (1991): 939-941.

169. Mason, E.A.; Evans III, R.B. "Graham's Laws: Simple Demonstrations of Gases in Motion, Part I, Theory." *J. Chemical Education* 46 (6) (1969): 358-364.

170. Masters, N.D.; Ye, W. "Octant flux splitting information preservation DSMC method for thermally driven flows." *Journal of Computational Physics* 226 (2007):2044–2062.

171. Matsumoto, S.; Klein, A.; Maeda, R. "Development of bi-directional valve-less micropump for liquid." *12th International Workshop on Micro Electro Mechanical Systems - MEMS*, 17-21 Jan. 1999, Orlando, FL, USA.

172. Mavriplis, C.; Ahn, J.C.; Goulard, R. "Heat Transfer and Flowfields in Short Microchannels Using Direct Simulation Monte Carlo." *J. of Thermophysics and Heat Transfer* 11 (4) (1997): 489-496.

173. Maxwell, J.C. “On Stresses in Rarefied Gases Arising from Inequalities of Temperature.” *Philos. Trans. R. Soc. Part 1*, 170, (1979): 231-256.

174. McNamara, S., Gianchandani, Y. “A Fabrication Process with High Thermal Isolation and Vacuum Sealed Lead Transfer for Gas Reactors and Sampling Microsystems.” *IEEE Sixteenth Annual International Conference on Micro Electro Mechanical Systems*, 19-23 Jan. 2003, Kyoto, Japan.

175. McNamara, S., Gianchandani, Y. “A Micromachines Knudsen Pump For On-Chip Vacuum.” *Transducers '03, The 12th Intl. Conf. On Solid State Sensors, Actuators, and Microsystems*, Boston, June 8-12, 2003.: 1919-1922.

176. Meng, A.H.; Nam-Trung Nguyen; Black, J.; White, R.M. “Focused Flow Micropump Using Ultrasonic Flexural Plate Waves.” *Biomedical Microdevices* 2:3, : 169-174, 2000.

177. Meng, E.; Xuan-Qi Wang; Mak, H.; Yu -Chong Tai “A check-valved silicone diaphragm pump.” *IEEE Thirteenth Annual International Conference on Micro Electro Mechanical Systems*, 23-27 Jan. 2000, Miyazaki, Japan.

178. Miller, G.A.; Buice Jr., R.L. “On the Knudsen Limiting Law of Thermal Transpiration.” *J. Phys. Chem.* 70 (12) (1966): 3874-3880.

179. Milligan, M.W. “Low-Density Gas Flow in Long Tubes.” *AIAA* 4 (4) 1966): 745-746.

180. Milligan, M.W.; Patterson, K.E. “Rarefied Gas Flow Through Long Square Tubes.” *Transactions of the ASME, J. of Eng. For Industry* 93 (2) (1971): 751-753.

181. Miyazaki, S.; Kawai, T.; Araragi, M. “A piezo-electric pump driven by a flexural progressive wave.” *IEEE Micro Electro Mechanical Systems. An Investigation of Micro Structures, Sensors, Actuators, Machines and Robots*, 30 Jan.-2 Feb. 1991, Nara, Japan.

182. Mizoguchi, H.; Ando, M.; Mizuno, T.; Takagi, T.; Nakajima, N. “Design and fabrication of light driven micropump.” *IEEE Micro Electro Mechanical Systems. An Investigation of Micro Structures, Sensors, Actuators, Machines and Robots,* 4-7 Feb. 1992, Travemunde, Germany.

183. Mohan, A; Tompson, R.V.; Loyalka, S.K. “Efficient Numerical Solution of the Clausing Problem.” *J. Vac. Sci. Technol.* A 25 (4) (2007):758-761.

184. Moroney, R.M.; White, R.M.; Howe, R.T. “Microtransport Induced By Ultrasonic Lamb Waves.” *Appl. Phys. Lett.* 59 (7), 12 August 1991, : 774-776.

185. Moroney, R.M.; White, R.M.; Howe, R.T. “Ultrasonically Induced Microtransport.” *IEEE* 1991 : 277-282.

186. Muntz, E.P. “Rarefied Gas Dynamics.” *Ann. Rev. Fluid Mech*. (1989) 21:387-417.

187. Muntz, E.P.; Sone, Y.; Aoki, K.; Vargo, S.; Young, M. “Performance Analysis and Optimization Considerations For A Knudsen Compressor in Transitional Flow.” *J. Vac. Sci. Technol.* A 20 (1) , Jan/Feb 2002, : 214-224.

188. Murphy, D.M. “Wall Collisions, Angular Flux, and Pumping Requirements in Molecular Flow Through Tubes and MicroChannel Arrays.” *J. Vac. Sci. Technol.* A 7 (5) (1989): 3075-3091.

189. Mutlu, S.; Cong Yu; Selvaganapathy, P.; Svec, F.; Mastrangelo, C.H.; Frechet, J.M.J., “Micromahcines Porous Polymer for Bubble Free Electro-Osmotic Pump”, *Technical Digest. MEMS 2002 IEEE International Conference. Fifteenth IEEE International Conference on Micro Electro Mechanical Systems*, 20-24 Jan. 2002, Las Vegas, NV, USA; p.19-23.

190. Nanbu, K. “Direct Simulation Scheme Derived From the Boltzmann Equation. I. Monocomponent Gases.” *J. of Physical Society of Japan* 49 (5) (1980): 2042-2049.

191. Nguyen, N.T.; Doering, R.W.; Lal, A.; White, R.M. “Computational Fluid Dynamics Modeling of Flexural Plate Wave Pumps.” *1998 IEEE Ultrasonics Symposium* (1998): 431-434.

192. Nguyen, N.T.; Meng, A.H.; Black, J.; White, R.M. “Integrated Flow Sensor For In Situ Measurement and Control of Acoustic Streaming in Flexural Plate Wave Micropumps.” *Sensors and Actuators* 79 (2000): 115-121.

193. Nishizawa, S.I.; Hirata, M. “DSMC Analysis of Thermal Transpiration of Capacitance Diaphragm Gauge.” *Vacuum* 67 (2002): 301-306.

194. Norberg, P.; Petersson, L-G; Lundstrom, I “Characterization of Gas Transport Through Micromachined Submicron Channels in Silicon.” *Vacuum* 45 (1) (1994): 139-144.

195. Ohwada, T.; Sone, Y.; Aoki, K. “Numerical Analysis of the Poiseuille and Thermal Transpiration Flows Between Two Parallel Plates on the Basis of the Boltzmann Equation For Hard-Sphere Molecules.” *Phys. of Fluids* A 1 (12) (1989), : 2042-2049.

196. Ok Chan Jeong; Sang Sik Yang “Fabrication of a thermopneumatic micropump with aluminum flap valves.” *Journal of the Korean Physical Society*; Dec. 2000; vol.37, no.6, p.873-7.

197. Olsson, A.; Enoksson, P.; Stemme, G.; Stemme, E. "A Valve-Less Planar Pump Isotropically Etched In Silicon." *J. Micromech. Microeng.* 6 (1996): 87-91.

198. Olsson, A.; Enoksson, P.; Stemme, G.; Stemme, E. "A Valve-Less Planar Pump In Silicon." 8th Intl. Conf. On Solid-State *Sensors and Actuators*, and Eurosensors IX (1995): 291-294.

199. Olsson, A.; Larsson, O.; Holm, J.; Lundbladh, L.; Ohman, O. "Valve-Less Diffuser Micropumps Fabricated Using Thermoplastic Replication." *Sensors and Actuators* A 64 (1998): 63-68.

200. Olsson, A.; Stemme, G.; Stemme, E. "The first valve-less diffuser gas pump." *The 10th Annual Intl Workshop on MEMS. An Investigation of Micro Structures, Sensors, Actuators, Machines and Robots*, 26-30 Jan. 1997, Nagoya, Japan.

201. Olsson, A.;Stemme, G.; Stemme, E. "A valve-less planar fluid pump with two pump chambers." *Sensors and Actuators* A 46-47 (1995): 549-556.

202. Oran, E.S.; Oh, C.K.; Cybyk, B.Z. "Direct Simulation Monte Carlo: Recent Advances and Applications." *Annu. Rev. Fluid Mech.* 30 (1998): 403-441.

203. Ozaki, K. "Pumping mechanism using periodic phase changes of a fluid." *IEEE Micro Electro Mechanical Systems.* 1995, 29 Jan.-2 Feb. 1995, Amsterdam, Netherlands.

204. Pao, Y-P; Tchao, J. "Knudsen Flow Through a Long Circular Tube." *Phys. of Fluids* 13 (2) (1970): 527-528.

205. Papadopoulos, D.H.; Rosner, D.E. "Enclosure Gas Flows Driven By Non-Isothermal Walls." *Phys. of Fluids* 7 (11) (1995): 2535-2537.

206. Park, J.H.; Bahukudumbi, P.; Beskok, A. "Rarefaction Effects on Shear Driven Oscillatory Gas Flows: A Direct Simulation Monte Carlo Study in the Entire Knudsen Regime." *Physics of Fluids*, Vol. 16, No. 2 (2004): 317-330.

207. Passian, A.; Warmack, R.J.; Ferrell, T.L.; Thundat, T. "Thermal Transpiration at the Microscale: A Crookes Cantilever." *Physical Review* Letters, Vol. 90, No. 12 (2003), : 124503-1 to 124503-4.

208. Piekos, E.S.; Bruer, K.S. "Numercal Modeling of Micromechanical Devices Using the Direct Simulation Monte Carlo Method." *J. of Fluids Eng*. 118 (1996): 464-469.

209. *Piezo Technical Information*, Piezo Systems Inc., Feb. 9, 2004, http://www.piezo.com/.

210. Pollard, W.G.; Present, R.D. “On Gaseous Self-Diffusion in Long Capillary Tubes.” *Physical Review* 73 (7) (1948): 762-774.

211. Poulis, J.A.; Pelupessy, B.; Massen, C.H.; Thomas, J.M. “Longitudinal Knudsen Forces.” *J. Sci. Instrum.* 41 (1961): 295-301.

212. Prasanth, P.S.; Kakkassery, J.K. “Direct Simulation Monte Carlo (DSMC): A Numerical Method for transition-Regime Flows - A Review.” *J. Indian Inst. Sci.* 86 (2006): 169-192.

213. Reynolds, O. “On Certain Dimensional Properties of Matter in the Gaseous State.” *Philos. Trans. R. Soc. Lond*on 170, 727 (1879), : 727-845.

214. Richter, A., Plettner, A., Hofmann, K. A., and Sandmaier, H. “A Micromachined Electrohydrodynamic (EHD) Pump.” *Sens. Actuators* A, 29, : 159–168. 1991.

215. Richter, A., and Sandmaier, H. “An Electrohydrodynamic Micropump.” *IEEE 3rd Int. Workshop on MEMS* (MEMS’90), : 99–104.

216. Robertson, J.K.; Wise, K.D. “Modeling a Microfluidic System Using Knudsen's Empirical Equation for Flow in the Transition Regime.” *J. Vac. Sci. Technol.* A 19 (1) (2001): 358-364.

217. Rosner, D.E.; Papadopoulos, D.H. “Jump, Slip, and Creep Boundary Conditions at Nonequilibrium Gas/Solid Interfaces.” *Ind. Eng. Chem. Res.* 35 (1996): 3210-3222.

218. Roy, S; Raju, R.; Chuang, H.F.; Cruden, B.A.; Meyyappan, M. “Modeling Gas Flow Through Microchannels and Nanopores.” *J. Appl. Phys.* 93 (8) (2003): 4870-4879.

219. Santeler, D.J. “New Concepts in Molecular Gas Flow.” *J. Vac. Sci. Technol.* A 4 (3) (1986): 338-343.

220. Santeler, D.J.; Boeckmann, M.D. “Molecular Flow Transmission Probabilities of Rectangular Tubes.” *J. Vac. Sci. Technol.* A 9 (4) (1991): 2376-2381.

221. Schabmueller, CGJ ; Koch, M ; Mokhtari, ME ; Evans, AGR ; Brunnschweiler, A. "Self-Aligning Gas/Liquid Micropump." *J. MEMS* 12 (4) (2004): 420-424.

222. Schomburg, W.K.; Fahrenberg, J.; Maas, D.; Rapp, R. “Active Valves and Pumps for Microfluidics.” *J. Micromech. Microeng.* 3 (1993): 216-218.

223. Schumacher, B.W.; Falckenberg, H.R.; Thiede, U. “Measurements On An Experimental Model of a New "Thermal Gradient" Vacuum Pump.” *Can. J. Phys*. 42 (1964): 259-272.

224. Seeger, J.I.; Boser, B.E. “Dynamics and Control of Parallel-Plate Actuators Beyond the Electrostatic Instability.” *Transducers '99, The 10th Intl. Conf. On Solid-State Sensors and Actuators*, Sendai, Japan (1999): 474-477.

225. Selvakumar, A.; Najafi, K “Vertical Comb Array Microactuators.” *J. MEMS*, Vol. 12, No. 4 (2003): 440-449.

226. Seong-Il Jeong; Seyed-Yagoobi, J. “An innovative pumping technology - electrohydrodynamic pumping through conduction phenomenon.” *AIP Conference Proceedings*; 2001; no.552, p.343-8.

227. Sharipov, F. “Rarefied Gas Flow Through a Long Tube at Any Temperature Ratio.” *J. Vac. Sci. Technol.* A 14(4), Jul/Aug 1996, : 2627-2635.

228. Sharipov, F. “Non-Isothermal Rarefied Gas Flow Through a Slit.” *Phys. of Fluids* 9 (6), June 1997, : 1804-1810.

229. Sharipov, F. “Application of the Cercignani-Lampis Scattering Kernel to calculations of rarefied gas flows. III. Poiseuille Flow and Thermal Creep through a long tube.” *Eur. J. Mech. B/Fluids* 22 (2003): 145-154.

230. Sharipov, F. “Rarefied Gas Flow Through a Long Rectangular Channel.” *J. Vac. Sci. Technol.* A 17 (5) , Sep/Oct 1999, : 3062-3066.

231. Sharipov, F. “Rarefied Gas Flow Through a Long Tube at Arbitrary Pressure and Temperature Drops.” *J. Vac. Sci. Technol.* A 15(4) (1997): 2434-2436.

232. Sharipov, F.; Seleznev, V. “Data on Internal Rarefied Gas Flows.” *J. Phys. Chem. Ref. Data*, Vol. 27, No. 3 (1998): 657-706.

233. Sherwood, T.K.; Cooke, N.E. “Mass Transfer at Low Pressures.” *A.I.Ch.E. J.* 3 (1) (1957): 37-42.

234. Shin, H. “On the Transfer of Energy Between a Gas and a Solid.” *J. Phys. Chemistry* 70 (4) (1966): 962-972.

235. Shinagawa, H.; Setyawan, H.; Asai, T.; Sugiyama, Y.; Okuyama, K. “An Experiment and Theoretical Investigation of Rarefied Gas Flow Through Circular Tube of Finite Length.” *Chem. Eng. Sci.* 57 (2002): 4027-4036.

236. Shinohara, J., Suda, M., Furuta, K., and Sakuhara, T., “A High Pressure Resistance Micropump Using Active and Normally Closed Valves.” *IEEE 13th Int. Workshop on MEMS* (MEMS’00), : 86–91.

237. Shulin Zeng; Chuan-Hua Chen; Mikkelsen, J.C., Jr.; Santiago, J.G. "Fabrication and Characterization of Electrokinetic MicroPumps." *IEEE 2000 Inter Society Conference on Thermal Phenomena*, (2000): 31-36.

238. Siu, M.C.I. "Equations for Thermal Transpiration." *J. Vac. Sci. Technol.* 10 (2) (1973): 368-372.

239. Smits, J.G. "Piezoelectric micropump with three valves working peristaltically (for insulin delivery)." *Sensors and Actuators* A (*Physica*l); Feb. 1990; vol.A21, no.1-3, (1990): 203-206.

240. Smits, J.G. "Piezoelectric micropump with microvalves." *Eighth University/Government/Industry Microelectronics Symposium*, 12-14 June 1989,Westborough, MA, USA.

241. Sokhan, V. P. ; Nicholson, D.; Quirke,N. "Fluid Flow in Nanopores: An Examination of Hydrodynamic Boundary Conditions." *J. Chem. Physics.* 115 (8) (2001): 3878-3887.

242. Sone, Y. "A Note on Thermal Creep in Rarefied Gas." *J. Phys. Soc. Japan*, 29 (1970), p.1655.

243. Sone, Y. "A Flow Induced by Thermal Stress in Rarefied Gas." *Phys. of Fluids* 15 (8) (1974), : 1418-1423.

244. Sone, Y. "Thermal Creep in Rarefied Gas." *J. Phys. Soc. Japan*, 21 (1966), : 1836-1837.

245. Sone, Y.; Fukuda, T.; Hokazono, T.; Sugimoto, H. "Experiment on a One-Way Flow of a Rarefied Gas Through a Straight Circular Pipe Without Average Temperature and Pressure Gradients." *CP585 Rarefied Gas Dynamics: 22nd International Symposium*, edited by T.J.Bartel, M.A. Gallis, 2001 American Institute of Physics.

246. Sone, Y.; Sugimoto, H. "Vacuum Pump Without a Moving Part and Its Performance." *Rarefied Gas Dynamics*: 23rd Intl. Sympos., (2003): 1041-1048.

247. Sone, Y.; Waniguchi, Y.; Aoki, K. "One-way Flow of a Rarefied Gas Induced in a Channel with a Periodic Temperature Distribution." Phys. Fluids 8 (8) (1996):2227-2235.

248. Steckelmacher, W. "Molecular Flow Conductances of Long Tubes with Uniform Elliptical Cross-Section and the Effect of Different Cross-Sectional Shapes." *J. Phys. D: Appl. Phys.* 11 (1978): 473-478.

249. Steckelmacher, W. "The Effect of Cross-Sectional Shape on the Molecular Flow in Long Tubes." *Vacuum* 28 (6/7) (1978): 269-275.

250. Steckelmacher, W. “Knudsen Flow 75 Years On: The Current State of the Art for Flow of Rarefied gases in Tubes and Systems.” *Rep. Prog. Phys.* 49 (1986): 1083-1107.

251. Steckelmacher, W. “A Review of the Molecular Flow Conductance for Systems of Tubes and Components and the Measurement of Pumping Speed.” *Vacuum* 16 (1) (1966): 561-584.

252. Steckelmacher, W., Lucas, M.W. “Gas Flow Through a Cylindrical Tube Under Free Molecular Conditions.” *J. of Phys. D: Appl. Phys.* 16 (1983): 1453-1460.

253. Stemme, E.; Stemme, G. “A valveless diffuser/nozzle-based fluid pump.” *Sensors and Actuators* A (*Physica*l); Nov. 1993; vol.A39, no.2, p.159-67.

254. Storvick, T.S.; Park, H.S.; Loyalka, S.K. “Thermal Transpiration: A Comparison of Experiment and Theory.” *J. Vac. Sci. Technol.* 15 (6) (1978), : 1844-1852.

255. Su, C.H. “Kinetic Equation of Classical Boltzmann Gases.” *Physics of Fluids* 7 (8) (1964): 1248-1255.

256. Sun, H.; Faghri, M “Effect of Surface Roughness on Nitrogen Flow in a Microchannel Using the Direct Simulation Monte Carlo Method.” *Numerical Heat Transfer, Part A*, 43 (2003): 1-8.

257. Takagi, H.; Maeda, R.; Ozaki, K.; Parameswaran, M.; Mehta, M. “Phase Transformation Type Micro Pump.” *5th International Symposium on Micro Machine and Human Science Proceedings*, 2-4 Oct. 1994, Nagoya, Japan.

258. Takahashi K, Weng J G and Tien C L “Marangoni Effect in Microbubble Systems.” *Microscale Thermophys. Eng.* 3, 1999, : 169–82.

259. Takata, S.; Sugimoto, H.; Kosuge, S. “Gas Separation By Means of a Knudsen Compressor.” *European Journal of Mechanics* A 26 (2007): 155-181.

260. Tamada, K.; Sone, Y. “Some Studies on Rarefied Gas Flows.” *J. Phys. Soc. Japan*, 21 (17) (1966), : 1439-1445.

261. Tao, J.C.; Ganzi, G.C.; Sandler, S.I. “Determination of Thermal Transport Properties from Thermal Transpiration Measurements. II.” *J. Chem. Phys.* 56 (8) (1972): 3789-3793.

262. Tao, J.C.; Revelt, W.; sandler, S.I. “Determination of Thermal Transport Properties from Thermal Transpiration Measurements. III. Polar Gases.” *J. Chem. Phys.* 60 (11) (1974): 4475-4462.

263. Tracy, D.H. “Thermomolecular Pumping Effect.” *Journal of Physics E (Scientific Instruments)*; July 1974; vol.7, no.7, p.533-6.

264. Turner, D.J. “A Mathematical Analysis of a Thermal Transpiration Vacuum Pump.” *Vacuum* 16 (8) (1966): 413-419.

265. Tysanner, M.W.; Garcia, A.L. “Measurement Bias of Fluid Velocity in Molecular Simulations.” *J. of Comput. Phys.* 196 (2004): 173-183.

266. Van De Pol, F.C.M.; Van Lintel, H.T.G.; Elwenspoek, M.; Bouwstra, S. “A Thermopneumatic Micropump based on Micro-Engineering Techniques.” *Sensors and Actuators*, A21-A23 (1990): 198-202.

267. Van Lintel, H.T.G.; Van De Pol, F.C.M.; Bouwstra, S. “A Piezoelectric Micropump Based on Micromachining Of Silicon.” *Sensors and Actuators*, 15 (1998): 153-167.

268. Van der Wijngaart, W.; Andersson, H.; Enoksson, P.; Noren, K.; Stemme, G. “The First Self-Priming and Bi-Directional Valve-less Diffuser Micropump For Both Liquid and Gas.” *IEEE* (2000): 674-679.

269. Vargo, S.E., Muntz, E. “Initial Results From the First MEMS Fabricated Thermal Transpiration-Driven Vacuum Pump.” *Rarefied Gas Dynamics: 22nd International Symposium, 2001 American Institute of Physics* 0-7354-0025-3/01.

270. Vargo, S.E., Muntz, E., Shiflett, G. “Knudsen Compressor As A Micro- And Macroscale Vacuum Pump Without Moving Parts or Fluids.” *J. Vac. Sci. Technol.* 17(4), Jul/Aug 1999, : 2308-2313.

271. Vestner, H.; Waldmann, L. “Generalized Hydrodynamics of Thermal Transpiration, Thermal Force and Friction Force.” *Physica* 86A (1977): 303-336.

272. Wachman, H.Y. “Thermal Accomodation Coefficient: A Critical Survey, The.” *ARS Journal* (1962): 2-12.

273. Wagner, W. “Convergence Proof for Bird's Direct Simulation Monte Carlo Method for the Boltzmann Equation.” *J. of Stat. Phys.* 66 (3/4) (1991): 1011-1044.

274. Wahlbeck, P.G. “Simulated Speed Distributions for Effusing Gases in the Transition Region.” *J. Phys. Chem.* A (2005) 109:8944-8949.

275. Wang, M.; Li, Z. “Simulations for Gas Flows in Microgeometries Using Direct Simulation Monte Carlo Method.” *Intl. J. Heat and Fluid Flow*. 25 (2004): 975-985.

276. Ward, J.W.; Mulford, R.N.R.; Bivins, R.L. “Study of Some Parameters Affecting Knudsen Effusion. II. A Monte Carlo Computer Analysis of Parameters Deduced from Experiments.” *J. of Chem. Phys.* 47 (5) (1967): 1718-1723.

277. Weng, C.I.; Li, W.L.; Hwang, C.C. “Gaseous Flow in Microtubes at Arbitrary Knudsen Numbers.” *Nanotechnology* 10 (1999): 373-379.

278. Williams III, J.C. “Thermal Transpiration - A Continuum gas Dynamics View.” *J. Vac. Sci. Tech.* 8 (2) (1970): 446-450.

279. Williams, B.E.; Forster, F.K. “Micropump design for optimum pressure/flow characteristics.” *Micro-Electro-Mechanical Systems (MEMS). 2000 ASME International Mechanical Engineering Congress and Exposition*, 11-16 Nov. 2001, New York, NY, USA.

280. Wong, C., Hudson, M., Potter, D., Bartel, T. “Gas Transport By Thermal Transpiration In Micro-Channels - A Numerical Study.” *ASME Intl. DSC* - Vol. 66, Micro-Electro-Mechanical (MEMS), Book No. G01091. 1998, : 223-230.

281. Wong, C.C.; Potter, D.L.; Bartel, T.J. “Investigation of Thermal Transpiration in Micro-Channel with DSMC.” *1998 International Mechanical Engineering Congress & Exposition - Application of Microfabrication to Fluid Mechanics* (SAND98-1441A).

282. Wright, SA ; Gianchandani, YB. "A Micromachined Titanium Sputter Ion Pump for Cavity Pressure Control". *Proceedings: IEEE MEMS WORKSHOP* (2006): 754-757.

283. Wu, Y. “Theory of Thermal Transpiration in a Knudsen Gas.” *J. Chem. Phys.* 48 (2) (1968): 889-894.

284. Wu, J.S.; Tseng, K.C. “Analysis of Internal Micro-Scale Gas Flows with Pressure Boundaries Using the DSMC Method. *CP585 Rarefied Gas Dynamics: Intl Symp.* (2001): 486-492

285. X Geng; H Yuan; Oguz, H.N.; Prosperetti, A. “Bubble-based micropump for electrically conducting liquids.” *J. Micromech. Microeng.* 11 (2001) 270–276.

286. Xie, C.; Fan, J.; Shen, C. “Rarefied Gas Flows in Micro-Channels.” CP663, *Rarefied Gas Dynamics*: 23rd Intl. Symp. (2003): 800-807.

287. Xing Yang; Zhaoying Zhou; Xiongying Ye; Mingfei Xiao. "Simulation and Experimental Studies on a Piezoelectrically Actuated Microdiaphragm Air Pump". *Journal of Microlith., Microfab., and Microsystems* 5 (2) (2006): 21106-1-7.

288. Yasumoto, I. “Thermal Transpiration Effets for Gases at Pressures Above 0.1 torr.” *J. Phys. Chem.* 84 (6) (1980): 589-593.

289. Young, R. M.; Han, Y.L.; Muntz, E.P.; Shiflett, G. “Thermal Transpiration in Microsphere Membranes.” *Rarefied Gas Dynamics*: 23rd Intl. Sympos., (2003): 743-751.

290. Young, R. M.; Han, Y.L.; Muntz, E.P.; Shiflett, G. “Characterization of a Radiantly Driven Multistage Knudsen Compressor.” *Proc. IMECE'03* (2003): 393-400.

291. Young, R. M. “Analysis of a Micromachine Based Vacuum Pump On A Chip Actuated By The Thermal Transpiration Effect.” *J. Vac. Sci. Technol.* 17(2), Mar/Apr 1999, : 280-287.

292. Zahn, J.D.; Deshmukh, A.A.; Pisano, A.P.; Liepmann, D “Continuous on-chip micropumping through a microneedle.” *Technical Digest. MEMS 2001. 14th IEEE International Conference on Micro Electro Mechanical Systems*, 21-25 Jan. 2001, Interlaken, Switzerland.

293. Zengerle, R.; Kluge, S.; Richter, M.; Richter, A. “A Bidirectional Silicon Micropump.” *IEEE* (1995): 18-24.

294. Zengerle, R.; Richter, A.; Sandmaier, H. “A Micro Membrane Pump With Electrostatic Actuation.” *Microelectromechanical Systems '92* (1992): 19-24.

295. Zheng, Y.; Garcia, A.L.; Alder, B.J. “Comparison of Kinetic Theory and Hydrodynamics for Poisseuille Flow.” *J. of Statistical Physics* 109 (3-4) (2002): 495-505.

296. Zieba, J. “Simulation of a Solenoid Actuator for a Device for Investigating Dynamic Air Permeability Through Flat Textile Products.” *Fibres and Textiles in Eastern Europe* Vol. 11, No. 2 (41) (2003): 85-87.

APPENDIX

List of Symbols

A	Area
c	Velocity
$\bar{c}$	Average Velocity
$\overline{c^2}$	Average of the Square of the Velocity
d	Channel Diameter
f_{loc}^{M}	Local Maxwellian
f_{0}^{M}	Absolute Maxwellian
$f(\boldsymbol{c},\boldsymbol{r},\boldsymbol{t})$	Phase Space Velocity Distribution Function
$\mathcal{F}(\boldsymbol{c},\boldsymbol{r},\boldsymbol{t})$	Phase Space Single Particle Velocity Distribution Function
G	Mass Flux
h	Channel Height
k	Boltzmann Constant $\left(1.3806504\times10^{-23}\ \mathrm{J/K}\right)$
Kn	Knudsen Number
l	Linear Direction Along Channel Axis
L	Channel Length
m	Molecular Mass
$\dot{M}$	Mass Flux
n	Number density
N	Number of molecules
N_c	Number of Molecules with Velocities Between c and $c+dc$
$\dot{N}$	Number Flux
P	Pressure
P_o	Pressure
O	Channel Circumference
Q	Volumetric Flowrate
Q_P	Reduced Pressure Induced Flow Rate
Q_T	Reduced Thermal Induced Flow Rate
$\dot{Q}_{dA}$	Flux of Some Quantity Q (dtdA)
r	Channel Radius
$\boldsymbol{r}$	Position Vector
R_o	Universal Gas Constant $\left(8.314472\ \mathrm{J/K\cdot mol}\right)$
t	Time

T	Temperature
T_o	Average Temperature
U	Flow Conductance
$\boldsymbol{v}$	Molecular Velocity Vector
V	Volume
w	Channel Width
W	Transmission Probability
z	Linear Direction Along Channel Axis
Z	Flow Resistance
α	Accommodation Coefficient
λ	Mean Free Path
μ	Viscosity
φ	Angle from z-axis
ρ	Density
σ	Molecular Diameter
σ_o	Molecule Cross Section
ϑ	Angle from x-axis
$d\omega$	Solid Angle in Spherical Coordinate System